NASA TECHNICAL MEMORANDUM

NASA TM X-72815

NASA TM X-72815

ADVANCED SUPERSONIC TECHNOLOGY CONCEPT AST-100 CHARACTERISTICS DEVELOPED IN A BASELINE-UPDATE STUDY

by Hal T. Baber, Jr.
NASA Langley Research Center

and

E. E. Swanson
Vought Corporation
Hampton Technical Center

January 16, 1976

NATIONAL AERONAUTICS AND SPACE ADMINISTRATION
LANGLEY RESEARCH CENTER, HAMPTON, VIRGINIA 23665

1. Report No.	2. Government Accession No.	3. Recipient's Catalog No.
TM X-72815		

4. Title and Subtitle	5. Report Date
ADVANCED SUPERSONIC TECHNOLOGY CONCEPT AST-100 CHARACTERISTICS DEVELOPED IN A BASELINE-UPDATE STUDY	January 16, 1976
	6. Performing Organization Code 31.000

7. Author(s)	8. Performing Organization Report No.
Hal T. Baber, Jr., NASA Langley Research Center E. E. Swanson, Vought Corporation, Hampton Tech. Cen.	

9. Performing Organization Name and Address	10. Work Unit No.
NASA Langley Research Center Hampton, Virginia 23665	743-04-01-01
	11. Contract or Grant No.

12. Sponsoring Agency Name and Address	13. Type of Report and Period Covered
National Aeronautics & Space Administration Washington, DC 20546	Technical Memorandum
	14. Sponsoring Agency Code

15. Supplementary Notes

16. Abstract

The Advanced Supersonic Technology configuration concept, AST-100, is an update of the Langley Research Center Reference Configuration baseline. The combination of wing thickness reduction, nacelle recontouring for minimum drag at cruise, and the use of the horizontal tail to produce lift during climb and cruise resulted in an increase in maximum lift-to-drag ratio. At cruise, the increase was about four percent over the previous Reference Configuration maximum lift-to-drag ratio. Lift-to-drag ratio improvement made possible a reduction in engine size. Lighter engines and lower fuel weight associated with this resizing result in a six percent reduction in takeoff gross weight compared to the Reference Configuration. AST-100 takeoff maximum effective perceived noise at the runway centerline and sideline measurement stations was 114.4 decibels. Since 1.5-decibels tradeoff is available from the approach noise, the required engine noise suppression is 4.9 decibels. Maximum overpressure (sonic boom) which would be generated by the AST-100 is slightly lower than that of the Reference Configuration. The AST-100 largest maximum overpressure would occur during transonic climb acceleration when the aircraft was at relatively low altitude. Calculated standard +8°C day range of the AST-100, with a 292 passenger payload, is 7348 km (3968 n.mi.) or 70.4 km (38 n.mi.) greater than the Reference Configuration range taken from NASA CR-132374 for a hot day at a cruise Mach number of 2.7. Fuel price is the largest contributor to direct operating cost (DOC). However, if the AST-100 were flown subsonically (M = 0.9), DOC would increase approximately 50 percent because of time related costs.

17. Key Words (Suggested by Author(s))	18. Distribution Statement
Aerodynamics; Aircraft Design, Testing and Performance; Aircraft Propulsion and Power; Aircraft Stability and Control; Advanced Supersonic Transport; Aircraft Noise; Sonic Boom	Unclassified - Unlimited

19. Security Classif. (of this report)	20. Security Classif. (of this page)	21. No. of Pages	22. Price*
UNCLASSIFIED	UNCLASSIFIED	133	$5.75

*For sale by the National Technical Information Service, Springfield, Virginia 22161

ADVANCED SUPERSONIC TECHNOLOGY CONCEPT AST-100 CHARACTERISTICS DEVELOPED IN A BASELINE-UPDATE STUDY

by Hal T. Baber, Jr.
NASA Langley Research Center

and

E. E. Swanson
Vought Corporation
Hampton Technical Center

SUMMARY

The Advanced Supersonic Technology configuration concept, AST-100, reported in this document is an update of the Reference Configuration baseline. In this study, it was found that the combination of wing thickness reduction (to the minimum practical), nacelle recontouring for minimum drag at cruise, and using the horizontal tail during climb and cruise resulted in an increase in maximum lift-to-drag ratio. At cruise, the increase over that of the Reference Configuration is about 4 percent.

Improvement in aerodynamic efficiency made possible a reduction in engine size from 363 kg/sec (800 lbm/sec) airflow to 323 kg/sec (712 lbm/sec). Lighter engines and lower fuel weight associated with this resizing result in a 6-percent reduction in takeoff gross weight compared to the Reference Configuration.

The AST-100 takeoff maximum effective perceived noise at the runway centerline and sideline measurement stations was 114.4 decibels. By applying the 1.5 decibel allowable tradeoff from the approach noise, which is below the 108 decibel limit, the required engine noise suppression is 4.9 decibels. Over the Mach number range considered, the maximum overpressure (sonic boom) which would be generated by the AST-100 is slightly lower than that of the Reference Configuration. The largest maximum overpressure associated with the AST-100 would occur during transonic climb acceleration when the aircraft was at relatively low altitude.

Calculated "hot" (standard +8°C) day performance of the AST-100, with a 292 passenger payload, is 7349 km (3968 n.mi.).

Lateral-directional stability and control results indicate the need for further lateral-control research in the Supersonic Cruise Aircraft Research (SCAR) program to improve the data base.

Fuel price is the dominant element in direct operating cost (DOC). At 30 cents per gallon, it accounts for 61 percent of DOC and, if doubled in price, would account for 70 percent of DOC. If the AST-100 were flown subsonically (M = 0.9) instead of supersonically, DOC would increase approximately 50 percent.

INTRODUCTION

The Langley Research Center has, since 1972, been actively engaged in, and contractually supporting, work in advanced supersonic technology for potential application to future U.S. transport aircraft. Early conceptual studies, for example reference 1, have identified configuration, stability and control, and performance problems. Continuing research has provided solutions to many of these problems, which were essentially aerodynamic in nature. An advanced supersonic technology concept study performed in 1973 generated a baseline configuration. The objective of this study, reported in reference 2, was to define a Reference Configuration and related characteristics achievable through integration of research results obtained in the interim between 1969 and 1973 (references 1 and 2).

The Reference Configuration provides a useful baseline for tradeoff studies and for the quasi application of future technology improvements. Thus, this configuration has been used as the baseline for a tradeoff study reported herein. The study objective was to update the Reference Configuration through application of recently obtained test data (from Langley full-scale tunnel and Ames 12-foot pressure tunnel) and advancements in analytical techniques and aerodynamic technology. Basic criteria for the study were as follows:

- Five abreast seating of 292 passengers, all tourist class with seat pitch of 0.864m (34 in.).
- Standard day cruise at M = 2.7.
- Range of 7408 km (4000 n.mi.) on standard day +8°C* at M = 2.62.
- Engine size based on either noise considerations (ref. 3), transonic acceleration (with hot day thrust margin of 1.2), or cruise, whichever is critical.
- Land on existing runways with tire footprint no greater than that of DC-8-50.

*"Hot day" as used herein is a so-called "simple hot day." That is, the temperature at any altitude as found in the U.S. Standard Atmosphere, 1962 tables is increased by the hot day increment (+8°C for mission analysis and +10°C for noise analysis) and the speed of sound is calculated for the increased temperature, whereas other state variables are assumed to be the same as for a standard day.

- Stability and control - Specifics can be found in the appropriate section, but generally stated the criteria were:

  Configuration to be trimmed,for minimum trim drag, throughout the flight envelope.

  No significant pitch-up in the takeoff or landing modes.

  Satisfactory short-period characteristics at approach speed.

  Cruise static margin at 1.0g of at least three percent of the reference chord to offset reduction in stability due to flexibility at the required 2.5g maneuver.

  Cruise directional stability such that the yawing moment derivative, C_{n_β} , is equal to or greater than zero for a 2.5g maneuver.

The current configuration is designated Advanced Supersonic Technology-100 (AST-100). Significant changes resulting from the study are: wing thickness reduction and nacelle resizing, with an attendant improvement in transonic and supersonic lift-to-drag ratios; and a resized rudder to insure adequate yawing moment to compensate for a failed outboard engine.

Lateral and direction stability and control analyses were not performed for the Reference Configuration prior to publication of reference 2. However, subsequent effort in this area was expanded to evaluate the AST-100 lateral and directional characteristics. These characteristics, along with the longitudinal stability and control, are presented in this report. Results from the control analysis illustrate the need for research on arrow-wing lateral control devices to generate experimental data for design of controls which provide adequate low-speed roll control.

Sonic Boom and direct operating cost analyses and engine definition was performed by personnel of the Aeronautical Systems Division, Langley Research Center. The remainder of the work reported herein was done by the Advanced Aircraft Technology Group of the Vought Corporation, Hampton Technical Center.

SYMBOLS

Computations in the course of this study were performed in U.S. Customary (English) Units. Results were converted to the International System of Units (SI) by using conversion factors given in reference 4 and are presented in this report along with the Customary Units.

ac	aerodynamic center
A	total equivalent body area, for cuts taken along Mach lines

A_E	equivalent body area due to lift and volume effects, for cuts taken along Mach lines
A_v	equivalent body area due to volume effect, for cuts taken along Mach lines
AR	wing aspect ratio
b	wing span
$\bar{c}_{ref}$	reference mean aerodynamic chord
c_r	rudder chord
c_{vt}	vertical tail chord
c.g., C.G.	center-of-gravity
cm	centimeter
C	Celsius
C_D	drag coefficient, $\frac{\text{Drag}}{q\ S_{W_{ref}}}$
C_{D_F}	skin friction drag coefficient
C_{D_i}	drag coefficient due to lift
C_{D_W}	wave drag coefficient
$\Delta C_{D_{TAIL}}$	drag increment due to 3.5 deg. angle of attack of the horizontal tail
C_L	lift coefficient, $\frac{\text{Lift}}{q\ S_{W_{ref}}}$
$\Delta C_{L_{TAIL}}$	lift increment due to 3.5 deg. angle of attack of the horizontal tail
C_l	rolling moment coefficient, $\frac{\text{Rolling Moment}}{q\ S_{W_{ref}}\ b}$
C_{l_β}	rate-of-change of rolling moment coefficient with angle of sideslip

C_m	pitching moment coefficient, $\frac{\text{Pitching Moment}}{q\ S_{W_{ref}}\ \bar{c}_{ref}}$
C_n	yawing moment coefficient, $\frac{\text{Yawing Moment}}{q\ S_{W_{ref}}\ b}$
C_{n_β}	rate-of-change of yawing moment coefficient with angle of sideslip
CWa	engine airflow corrected to the compressor inlet $(Wa\sqrt{\Theta_{ti}}/\delta_{ti})$
C_{Y_β}	rate-of-change of side force coefficient with angle of sideslip
D	drag
dB	decibels
DEG	degree
EAS	equivalent airspeed
EPNL	effective perceived noise level
ft	feet
FAA	Federal Aviation Administration
F_g	gross engine thrust
F_N	net engine thrust
GE	General Electric
h	altitude
h_o	vertical distance from ground to .667 $\bar{c}_{ref}$ aft of LEMAC
HP	HORSEPOWER
HR = hr	hour
INIT	initial
in.	inches
i_t	horizontal tail incidence angle measured from wing reference plane

kg	kilograms
km	kilometers
kt	knots
kw	kilowatts
K	Kelvin
k_1	control effectiveness parameter
k_2	flexibility factor
lbf	pound force (avoirdupois)
lbm	pound mass (avoirdupois)
L	lift
L_α	$(1/mV)\frac{\partial L}{\partial \alpha}$
$L_{1, 2, 6}$	leading-edge flap designations
L/D	lift-to-drag ratio
l_t	tail length
LEMAC	leading-edge of the mean aerodynamic chord
m	meter
mm	millimeter
mps = m/sec	meters per second
mV	product of mass and velocity
M	Mach number
MAX	maximum
MIN	minimum
MIN DEM	minimum demonstrated
MLW	maximum landing weight
n.mi.	nautical miles

n_{z_α}	incremental load-factor per unit angle-of-attack
N	Newton
NLW	normal landing weight
OASPL	overall sound pressure level
OGE	out-of-ground effect
OW	operating weight
PR	pilot rating
PNL	perceived noise level
Δp	incremental pressure change
Δp_{max}	maximum positive pressure above ambient or the pressure change at the rear shock, whichever is larger
q	dynamic pressure
R	Rankine
sec	second
S_{wf}	wing fin area/side
S_{ht}	exposed, projected horizontal tail area
$S_{W_{ref}}$	reference wing area
S_v	ventral fin area
S_{vt}	vertical tail area
SFC	specific fuel consumption
SLS	sea-level, static
$t_{1,2,3,4}$	wing trailing-edge flap designation
TOGW	takeoff gross weight
TSFC	thrust specific fuel consumption

T/W	thrust-to-weight ratio
$T_{2_{min}}$	minimum time to double amplitude
U_2	ventral fin designation
V	velocity
V_{app}	approach velocity
V_{cw}	cross wind velocity
$V_{min\ dem}$	minimum demonstrated velocity
$\bar{V}$	horizontal tail volume coefficient, $\frac{S_{ht}\, l_t}{(S_{W_{ref}}\, \bar{c}_{ref})}$
W	weight or mass
Wa	engine air mass flow rate
WE	weight empty
X	airplane longitudinal coordinate
ZFW	zero fuel weight
α_t	horizontal tail angle-of-attack
α_{wrp}	wing reference plane angle-of-attack
β	sideslip angle
γ	climb angle
δ_e	elevator deflection measured from tail chord plane
δ_f	flap deflection
δ_r	rudder deflection
δ_{ti}	ratio of total pressure to standard sea level pressure (total conditions at compressor inlet)
Δ	increment

ζ	damping ratio
θ_{ti}	ratio of total temperature to standard sea level temperature (total conditions at compressor inlet)
$\dot{\theta}$	pitch rate
$\ddot{\theta}$	pitching acceleration
λ_c	ratio of control surface chord to total surface chord
Σ	total
τ	control effectiveness parameter
$\tau_{R_{max}}$	maximum roll-mode time constant
ϕ	bank angle
ω_n	undamped natural frequency

Additional subscripts

AVAIL	available
avg	average
b	baseline
d	design
e	nozzle exit
r	required
max	maximum

CONFIGURATION DEVELOPMENT

Background

Results of recent wind tunnel tests (unpublished) along with revised analytical techniques have indicated potential improvements in supersonic cruise aerodynamic technology. This new technology was utilized to evaluate wing thickness reduction, nacelle recontouring for minimum drag at cruise, and the use of the horizontal tail in a lifting attitude during climb and cruise, for possible increase in lift-to-drag ratio (L/D), and hence performance improvement over the

concept of reference 2. Basic aircraft geometry including wing area and planform from the Reference Configuration was held constant. Passenger compartment arrangement and fuselage shape are essentially the same as the Reference Configuration. Minor fuselage refairing was required to maintain a favorable Mach number, M = 2.7, cross-sectional area distribution because of wing thickness reduction and rearward movement of the wing for balance.

Wing Thickness Selection

A series of iterations were performed in which chordwise and spanwise thickness distribution was varied and analyzed for effect on zero-lift wave drag at M = 1.2 and 2.7. In addition to the conventional criteria of basic wing strength, the constraint of housing the main landing gear in the wing, without protuberances, was imposed. Initially, the fuselage, empennage, and nacelles remained the same as for the Reference Configuration, and no attempt was made to optimize the M = 2.7 area distribution curve. In the wing thickness analysis, the thickness distributions of the Reference Configuration and 509B (ref. 5) wings were compared as shown in figures 1 and 2. The 509B wing is believed to be representative of the minimum thickness achievable without incurring significant structural weight penalty. The 509B wing wave drag is lower than that of the Reference Configuration by 11 counts at M = 1.2 and 4.4 counts at M = 2.7. Therefore, the 509B wing was considered initially to be a candidate wing for the AST-100. However, the tires would not fit within the mold lines of the thin wing of the 509B with allowance for minimum tire growth and clearance with structure. A new thickness distribution was developed to provide minimum tire-gear clearance, with the outboard section from about 60 percent semi-span to the tip sized by flutter criteria rather than strength. Thickness was increased from 2.8 percent to 3 percent from the wing fin location to the tip to reduce structural penalty in this area. In addition, the maximum thickness was moved rearward from 50 percent to 60 percent chord to increase the depth of the rear spar. Figures 3 and 4, respectively, show the AST-100 (initial) spanwise thickness distribution and chord-wise maximum thickness location. Unfortunately, these changes results in wave drag increases over the Reference Configuration of 15.7 counts at M = 1.2, and 2.0 counts at M = 2.7. To analyze this large increase in wave drag, the 509B wing was modified to increase tip thickness to three percent. This increased wave drag by 5.1 counts at M = 1.2, and 1.6 counts at M = 2.7 over the original 509B wing.

To further examine the influence of the chordwise and spanwise thickness distribution on wave drag, an interim AST-100 wing was generated with inboard maximum thickness location forward of that of the AST-100 (initial) wing. Inboard spanwise thickness was the same as the AST-100 (initial). The tip section was the same as the Reference Configuration. Wave drag for this concept was close to that of the AST-100 (initial). The selected profile for the AST-100 designated AST-100 (final) is shown in figures 5 and 6. The final AST-100 wing was selected as having characteristics closest to optimum with achievable geometry. For example, the maximum t/c chordwise location is as far rearward as practical and, of the wings considered in this study, it has the lowest volume and hence the lowest wave drag. At M = 1.2 the AST-100 wave

drag is 3 counts lower than that of the Reference Configuration and 1.7 counts lower at cruise. Table I is a brief summary of results from some of the wing thickness distributions studied. These results indicate that the wave drag at M = 1.2 and 2.7 is quite sensitive to the combination of chordwise and spanwise distribution and wing volume.

The AST-100 (final) wing was located to satisfy balance requirements. Correct nacelle and empennage geometry was incorporated and the fuselage was then re-contoured for minimum drag. The AST-100 (final) wing, along with the aforementioned changes, was then used in developing the drag polars for the final performance analysis. A thickness map of the selected wing configuration is shown in figure 7.

AST-100 Description

The AST-100 passenger seating arrangement, shown in figure 8, is the same as that of the Reference Configuration. Seating is 5 abreast, all tourist class, to accommodate 292 passengers with a seat pitch of 0.864 m (34 in.). Volume is available below the cabin floor forward of the wing structural box for passenger baggage and containerized cargo. However, no cargo has been considered in this study. Basic mission fuel is contained in itegral fuel tanks in the wing. A 15142 liter (4000 gal.) reserve fuel tank for extended range and/or center-of-gravity control is located in the aft fuselage. Figure 9 shows the general arrangement of this arrow-wing configuration with geometric characteristics presented in Table II.

The main landing gear is a two-strut arrangement with 12 wheels per strut. A cursory floatation analysis based on a final takeoff gross weight (TOGW) of 325,679 Kg (718,000 lbm) and a tire size of 36 x 11 indicated that floatation criteria for landing on a runway of 0.610m (24 in.) flexible pavement with a subsoil California Bearing Ratio (CBR) of 15 was satisfied. Since detailed design of the main landing gear was beyond the scope of this study, volume for clearance was provided based on wheel diameter and strut length only. Nose landing gear was located forward of that of the Reference Configuration. This reduced flight crew compartment overhang and should improve ride quality in high-speed taxi conditions.

The AST-100 engine is a scaled version of the single spool variable geometry turbine non-afterburning turbojet Reference Configuration engine. Additional engine information can be found in the PROPULSION section. Nacelle geometry was revised from the Reference Configuration "D" pod for cruise drag reduction as previously noted. Figure 10 shows a comparison of the two pod shapes. Typical engine installation is presented in figure 11.

Wing control surfaces are essentially the same as those of the Reference Configuration. However, a minor modification to the inboard flaps, as an increase in span, was possible due to nacelle contour changes, a small increase in inboard nacelle displacement from the fuselage centerline, and fuselage refairing. This inboard flap change increased the area thereof by 2.29 m^2 (24.6 ft^2) per flap, or an increase of nearly 17 percent over the Reference Configuration.

Identification of the various wing control surfaces along with their respective sizes can be found in Table III.

LOW-SPEED AERODYNAMICS

Method

Low-speed aerodynamic characteristics were drived primarily from experimental data of reference 6. Supplementary data such as air conditioning and propulsion drags, and landing gear drag were taken from references 2 and 1, respectively.

In the low-speed regime, three flight modes were considered; namely, take-off and initial climb, climb-out, and approach. The conditions and parameters associated with each of these is shown in Table IV.

Drag data (horizontal tailoff) from reference 6 was adjusted for skin friction difference between model and full-scale Reynold's numbers by the use of reference 7. The basic wind tunnel data from which the AST low-speed data was developed is plotted in figure 12(a) & (b). The data was corrected for leading edge suction differences between model test and full-scale flight conditions by the use of a modified form of the equation given in reference 8. In reference 8, the classical form of the drag-due-to-lift, $C_L^2/\pi AR$, for an elliptically loaded wing was used for 100 percent suction. Hence, the expression used for leading-edge suction parameter s, defined as the measured suction in percent of the total theoretical suction was

$$s = \frac{C_L \tan\alpha - C_{D_i}}{C_L \tan\alpha - C_L^2/\pi AR} \times 100 .$$

The values of s so determined are plotted on figure 12(a) & (b) as a function of C_L. This curve is designated $s_{\text{model test}}$. In addition drag coefficients for 100 percent suction and 0 percent suction, calculated as $C_L^2/\pi AR$ and $C_L \tan\alpha$, respectively are also plotted on figure 12(a) & (b). The suction increment from test Reynold's number, R_N, to full-scale R_N was taken at selected C_L's from scaling curves generated in tests (unpublished) in the Ames Research Center 12-Foot Pressure Tunnel. This increment was then added to the test suction values plotted in figure 12(a) & (b) to obtain suction values for full-scale, which are also plotted on the same figures. Rearranging the equation and substituting, from figure 12(a) & (b), for $C_L^2/\pi AR$, $C_L \tan\alpha$ and s the appropriate values of $C_{D\ 100\%}$, $C_{D\ 0\%}$, and s full-scale, the full-scale drag-due-to-lift was determined.

An incremental downwash angle on the horizontal tail of 4° for flap-deflection from 20° to 40° was determined by interpolation using reference 6 data and unpublished results from tests in LRC's 7- by 10-foot tunnel. The latter source was also used to estimate downwash due to 5° flap deflection (climb-out case). These downwash angles were algebraically added to the angle of attack, and the tail incidence/elevator deflection angles (averaged) for an effective angle of attack to calculate C_{D_i} as $C_L \tan\alpha$, where C_L was obtained as ΔC_L from tail-on and tail-off data of reference 6. The ΔC_{D_i} thus obtained for the incremental flap deflection from 20° to 40° was subtracted from the reference 6 data for $\delta_{Flap} = 40°$. In addition, the difference between model and full-scale horizontal tail skin friction, as estimated by use of the reference 7 computer program was also subtracted from reference 6 data for $\delta_{Flap} = 40°$ to obtain a full-scale tail $C_{D\ total}$ of 0.0027 for the $\delta_{Flap} = 20°$. This model drag coefficient, as corrected to full-scale, was compared to an estimated drag coefficient "buildup" of induced drag and profile drag and found to be higher by 0.0035. This difference was attributed to interference drag. A similar drag coefficient "buildup" for the horizontal tail was done for the climb-out configuration ($\delta_{Flap} = 5°$). With the interference drag coefficient assumed to be 0.00035, a total drag coefficient of 0.0009 was estimated for the horizontal tail.

The tail drag coefficients, based on the proper reference area, were then added to the reference 6 tail-off C_D. For takeoff, this C_D value was corrected for ground effects by the method used in reference 2. Air conditioning and propulsion drag coefficients were taken from reference 2 with the latter being corrected to the AST-100 engine airflow rate. Landing gear drag, for takeoff and approach, obtained from reference 1 is shown in figure 13.

Low-Speed Drag Polars

Takeoff and initial climb.- The takeoff and initial climb drag polar, obtained by the methods just described is shown in figure 14. Significant parameters are presented in Table IV with pertinent configuration geometry shown in Table III. This polar reflects the ground plane effect for an average height of the center of gravity above ground, h, to wing span, b, ratio of 0.2. From figure IV-1A-26 (ref. 2) the lift increases 18 percent at an $h/b = 0.2$ whereas figure IV-1A-33 (ref. 2) shows that C_D increases non-linearly with angle of attack, resulting in an increase of 0.0052 at the angles associated with the takeoff/initial climb C_L of 0.44.

Climb-out.- The climb-out polar in figure 15 is for landing gear retracted and trailing-edge flaps at 5° (see table IV). Ground effect is not included in this polar. Profile drag is reduced significantly due to landing gear being up and flaps retracted from 20° to 5°. Above a lift coefficient of 0.6, the polars of

figures 14 and 15 are similar because drag reduction due to gear and flap retraction is more than offset by the lack of ground effect on lift for the "climb-out" condition.

Approach.- The approach polar is presented in figure 16. For the approach, the airplane is trimmed at the most aft center of gravity, 0.5600 $\bar{c}_{ref}$, compared to climb center of gravity at 0.5375 $\bar{c}_{ref}$. (See Table IV). An important difference between this polar and the one on figure 14 is that this one does not include ground plane effects. Since for out-of-ground effect condition the drag is reduced to a lesser extent than the lift, the L/D is significantly reduced above a C_L of 0.20 compared to the takeoff and initial climb polar.

Lift-to-Drag Ratios

Lift-to-drag ratios, taken from the polars of figures 14, 15, and 16 as a function of lift coefficient are presented in figure 17. Trends are as expected, with the landing gear retracted and 5° flap deflection (climbout) configuration producing the highest lift-to-drag ratios to a C_L of 0.60.

Values of L/D at design lift coefficients for the AST-100 are compared with those of the Reference Configuration (ref. 2) in Table IV. The lift-to-drag ratio, taken at the appropriate design C_L for takeoff and initial climb and climbout, is about 0.82 higher for the AST-100. The L/D increase in the approach mode was not as large, with the increment being 0.26. Similar improvements in maximum L/D were noted at the optimum lift coefficients. Improvements in L/D for AST-100 compared to that of the Reference Configuration are attributed to updated test data (ref. 6) and the application of leading edge suction scaling effects.

HIGH-SPEED AERODYNAMIC CHARACTERISTICS

Method

The method chosen for aerodynamic analysis of the AST-100 involved combining analytically corrected zero-lift drag increments with lift-dependent drag based on experimental data and a semi-empirical estimate of the horizontal tail contribution to drag due to trim incidence. Zero-lift drag for the AST-100 was determined from a superposition of skin friction and roughness drag, wave drag, propulsion bleed drag, and air conditioning drag as discussed in detail in reference 2. The various drag increments presented in this reference were adjusted to reflect geometric differences between the AST-100 and the Reference Configuration. Procedures used to establish each of these drag contributions are outlined in several sub-sections which follow.

Skin Friction and Roughness Drag.- The T' method described in reference 9 was used to compute skin friction drag. Friction drag for a given Mach number/altitude combination was computed by representing various configuration

components by appropriate wetted areas and reference lengths. Assumed conditions were smooth flat plate, adiabatic wall, and turbulent boundary layer. Transition was considered to be fixed at the leading edge of each component. Components such as wing or tail, which have significant variations in reference length, were subdivided into strips to improve the accuracy of friction drag estimates.

Below cruise, the ratio of roughness drag to skin friction drag developed in reference 2 for the Reference Configuration was used to determine roughness drag increments for the AST-100. For the Mach 2.62 cruise condition, the roughness drag increment was assumed to be 6 percent of the skin friction drag.

Skin friction and roughness drag data established for AST-100 at M = 0.6, 1.2, and 2.62 in the manner just described were used to adjust the values for the Reference Configuration to reflect the effect of AST-100 geometry.

The skin friction drag data base for the Reference Configuration was limited to 18,288m (60,000 ft). For higher altitudes, a linear correction factor of $dC_D/dh = 0.123031 \times 10^{-6}$ per meter (0.03750×10^{-6} per foot) was used to account for skin friction and roughness drag variation with altitude. This Reynolds number effect was included in the range calculations for this study.

Component wetted areas and skin friction drag coefficient for the three Mach numbers just cited, along with applicable altitudes, are presented in Table V.

Wave drag.- The supersonic area rule was the basis for AST-100 wave drag computations. The computer program employed is described in reference 10. Typical (in this case M = 2.62) equivalent area distributions for fuselage and overall configuration are presented in figure 18. With equivalent area distributions established, wave drag values were then computed for M = 1.2 and 2.62. These wave drag points were used to adjust the wave drag data of reference 2 for other Mach numbers to account for the AST-100 geometry, as previously indicated for skin friction and roughness drag increments.

Air-conditions and propulsion bleed drag.- Air-conditioning and propulsion bleed drag increments were obtained from reference 2. No modifications or corrections were applied to the air-conditioning drag values. The data from reference 2 was for 363 kg/sec (800 lbm/sec) airflow engines. Therefore, propulsion bleed drag values were scaled by the ratio 712/800 to make them consistent with the 323 kg/sec (712 lbm/sec) airflow engines of the AST-100. These two drag increments as used in the AST-100 performance analysis, are presented in figure 19 as a function of Mach number.

Lift-dependent drag.- Reference 2 was the source of lift-dependent drag for the AST-100. The characteristic polar shapes contained therein are based on wind-tunnel data which were subsequently corrected for differences in wing reference area and aspect ratio as indicated in the reference. Since wing area and aspect ratio for the AST-100 is identical to that of the Reference Configuration the drag polar data from reference 2 were applicable to the former without correction.

Horizontal tail incidence drag.- The horizontal tail is set at an angle of attack of 3.5 degrees (relative to the local flow) for $(L/D)_{max}$ to improve cruise performance. A small drag penalty is associated with the lift so generated. Semi-empirical estimates of this tail lift increment, in coefficient form, were made from delta wing theoretical and experimental data of reference 11 and modified by information from references 12 or 13, as appropriate, to account for the AST-100 horizontal tail being of clipped-delta planform. Drag coefficient due to lift, C_{D_i}, was calculated as a component of the normal force coefficient by writing the latter as a function of C_L and tail angle of attack and using C_L values obtained in the manner just described. These incremental lift and drag values are shown in figure 20.

Drag Polars

Overall drag polars for the AST-100 were developed by combining zero-lift drag increments (including air conditioning and propulsion bleed drag) and the horizontal tail lift and drag increments with the characteristic polars from reference 2. The resulting polars are tabulated, for Mach number 0.6 through 2.62, in Table VI. Three typical drag polars are plotted in figure 21 for M = 0.6, 1.2, and 2.62.

Maximum Lift-to-Drag Ratios

Maximum lift-to-drag ratios were graphically determined from the data of Table VI plotted as per figure 21. The resulting $(L/D)_{max}$ values are shown in figure 22 as a function of Mach number along with comparable values for the Reference Configuration. From figure 22 it can be seen that $(L/D)_{max}$ for AST-100 is higher than that of the Reference Configuration over the Mach number range considered. The combination of wing-thickness reduction and nacelle and fuselage recontouring resulted in an increase in maximum (L/D) of about 0.35, or 4 percent, at cruise.

STABILITY AND CONTROL

Subsequent to publication of reference 2, a 0.10- scale model of the Reference Configuration was tested in the LRC 30 x 60-Foot Full Scale Tunnel. Analysis of these data, reported in reference 6, indicated that the Reference Configuration has, compared to the estimated aerodynamic characteristics of reference 2, lower longitudinal stability at low angles of attack, less negative wing-body zero-lift pitching moment, and gradual pitch-up at the lift coefficient associated with the defined minimum flight speed.

The AST-100 is, therefore, believed to be a more realistic baseline configuration since the low speed aerodynamic characteristics developed herein are based

on improved experimental data of reference 6 and recent unpublished data obtained in the ARC 12-Foot Pressure Tunnel.

Criteria

Prior to determining stability and control characteristics of the AST-100, criteria were set forth as follows:

Longitudinal

(Take-off) - Forward center of gravity set at a position for neutral stability; center-of-gravity range of 66.cm (26 inches); landing gear location set by nose-wheel lift-off speed, consistent with maximum lift coefficient in ground effect; control to geometry limit in full ground effect, and no significant pitch-up.

(Landing) - Aft center-of-gravity limit based on the ability to provide nose down pitching acceleration of 0.08 rad/sec^2 at the minimum demonstrated speed, at the normal landing weight (critical condition); satisfactory dynamic short-period characteristics at the approach speed with stability augmentation, and no significant pitch-up.

(Cruise) - A positive static margin $\geq$ 3 percent at $M = 2.7$ to compensate for for loss of stability due to structural flexibility at the required 2.5g pull-up maneuver condition.

Lateral-Directional

(General) - Negative roll due to positive sideslip (positive dihedral effect).

(Taxiing) - For cross-wind taxiing, minimum control speed shall be sufficiently low such that nose-wheel steering can be used.

(Take-off) - Directional control sufficient to trim the airplane in a 15.4 m/sec (30Kt) 90 degree cross-wind. Directional control sufficient to counteract an outboard engine failure at full thrust engine failure speed for balanced field length of 3200m (10,500 ft.).

(Landing) - Airplane shall possess, in the approach mode, inherent Dutch-roll stability with acceptable levels of undamped natural frequency ($\omega_\eta \geq 0.4$ rad/sec); acceptable levels of damped natural frequency obtained by use of a yaw damper. Lateral control, at or above the normal approach speed, shall be sufficient to produce a 30 degree roll response in 2.5 seconds after initiation of a rapid, full control (assuming a 0.25 second ramp at initiation of control input); directional control at or above the normal approach speed, shall be sufficient to produce a 10 degree sideslip angle with not more than 75 percent of full lateral control to maintain wings-level flight.

(Cruise) - Directional stability such that $C_{n_\beta} \geq 0$ at $M = 2.7$ for the 2.5g maneuver.

Data Base

High-lift configuration longitudinal stability and control data were obtained, as previously noted, from reference 6 and unpublished ARC data. This experimental data included leading edge flap deflection, trailing edge flap deflection, thrust, and horizontal tail incidence/elevator deflection effects. Transonic and supersonic data were obtained from unpublished results from LRC 8-Foot Transonic Tunnel Test No. 503 and LRC Unitary Plan Wind Tunnel Test No. 827, respectively, These data were corrected for horizontal tail volume differences and based on the reference dimensions of the AST-100 by the method presented in reference 2.

Lateral-directional stability and control data for the high-lift configuration were taken from reference 1, and unpublished results from LRC 7 x 10-Foot High Speed Tunnel Test No. 893, corrected for vertical tail volume, ventral position and size differences and based on AST-100 reference dimensions. Reference 1 was also the source of supersonic data. The data were corrected for vertical tail volume, ventral position and size differences and based on AST-100 reference dimensions.

Wing flexibility associated with lateral control deflections, high-speed wing twisting, and fuselage bending effects were taken from reference 1.

Controls

Longitudinal, lateral, and directional control elements, which are partially identified in Table III were considered to be as follows:

Longitudinal	Lateral	Directional
Leading-edge flaps	Outboard ailerons	All-movable rudder (full-span, three segment)
Trailing-edge flaps	Outboard-spoiler-slot and inverted slot deflectors	
All-movable horizontal tail/geared elevator	Inboard flaperons	

Static Longitudinal Stability and Control

The effect of horizontal tail size and control deflection on stability and trim of the AST-100 was investigated for the approach mode at a T/W of 0.164. Results are plotted on figure 23. A subsequent paragraph presents the selection of horizontal tail size in terms of tail volume coefficient and as related to center-of-gravity limits to satisfy longitudinal stability and control criteria.

Longitudinal control power capability was estimated for various combinations of tail incidence, i_t, and elevator deflection, δ_e. The data indicated that an

i_t/δ_e combination of ± 20/25 degrees would give maximum control effectiveness. Data at maximum incidence/deflection were corrected to full-scale Reynold's number by the use of information from reference 2 (fig. VI-2-8). Pitching moment increments for various combinations of tail incidence/elevator deflection, from tunnel test data corrected for the difference in horizontal tail arm and based on full-scale exposed tail area, are presented in figure 24.

Analysis of reference 6 data indicated a forward shift in aerodynamic center of approximately 4 percent $\bar{c}_{ref}$ which, combined with less negative wing-body zero-lift pitching moments, negates the tail up-load required to trim the Reference Configuration. As a result, for the AST-100 approach, a slight tail down-load is required to trim, notwithstanding a 2.26 percent negative static margin during the approach mode of flight. For climb and cruise performance computations the horizontal tail/elevator were considered to be at the incidence/deflection required for minimum trim drag and hence produce maximum L/D. The tail, for this condition, therefore, provides an up-load. Required center-of-gravity locations to achieve the condition of minimum trim drag are presented in figure 25 as a function of Mach number.

Supersonic stability of the AST-100 was estimated from the aerodynamic center data of reference 2 (figure Vi-2-12) which was developed for low-lift coefficients. This data was corrected for the more rearward location of the AST-100 wing and additional flexibility associated with the larger horizontal tail. The resulting flexible airplane aerodynamic center location is shown on figure 25 as a function of Mach number. It can be seen that there is a large static margin for 1g level flight at supersonic speeds. This is more than adequate to compensate for loss of stability in the 2.5g maneuver at cruise conditions. Further, from figure 25, static stability in the transonic region is lower than that at supersonic speeds, which is highly desirable from a transonic maneuverability consideration.

Takeoff and climb-out center-of-gravity limits were estimated based on TOGW, and pitch moment of inertia, takeoff T/W and takeoff $C_{L_{max}}$ in ground effect (for take-off) and out of ground effect (for climb-out). Landing center-of-gravity limits were influenced by normal landing weight (and pitch inertia) and required pitching acceleration to comply with control criteria. By noting the maximum trim capability at minimum demonstrated speed from figure 23 and determining the center-of-gravity position for neutral stability, at the approach speed, forward and aft center-of-gravity limits were calculated. Results are shown on figure 26 as a function of tail size expressed as horizontal tail volume coefficient, $\bar{V}$. It can be seen that the tail size required to satisfy longitudinal stability criteria is 0.0472 which corresponds to a tail area of 39.95 m^2 (430 ft^2). Tail area as used here included the elevator.

Parameters affecting nose-wheel lift-off, and which were considered in the analysis, are: wing body zero-lift pitching moment (in ground effect), horizontal tail maximum lift coefficient (in ground effect), takeoff maximum airplane lift coefficient (in ground effect), landing gear location rearward of the center-of-gravity limit, and takeoff center-of-gravity range. Nose wheel lift-off was established by performing take-off control calculations to

determine landing-gear location rearward of the take-off aft center-of-gravity position. These calculations required the assumption of reasonable values of nose wheel lift-off speed (corresponding to C_L = 0.52), T/W (= 0.296) and tail $C_{L_{max}}$ (= 1.896). The result was an acceptable landing-gear location of 167.6cm (66 in.) aft of the 0.56 $\bar{c}_{ref}$ thereby confirming the validity of the nose wheel lift-off conditions assumed for the calculations.

Finalized static stability and trim data for the AST-100 in the initial climb, climb-out at engine "cutback", and approach modes of flight are presented in figures 27, 28, and 29, respectively. As can be seen on figure 29, the critical design case was for normal landing weight (at lowest approach speed) rather than for maximum landing weight, for which the pitch moment of inertia was larger. From the data of figures 25, 27, 28, and 29, the AST-100 center-of-gravity range is from 42.95 to 56.00 percent of the reference mean aerodynamic chord.

Static Lateral-Directional Stability and Control

AST-100 static lateral-directional stability and control characteristics are based on estimates for the Reference Configuration made subsequent to publication of reference 2. These earlier estimates were modified to account for differences in aft fuselage length, and ventral fin size and location. This unpublished analysis indicated that the critical directional stability condition was for cruise at M = 2.7 with the flexible airplane required to exhibit at least a zero level of directional stability ($Cn_\beta \geq 0$) in a 2.5g pull-up maneuver. Prior analyses have indicated that a vertical tail of 15.8m^2 (170 ft^2) would provide sufficient directional stability in the high-lift configuration but inadequate stability in the 2.5g maneuver at M = 2.7. To reduce dependency upon the vertical tail for stability, this deficiency in directional stability can be alleviated by use of a large aft fuselage-mounted ventral fin. It must, however, be compatible with the ground clearance angle for landing. The ventral fin designated U_2 in LRC Unitary Plan Wind Tunnel Test No. 827 (unpublished) has a full-scale area of 20.25m^2 (218 ft^2). This ventral (with vertical tail) will provide adequate directional stability and can be accommodated on the AST-100.

Wing-body test data from LRC Test No. 827 for a wing leading-edge radius of 0.5 percent wing chord was used to develop AST-100 lateral-directional stability characteristics. Based on trends of wing-mounted fin and ventral fin data, the vertical tail contribution to side force was extrapolated. Using this side-force trend, the vertical tail contribution to directional stability was estimated. This estimated data was corrected for tail size and location. Measured wing-mounted fin contribution to lateral-directional stability was taken from LRC Test No. 827 results and corrected to AST-100 fin area. Finally, measured contribution of the ventral, U_2, was also found in LRC Test No. 827 data. Before summing, all component data were based on AST-100 reference dimensions. Test model leading-edge sweep was 74/65 degrees compared to 74/70/65 for the AST-100. Consequently, test rolling moment due to sideslip was corrected for

leading sweep by the method of reference 14. Flexibility effects applied to the developed data were taken from reference 1.

Estimated cruise (M = 2.7) static lateral-directional stability characteristics for a flexible AST-100 are shown on figure 30 as a function of lift coefficient. The lift coefficient of 0.098 for 1g cruise is the highest coefficient consistent with conditions at the end of cruise. From this figure it can be seen that there is sufficient directional stability to meet the criterion of $Cn_\beta \geq 0$ in a 2.5g "pull-up" maneuver.

Whereas for a normal takeoff, the thrust is less than maximum available, it is increased to the maximum of the operating engines in the event of an engine failure. This, therefore, is the critical condition for directional control sizing. For the previously selected vertical tail size of 15.8m^2 (170 ft^2), a directional control surface sizing parametric study was performed. Conditions were, a TOWG of 325,679Kg (718,000 lbm), an aft center-of-gravity at 0.56 $\bar{c}_{ref}$, and full-thrust engine-failure speed of 97.2 m/sec (189Kts).

A three dimensional control effectiveness (i.e. rate-of-change of fin angle-of-attack with control surface deflection), τ_{3dim}, has been developed and presented in reference 15 to account for control chord and span dimensions as follows:

$$\tau_{3dim} = \frac{1 + \left[AR_s + (AR_s)^{\frac{1}{2}} \right] \tau_{2\,dim\,(avg.)}^{\frac{1}{2}}}{1 + \left[AR_s + (AR_s)^{\frac{1}{2}} \right] \tau_{2\,dim\,(avg.)}^{-\frac{1}{2}}}$$

Where:
$$AR_s = \frac{\text{span of control surface}}{\text{average surface chord}}$$

$$\tau_{2dim\,(avg.)} = \frac{3.2\lambda_c}{1 + 2.2\lambda_c}$$

$$\lambda_c = \frac{c_r}{c_{vt}}$$

An effectiveness parameter, K_1, was developed as a function of control deflection, and a flexibility factor, K_2, was assumed so that $\tau' = K_1 K_2 \tau_{3\,dim}$. The factors, K_1 and K_2, are presented in figure 31.

Vertical tail contribution to lateral-directional stability for the Reference Configuration was developed (aforementioned unpublished analysis) subsequent to reference 2 publication. This data was corrected for AST-100 vertical tail location and is presented in figure 32. Data from this figure, in combination with calculated values of τ', was used to calculate yawing moment capability which is presented in parametric format in figure 33. It can be seen that there are numerous combinations of rudder size and control deflection which will

satisfy static yaw balance for the failed outboard engine condition. As a compromise between maximum aerodynamic benefits from an all-movable vertical tail and control actuation problems associated therewith, a full-span 40 percent chord rudder with a maximum deflection of 35 degrees was selected.

Maximum rigid lateral control contributions from outboard ailerons, outboard spoiler-slot and inverted spoiler-slot deflectors, and inboard flaperons have been estimated previously (unpublished analysis). Estimated rigid contributions were modified by factors from reference 1 to account for flexibility associated with control deflection. Results, along with yawing moment contributed by these controls, are presented in figure 34 as a function of lift coefficient.

Through the use of Laplace transform techniques, the single degree-of-freedom roll equation was solved to express roll angle, ϕ, as a function of time for a ramp control input. The resulting equation was used to determine rolling moment L, (and subsequently the coefficient C_l) required to achieve a given roll angle in a specified time. Available rolling moment, in coefficient form, was derived from figure 34. Available and required rolling moment coefficient are plotted as a function of equivalent airspeed in figure 35 for takeoff and figure 36 for approach. For takeoff, reference 16 permits the required bank angle (30 deg.) to be reduced by the ratio of maximum landing weight inertia to TOGW inertia. Since this ratio, for the AST-100, is .863 the required (reduced) bank angle is 25.9 degrees. Satisfactory roll response, at and above lift-off speed, is indicated in figure 35. Figure 36 indicates satisfactory roll response in the approach mode above 97.7 m/sec (190Kts). Further, it should be noted that, at speeds less than the normal approach speed of 80.5 m/sec (156.4Kts), the roll response would be inadequate to meet a Level 2 (ref. 16) roll requirement.

Two conditions, steady sideslip during the approach and during takeoff ground roll in 90-degree cross wind, were considered in determining lateral and directional control required to trim.

For the approach, lateral and directional control deflections were estimated by solving the two degree-of-freedom roll and yaw steady-state trim equations for positive sideslip angles of 6, 8, and 10 degrees at zero bank angle (wings level). Results, shown in figure 37, indicate adequate directional control and positive dihedral effect (left rudder and right roll control). Achievable sideslip data for the lateral control limits of 75 and 100 percent were developed by cross plotting data from the lower part of figure 37 as the upper part of figure 38. The lower part of figure 38 was produced by cross plotting data from the upper part of figures 37 and 38. These results clearly indicate that a 10-degree sideslip (wings level) cannot be achieved with 75 percent (or less) of maximum roll control at speeds below 102.9m/sec (200 Kts). Furthermore, adherence to 75 percent of maximum roll control capability limits the effective dihedral to 7 degrees of sideslip at 77.7 m/sec (151Kts). To increase the achievable-sideslip angle will require an increase in roll control capability and/or a decrease in positive dihedral effect. Neither of these potential solutions were pursued since further iteration for sizing was beyond the scope of this study. Refinement effort to overcome these deficiencies (roll angle response and "wing level" sideslip) would be hindered by limitations of the present experimental knowledge of the effectiveness of lateral controls on

arrow wings under the influence of aeroelastic deformations. Hence, the need for further lateral-control research is indicated.

Take-off ground roll cross-wind directional control capability was evaluated on the basis of minimum achievable sideslip angle (9.3 deg) with maximum lateral control and associated airplane speed (77.7 m/sec, 151Kts) selected from figure 38. Operationally allowable cross-wind speed, calculated as $V_{CW} = V\tan\beta$, is 12.7 m/sec (24.7Kts). The rationale here is that since the AST-100, in the approach mode, is limited to cross-winds $\leq$ 12.7 m/sec (24.7Kts) rather than the goal of 15.4 m/sec (30Kts), the cross-wind criterion for ground roll should be consistent with the approach cross-wind constraint. Directional control requirements, in terms of rudder deflections, were determined by equating yawing moment, $\delta_r C_{n_{\delta_r}}$ (due to rudder deflection) to airplane yawing moment (due to sideslip) expressed as $C_{n_\beta}\beta$. It was assumed that rotation about the longitudinal axis of the aircraft was not required. Results, as a function of take-off ground roll speed, are shown in figure 39. It can be seen that, in a 12.7 m/sec (24.7Kts) cross-wind, directional control cannot be maintained at ground-roll speeds less than about 46.3 m/sec (90Kts). The implication is that, in such cross-winds, nose-wheel steering and/or differential thrust would have to be used during the initial segment of take-off ground roll.

Dynamic Stability

For the AST-100, only the approach mode of flight was considered in evaluating the inherent longitudinal short-period and lateral-directional stability characteristics. This was done by performing a simple controls-fixed dynamic analysis to obtain roots of the characteristic-uncoupled equations of motion and comparing these roots with handling qualities criteria selected from references 16 and 17.

For the longitudinal mode, examination of the roots of the characteristic equation of motion indicated that the AST-100 inherent characteristics, for the critical case of approach with a center-of-gravity at .56 $\bar{c}_{ref}$ (2.25 percent negative static margin), are unacceptable when compared with the referenced criteria. The problem was alleviated by incorporating a modest level of pitch-rate damping which appeared promising, based on a simple Hardened Stability Augmentation System (HSAS) concept presented in reference 18. Since the damping ratio, with an assumed HSAS pitch-rate damping gain of 3 degrees of i_t/degree per second of $\dot{\theta}$, is greater than 1.3 the short period characteristics would still be unacceptable. As the low-speed approach with the center-of-gravity at the aft limit is the only condition at which the airplane would be flown unstable (see fig. 25), the use of SAS that included a pitch-stiffness function in lieu of the simple HSAS seemed feasible. A pitch-stiffness gain of 1 degree of i_t/degree change in attitude, θ, combined with the aforementioned pitch-rate damping gain produced acceptable short period characteristics as shown on figures 40 and 41.

Examination of the roots of the characteristic equations of motion (see Table VII) indicates that the inherent AST-100 lateral-directional dynamic stability characteristics are: a stable spiral mode; and unacceptable roll-damping mode; and an unstable Dutch-roll mode with acceptable undamped natural frequency. Inherent Dutch-roll characteristics, at normal and maximum landing weights, for the approach mode are presented in figure 42. The effect of increased damping ratio is illustrated here. It can be seen that a yaw damper capable of providing a damping ratio slightly greater than 0.2 would correct the AST-100 Dutch-roll characteristics from unsatisfactory to satisfactory.

PROPULSION

Engine Description

The engine cycle selected for the AST-100 study was the same as for the Reference Configuration. This engine is a single spool, non-after-burning, JP-4 fueled turbojet with a variable geometry turbine and nozzle. The exhaust nozzle is convergent-divergent and completely variable in both throat and exit areas. Nozzle areas were varied throughout the flight envelope to achieve a fully expanded flow within the nozzle.

Several changes in the baseline Reference Configuration such as reduced wing thickness and nacelle recontouring, which were discussed in CONFIGURATION DEVELOPMENT, resulted in drag reduction. This in turn resulted in a reduction in the engine size required and, consequently, a reduction in engine weight and nacelle size.

Turbine geometry was sized to meet engine flow requirements at the design point. However, at part power, turbine geometry was allowed to vary such that the engine could continue operation at the compressor design point with lower turbine inlet temperature. Compared to an engine with a fixed geometry turbine, this mode of operation can yield a given thrust level at reduced fuel consumption.

In the course of the study, several engines were studied. The one selected for the AST-100 was designated AST-JP-2; the numeral 2 simply denoting the second in a series.

Performance

Results of preliminary takeoff, noise, and mission analysis studies dictated engine size for the engine cycle selected. Design point parameters for the AST-JP-2 were:

- Overall pressure ratio of 15:1
- Turbine inlet temperature of 1700°K (3060°R)
- Uninstalled corrected compressor airflow of 323 kg/sec (712 lbm/sec)

An engine defined by these parameters would produce an uninstalled sea-level standard day static thrust of 327,390N (73,600 lbf).

Required engine performance parameters were computed by the use of the ratio of required corrected airflow to the baseline corrected airflow. For example, required gross thrust, F_{g_r} was determined as

$$F_{g_r} = F_{g_b} \frac{CWa_r}{CWa_b}$$

Effects such as inlet, nozzle, thrust reverser, service air bleed of 0.454 kg/sec (1 lbm/sec) and power extraction of 149KW (200 HP) are included in the installed performance for the AST-JP-2 engine.

The computer program used in the reference 2 study was employed to generate two sets of installed performance data. One set, for a simple hot day of standard +10°C atmospheric conditions was used in the takeoff and approach noise analysis. The other set, for a simple hot day of standard +8°C atmospheric conditions, was used in the mission analysis portion of the study. The data are presented in figures 43 through 52. Static thrust and related thrust-to-weight ratio are summarized in the following table.

	Uninstalled		Installed	
Sea Level	Static Thrust, N(lbf)	T/W	Static Thrust, N(lbf)	T/W
Standard Day	327,390 (73,600)	.41	306,447 (68,892)	.38
Std. + 8°C Day	- - - - - - - -	- -	293,485 (65,978)	.37
Std. + 10°C Day	- - - - - - - -	- -	290,360 (65,276)	.36

Engine Weight

Through the use of scale factors which are a function of the corrected airflow ratio (previously defined), it was possible to compute engine weight and dimensions. These scale factors, taken from reference 19 and presented in figure 53, are considered to be typical for a single and two-spool turbojet engine. AST-JP-2 engine weight was calculated to be 5914 kg (13011 lbm) by scaling from the weight of the General Electric GE-4 engine with the scale factors shown in figure 53. The weight of the gas generator, nozzle, and thrust reverser is included in the engine weight.

Nacelle

As noted in a previous section, the engine nacelle was recontoured to reduce the drag thereof below that of the Reference Configuration "D" nacelle. The AST-JP-2 nacelle was defined geometrically by scaling the GE-4 nacelle to match the AST-JP-2 airflow of 323 kg/sec (712 lbm/sec). Once again, scaling was by use of data from figure 53. To the correctly sized engine, a fully expanded

exhaust nozzle was added to meet the following conditions:

M = 2.7

Altitude = 19812m (65000 ft)

Standard + 8°C atmosphere

Air intake capture diameter and length were sized from data in reference 1 as a function of airflow modified by the appropriate scale factor from figure 53. The cylindrical cowl, from the compressor face to the nozzle exit, was sized at the same diameter as the nozzle exit. The air intake was given a conic section shape to match the capture diameter and cowl diameter over the scaled air intake length. An isentropic spike was selected as the air intake centerbody. A sketch of the resulting nacelle profile, along with tabulated dimensions, is shown in figure 54.

MASS CHARACTERISTICS

Method

It was necessary to establish the mass and size characteristics of a configuration which could achieve, within the given criteria, the desired mission goal stated in the INTRODUCTION. A number of candidate aircraft configurations were subjected to a computerized mass properties evaluation and sizing synthesis on the basis of TOWG and thrust-to-weight ratio (T/W). The structural mass analysis was based on an all titanium primary structure. Design features/ fabrication techniques for major components were assumed to be as follows:

- Wing and Aerodynamic Surfaces - Stresskin titanium skin/core sandwich panels
- Fuselage - Titanium skin/stringer/frame construction
- Landing Gear - Two strut main gear and single strut nose gear structure of high strength steel alloy
- Engines - Single spool, non-afterburning turbojet with variable geometry turbine and exhaust nozzle

All mass evaluations were performed using a Vought developed LRC "in-house" Computerized Statistical Mass Properties Estimating Program. This program was used to generate mass data for the Reference Configuration. Hence, its use in the present study ensured that all evaluations were performed on a consistent basis and thus any trends developed from design variations would be real value differences. Payload, cruise speed, and range parameters were held constant, while design gross mass (DGM) and T/W were varied. The sizing synthesis and configuration selection involved the generation of a matrix of approximately 100 candidate aircraft with an array of DGM's varying from 308,445 kg (680,000 lbm) to 340,195 kg (740,000 lbm) with the standard day, sea level uninstalled T/W's varying from 0.36 to 0.50. Data from this program were then used in mission performance evaluations reported in the MISSION ANALYSIS

section. The AST-100 with a design gross mass of 325,679kg (718,000 lbm) was selected as the configuration having the capability of meeting mission goals. This is a 6 percent reduction in take-off gross weight compared to the Reference Configuration (ref. 2).

Mass and Inertia

Gross mass breakdown in the form of a bar chart is presented in figure 55 where the major items of weight are identified and are also shown as a percentage of TOGW. A mass summary by principal subsystems of structure, propulsion, systems and equipment, fuel and payload, is presented in Table VIII. To give the reader insight into the mass accountability "bookkeeping," a detail mass distribution, by subsystems, is shown in Table IX.

Moments of inertia for the AST-100 about the three axes, X, Y, and Z, were calculated for two flight conditions, takeoff and approach, since these are the flight modes for which dynamic stability and control analyses were performed. For the approach mode, inertias were calculated for both normal and maximum landing weight (TOGW - .5x mission fuel weight). These inertia data are given in Table X.

Balance characteristics of the AST-100 were tailored so that all takeoff, cruise and landing center-of-gravity points lie within the limits dictated by longitudinal stability and control criteria. Combinations of fuel burn-tank sequencing were investigated, and the most forward and aft boundaries, compatible with the stability and control constraints determined. A plot of these boundaries, varying with weight, is presented in figure 56. Aerodynamically constrained center-of-gravity limits are as follows:

	Percent $\bar{c}_{ref}$		
	Forward Limit	Aft Limit	Position for Min. Trim Drag
Takeoff	53.75	56.00	
Landing	42.00	56.00	
Begin Cruise			48.50
End Cruise			49.80

All required center-of-gravity locations throughout a typical flight profile lie within the boundaries shown in figure 56, which are attainable by proper fuel burn/transfer management.

ENVIRONMENTAL FACTORS

Noise

AST-100 noise characteristics have been calculated for both takeoff and approach conditions. Jet exhaust noise as effective perceived noise level (EPNL) and the airframe noise as overall sound pressure level (OASPL) were calculated for the measurement stations prescribed in reference 3. The relative location of these stations is shown in figure 57.

Engine noise calculation is based on method 2 of reference 20. Details of the noise prediction method are given in section VI-5 of reference 2. However, the method used in the present study included some modifications taken from reference 21. One of these was the use of the variation of OASPL with relative jet velocity from reference 21 instead of from reference 20. The difference between these two can be seen in figure 58. Further, the variation of density exponent with jet relative velocity is taken from reference 21 rather than using a constant value of 2 as per the reference 20 method. Finally, the variation of directivity corrections with frequency and jet relative velocity were also taken from reference 21 instead of from the reference 2 study.

Engine performance, speed of sound, and atmospheric absorption factors for noise attenuation were based on a 25°C (77°F) day and 70 percent humidity.

Takeoff Noise Analysis.- Takeoff noise level evaluation consisted of an engine sizing parametric study and a final noise analysis compared to the criteria of reference 3. The effects of trailing edge flap angle and engine power setting on takeoff noise level at the measurement stations shown in figure 57 were included in the study. For this study TOGW was held constant at 326,363 Kg (718,000 lbm). Deflection of the three inboard flaps was varied from 5° to 20°. Speed at start of rotation and lift-off varied, of course, with flap angle. For each flap deflection and power setting selected, a takeoff noise profile was generated. At maximum gross thrust, the exhaust gas velocity at sea level standard day + 10°C takeoff is 971 m/s (3188 ft/s),(see fig. 50(a)). This results in unacceptable noise levels. Therefore, the effect of reduced power settings, corresponding to jet exit velocities from 701 m/s (2300 ft/s) to 762 m/s (2500 ft/s) for a sea level standard + 10° day, was examined. Each takeoff profile was constrained to pass through the thrust "cut back" point of 214m (700 ft) altitude at a down-range distance of 5944m (19500 ft). At the "cut back" point, the three inboard trailing edge flaps were retracted to 5° and engine power reduced to the minimum allowed by reference 3.

Figure 59 shows the effect of takeoff distance, to clear a 10.68m (35 ft) obstacle, on the EPNL at the 6486m (3.5 n.mi.) point from brake release as a function of flap deflection and power setting. If the initial engine power (jet exit velocity) is reduced, then the acceleration is lower and hence aircraft speed at the 6486m (3.5 n.mi.) point is lower. At lower speed, this L/D is reduced, and consequently, a higher "cut-back" thrust level is required to meet the "one engine out" requirement of reference 3. Thus, for a given takeoff

distance, the lower the initial power setting (jet exit velocity), the higher the thrust required after "cut back" and, hence, the higher the noise level at the measurement point as shown in figure 59.

The effect of takeoff distance on the EPNL at the sideline measurement point (fig. 57) was also determined as a function of flap deflection and power setting. Results are shown in figure 60. It can be seen that, for a given power setting (jet exit velocity), sideline noise is slightly dependent upon takeoff distance and flap deflection and, conversely, more strongly dependent upon engine power level.

Installed T/W varies for each power setting (jet exit velocity). For example, using the upper plot of figure 61 it can be seen that, for an uninstalled T/W of 0.41 and a jet velocity of 701 m/s (2300 ft/s), the installed T/W is 0.259, whereas at 762 m/s (2500 ft/s), the installed T/W is 0.282. Using these installed T/W's, the variation in noise level with jet exit velocity can be obtained and then related to uninstalled T/W's.

The effect of uninstalled T/W on EPNL at the 6486m (3.5 n.mi.) point for a takeoff distance of 3200m (10,500 ft) and three jet exit velocities can be seen in figure 61. For each T/W the takeoff distance was held constant by changing the flap deflection and initial rotation speed. For each jet exit velocity, and hence each T/W, there is a value of EPNL at which the sideline noise is equal to the centerline noise. The locus of these points is also shown on figure 61.

Reference 3 limits the EPNL at the two takeoff measurement points and the measurement point for approach to 108dB (see fig. 61). However, reference 3 allows noise tradeoffs to be made between the three measurement points with the provision that no more than 2dB can be applied to noise exceedence at any point and that the sum of exceedence cannot be greater than 3dB. The approach noise, to be discussed later, is less than 108dB. Since reference 3 permits 3dB of the difference between the allowable noise level and the actual approach noise level to offset the exceedence at the two takeoff noise measurement points, the limit at these points can be raised to 109.5dB (see fig. 61).

In order to meet the aircraft mission requirements without excessively large engines, the T/W range of engines investigated in this analysis have noise levels which, without suppression, exceed the limits of reference 3. Therefore, jet noise suppression is required. Required suppression as a function of uninstalled T/W is shown in figure 62. It should be noted that for a 3200m (10,500 ft) takeoff distance, noise suppression is required over the range of T/W's considered in this study. Since suppression is required, the decision was made to size the engine for cruise rather than on the basis of noise. For the AST-100 the selected uninstalled T/W was 0.41. This corresponds to an installed, full-power thrust of 290,360N (65276 lbf) per engine at sea level standard +10°C day conditions. Based on the trade-off study reported in reference 2, the AST-100 trajectory was constrained so that the aircraft would reach the "cut back" altitude of 213m (700 ft) at 5944m (19,500 ft) from brake release to maximize speed at "cut back." At this point, flaps were retracted from 20° to 5°.

The variation of takeoff noise level with reduced power setting corresponding to jet exit velocities from 701 m/s (2300 ft/s) to 762 m/s (2500 ft/s) was determined and is presented in figure 63. As initial thrust level (jet velocity) increases, the sideline noise level increases. As a consequence of the thrust level increase, aircraft speed at the 6486m (3.5 n.mi.) point increases. With the speed increase, L/D increases with the result that a lower thrust level is required, after "cut back," to maintain the "one engine out" requirement of reference 3. Thus, as the takeoff thrust level (jet level) increases, the thrust level required at "cut back" is lower and the centerline noise level is reduced as shown in figure 63. It can be seen that the minimum amount of suppression required occurs at the condition where the sideline noise and centerline noise are equal; in this case, at a jet exit velocity of 752.9 m/s (2470 ft/s).

Takeoff thrust level corresponding to partial power jet velocity of 752.9 m/s (2470 ft/s) is 224,336N (50,433 lbf) per engine for a standard +10°C day. With this thrust level, the AST-100 trajectory was set to reach the "cut-back" point at an altitude of 216m (710 ft) rather than 213m (700 ft) in an effort to meet the airframe noise constraint of 108dB at the runway centerline measurement point.

The takeoff trajectory, including the cut-back point and the two noise measurement locations, is shown in figure 64. Lift-off occurred at 107.0 m/s (208.1 knots) with the speed at the 6486m (3.5 n.mi.) point being 124.0 m/s (240.9 knots). At this point, with 5° flap deflection, lift coefficient, C_L, is 0.378, which corresponds to an L/D of 10.1.

The variation of EPNL along the runway centerline and along a sideline position 649m (0.35 n.mi.) from the centerline is presented in figures 65 and 66, respectively. Also shown is the reference 3 allowable noise level and the amount of suppression (4.9dB) required. From these figures it can be seen that the maximum centerline noise at the 6486m (3.5 n.mi.) point is 114.4dB and the sideline maximum is 114.4dB.

Contour plots of EPNL (unsuppressed engine) for 115dB and 108dB are presented in figure 67.

Approach Noise Analysis.- For the aircraft in the approach mode, noise level was evaluated for the measurement point defined in reference 3. This point is 1852m (1.0 n.mi.) from the 15.24m (50 ft) altitude threshold point along the runway centerline as shown in figure 68. For the approach, trailing edge flaps were deflected to 20°. Lift coefficient during approach was 0.55, which is the same as for the Reference Configuration. The normal landing weight of 206,364kg (454,000 lbm) was used for this analysis. At these conditions, the approach speed was 81.75 m/s (158.8 knots) and the L/D was 5.9. With the aircraft flying at 3° approach, the EPNL at the reference 3 measurement point was calculated to be 103.1dB.

Airframe Noise Analysis.- The airframe overall sound pressure level (OASPL) was computed by the use of the following equation:

$$OASPL = 10 \log_{10} \left[\frac{V^{3.17} W^{0.88}}{R^{1.62} S^{0.16} AR^{2.06}} \right] + 41.29$$

where: V = aircraft speed in m/s
W = aircraft weight in Kg
R = aircraft altitude in m
S = wing area in m^2
AR = wing aspect ratio

The airframe OASPL value from this equation is applicable to the runway centerline directly under the aircraft. Parameter input values and the corresponding airframe OASPL at the two measurement points, as defined in reference 3, were as follows:

Parameter	Takeoff Point 6.49km (3.5 n.mi.) From Brake Release	Landing Point 1.85km (1.0 n.mi.) From 50 ft. Obstacle
AR (gross)	1.726	1.726
$S_{W_{gross}}$, $m^2(ft^2)$	1021.56 (10,996)	1021.56 (10,996)
V, m/s (knots)	124.00 (240.9)	81.75 (158.8)
R, m(ft)	245.50 (835)	112.47 (369.0)
W, kg(lbm)	325,679 (718,000)	205,930 (454,000)
OASPL, dB	108	107

Since OASPL is not a time dependent function, the above values are the maximum that an observer at either measurement point would perceive. Because EPNL is a time-related function, the reference 3 EPNL limitation of 108dB is not directly applicable to the airframe OASPL. However, the EPNL will be less than 108dB if the maximum value of OASPL is equal to or less than 108dB.

Sonic Boom

Sonic Boom Analysis.- Equivalent area distributions, due to volume and lift, required for sonic boom analyses, were computed by the use of methods described in references 10 and 22, respectively. These methods were modified to include angle of attack effects. Using these equivalent areas and the procedures of references 23 and 24, near field pressure signatures located at three body lengths below the aircraft, were defined. By the method of reference 25, these near-field pressure signatures were extrapolated to ground level. This method permits the incorporation of variations in atmospheric properties and flight conditions such as acceleration and flight path angle. Hence, the effects thereof are included. A reflection factor of 1.9 was used in these analyses.

For comparison purposes, both the AST-100 and Reference Configuration were analyzed for sonic boom through climb and cruise segments. Aircraft properties and flight conditions used in these analyses are listed in Table XI(a) and (b).

Sonic Boom Results.- Equivalent area distributions which are typical of those for transonic and supersonic climb, along with that for the start of cruise, are shown in figures 69, 70, and 71, respectively. Associated pressure signatures for these conditions are shown in figure 72. From these and other similar plots of the variation of overpressure increment with time, the maximum overpressure, Δp_{max}, was obtained and plotted against Mach number. The result is in figure 73.

At low supersonic Mach numbers Δp_{max} increases rapidly as Mach number decreases. Further analysis indicated that a caustic (super boom) would occur on the ground for the AST-100 at a Mach number slightly below 1.15 and for the Reference Configuration slightly below $M = 1.17$. This is due to the shock focusing effect of acceleration at low flight altitudes (see ref. 26).

At higher Mach numbers the Δp_{max} curves typically exhibit two peaks. In this case, the first at $M = 1.6$, is attributed to the opposing effects of increasing lift and increasing altitude. The second peak, at $M = 2.2$ for the Reference Configuration and $M = 2.4$ for the AST-100, is the result of shock coalescence into the higher-strength N-wave signature.

At low supersonic Mach numbers more complex mid-field signatures occur as illustrated by figure 72(a).

Over the Mach number range considered, the Δp_{max} which would be generated by the AST-100 is slightly lower than that of the Reference Configuration. This is because of the smaller equivalent body area due to volume effects and lower weight of the AST-100 compared to the Reference Configuration.

MISSION ANALYSIS

Mission analysis objective for the AST-100, as taken from the Reference Configuration criteria, was a design range of 7408Km (4000 n.mi.) and 292 passengers plus baggage, which translates into a payload of 27,682kg (61,028 lbm). Although the AST-100 is sized for $M = 2.7$ cruise at standard conditions, it is required that it achieve the range objective on a hot (standard +8°C) day. On the basis of equal stagnation temperature, a standard +8°C day Mach number of 2.62 corresponds to $M = 2.7$ at standard conditions and hence was selected as the cruise Mach number for mission analysis in order not to exceed $M = 2.7$ stagnation temperature. The desired mission profile was taken from reference 2 and is presented in figure 74. Fuel reserves allowance from FAR 121.648 SST Fuel Requirements (tentative standard proposed by the FAA) was modified for a change in holding altitude from 457m (1,500 ft) to 4572m (15,600 ft).

As pointed out in the CONFIGURATION DEVELOPMENT section, the wing area and planform of the Reference Configuration were retained for the AST-100. However, resizing in terms of engine size and overall aircraft weight was performed. Resizing was accomplished through a parametric study, which determined the effect of (T/W) ratios on range for various takeoff gross weights.

Plots of TOGW as a function of T/W for the design range and range as a function of T/W for various TOGW's are presented in figure 75. Figure 76 is a similar type plot with the independent variable being installed T/W rather than uninstalled T/W. Based on a takeoff field length constraint of 3200m (10,500 ft), an uninstalled T/W = 0.41 and a design range of 7408km (4000 n.mi.), a TOGW of 325,679kg (718,000 lbm) was found from figure 75. This is the final takeoff gross weight for the AST-100.

The NASA Mission Analysis Computer Program (PAB-2011) was used for a final mission performance evaluation of the AST-100. The following data were inputs to the program:

(1) Takeoff gross weight - 325,679kg (718,000 lbm)

(2) Payload - 292 passengers plus baggage, 27,682kg (61,028 lbm)

(3) Operating Weight - 149,448kg (329,476 lbm)

(4) Desired Range - 7408km (4000 n.mi.)

(5) Cruise Mach number - 2.62 at standard + 8°C day

(6) Descent distance (part of range) - 370km (200 n.mi.)

(7) Low and high speed drag polars for AST-100

(8) Installed thrust and fuel flow data for AST-100 engines with a sea level static installed thrust of 293,485N (65,978 lbm) per engine (standard day +8°C ambient temp.) and corrected airflow of 323kg/sec (712 lbm/sec)

(9) Climb speed schedule - figure 77

Significant final performance results for the AST-100 as obtained from PAB-2011 program are:

(1) Start of cruise L/D - 8.91

(2) Start of cruise altitude - 18,898m (62,000 ft)

(3) Required trip fuel - 119,295kg (263,000 lbm)

(4) Range - 7,349km (3968 n.mi.)

Extensive mission segment data are presented in Table XII. A simplified flight profile representation of mission performance is shown in figure 78.

Computed performance of the AST-100 indicates a range that is 59.3km (32 n.mi.) short of the objective of 7,408km (4000 n.mi.) or 0.8 percent less. Due to the difference being so small, there was no merit in further iterations. It should be noted, however, that the AST-100 range on a standard +8°C "hot" day exceeds that of the Reference Configuration (ref. 2) on a standard day (M = 2.7 cruise) by 70.4km (38 n.mi.) and at 19,958kg (44,000 lbm) lower TOGW.

DIRECT OPERATING COST

Component elements of direct operating cost (DOC) were estimated for the AST-100 by the use of the model of reference 27 (updated to 1975 cost experience). Nominal values and assumptions used in the DOC analysis are listed in Table XIII. A detail breakdown of DOC is given in figure 79 in the form of "pie" charts and is tabulated in Table XIV. At a price of 30 cents per gallon, fuel cost is dominant; figure 79 shows that it accounts for about 61 percent of DOC. If fuel price is doubled, it then accounts for 70 percent of DOC. As can be seen from figure 79, aircraft depreciation is the other major contributor to DOC. Collectively, fuel and depreciation account for 80 percent of the direct operating cost. The importance of fuel price increases is further illustrated in figure 80.

Due to the significance of fuel price and depreciation (as related to purchase price), technological improvements can make a major contribution in the area of fuel consumption and fabrication techniques to enhance economic performance. Innovations which reduce specific fuel consumption, increase lift-to-drag ratio, and reduce airplane weight and cost should be given high priority for implementation. These innovations will have a greater impact on the operation of supersonic airplanes than on subsonic airplanes since fuel consumption is a relatively less important part of DOC for the latter, Further, should fuel cost continue to rise at a faster rate than other costs, such technological innovations will become progressively more important. Conversely, however, the supersonic airplane is less sensitive to other costs. For example, from figure 80, it can be seen that doubling airplane cost increases DOC about 28 percent, whereas doubling fuel cost increases DOC about 60 percent. Reasonable variations in annual utilization rates or period of depreciation can be seen to have a much smaller effect on DOC.

The effect on DOC of operating the AST-100 subsonically ($M = 0.9$) at two load factors is shown in figure 81 along with supersonic ($M = 2.62$) operation at the same load factors. Calculations for the 55 percent load factor cases included the slightly favorable influence of off-loading fuel which yeilds about a 2 percent reduction in DOC. If the airplane is flown at the lower speed, DOC increases approximately 50 percent. Comparison of costs at these two speeds reveals that fuel costs are nearly the same but wide variations exist in time related costs. Costs such as crew and maintenance rise drastically because of the extra time required to complete the mission. The severe penalties paid for operation of the AST-100 at subsonic speed mean that low-speed flight time must be held to an absolute minimum. Likewise, supersonic design must not be compromised for subsonic operation.

CONCLUDING REMARKS

The AST-100 has been defined by: application of additional experimental data, obtained since establishment of the Reference Configuration as the Advanced Supersonic Technology (AST) baseline concept; the use of improved analytical techniques; and more extensive analyses, especially in the stability and control area. Therefore, the AST-100 is a viable replacement for the Reference Configuration as the updated AST baseline.

Reduction of wing thickness in the root area, recontouring engine nacelles for minimum drag and the use of the horizontal tail to produce lift during climb and cruise, has resulted in an overall improvement in maximum lift-to-drag ratio for the AST-100 over the Reference Configuration, the difference at cruise being approximately 0.35.

Mission range for the AST-100, computed for a standard +8°C day, is 59.3km (32 n.mi.) less than the design goal of 7408km (4000 n.mi.), or 0.8 percent less.

Resizing engines to 323 kg/sec (712 lbm/sec) airflow for the AST-100 compared to 362kg/sec (800 lbm/sec) airflow for the Reference Configuration implies a significant reduction in block fuel and total reserve fuel required, as was indeed the case.

Takeoff at jet exit velocity of 752.9m/sec (2470 ft/sec) is the condition for equal noise at the centerline and sideline measurement stations, which is the condition for minimum-required suppression. Noise exceedence at both stations would be 6.4dB. Application of 1.5dB tradeoff at each station, from the approach noise, results in 4.9dB required suppression.

Results from the AST-100 lateral-directional stability and control analysis indicated that the arrow-wing concept has several inherent deficiencies, especially in the high-lift approach mode. Namely, these are roll angle response and inadequate "wing-level" sideslip capability. Any attempt at configuration refinement to eliminate these deficiencies would be impeded by the lack of experimental data for lateral controls on aeroelastically deforming arrow wings. This emphasizes the need for further lateral-control research in the Supersonic Cruise Aircraft Research (SCAR) program.

Direct operating cost analysis showed that fuel price has a dominant role in the DOC of a supersonic cruise aircraft with depreciation being the next largest element. Hence, innovations which reduce specific fuel consumption, increase lift-to-drag ratio, and reduce aircraft weight and cost should be given high priority for implementation. Finally, the analysis indicated that such a severe penalty, associated with time related costs, would be paid for operation at subsonic speed that this mode of operation would have to be held to an absolute minimum.

REFERENCES

1. The Boeing Company: Mach 2.7 Fixed Wing SST Model 969-336C (SCAT-15F), Document No. DGA-11666-1, Nov. 1969

2. LTV Aerospace Corporation, HTC: Advanced Supersonic Technology Concept Study, Reference Characteristics, NASA CR-132374, Dec. 21. 1973

3. Department of Transportation, Federal Aviation Administration Noise Standards: Aircraft Type and Airworthiness Certification, Federal Aviation Regulations Part 36, June 1974

4. Mechtly, E. A.: The International System of Units - Physical Constants and Conversion Factors (Second Revision), NASA SP-7012, 1973

5. LTV Aerospace Corp., HTC: Advanced Supersonic Technology Liquid Hydrogen Concepts Study, Summary Report, NASA CR-132506, March 1975

6. Coe, Paul L., Jr.: McLemore, H. Clyde; and Shivers, James P.: Effects of Upper-Surface Blowing and Thrust Vectoring on Low-Speed Aerodynamic Characteristics of a Large-Scale Supersonic Transport Model, TM X-72792

7. Airplane Turbulent Skin-Friction Drag. NASA Program Number D1266

8. Henderson, William P.: Studies of Factors Affecting Drag Due to Lift at Subsonic Speed, NASA TN-D 3584, Oct. 1966

9. Somer, Simon C.; and Short, Barbara J.: Free Flight Measurements of Turbulent Boundary Layer Skin Friction in the Presence of Severe Aerodynamic Heating at Mach Numbers from 2.8 to 7.0. NACA TN 3391, 1955

10. Harris, Roy V., Jr.: An Analysis and Correlation of Aircraft Wave Drag. NASA TM X-947, 1964

11. Purser, Paul E; and Fields, E. M.: Some Research on the Lift and Stability of Wing-Body Combinations. NACA RM L55G06A, July 1957

12. Emerson, Horace F.: Wind Tunnel Investigation of Effect of Clipping the Tips of Triangular Wings of Different Thickness, Camber, and Aspect Ratio - Transonic Bump Method. NACA TN-3671, 1956

13. Laberg, J. G.: Supersonic Wind Tunnel Tests of Eleven Small Aspect Ratio Wings. National Aeronautical Establishment. AD 36-420, 1954

14. Air Force Flight Dynamics Laboratory: Stability and Control Methods. USAF Stability and Control Datcom, Oct. 1960, Revised Jan. 1975

15. DeYoung, J.: Symmetric Loading of a Wing in a Wide Slipstream. Grumman Aircraft Engineering Report No. ADR 01-04-66.1, Oct. 1966

16. Anon.: Flying Qualities of Piloted Airplanes. Military Specification MIL-F-8785B (ASG), Aug. 1969

17. Shomber, H. A.; and Gertsen, W. M.: Longitudinal Handling Qualities Criteria: An Evaluation. Journal of Aircraft, Vol. 4, No. 4, 1967

18. Tomlinson, L. R.: SST Longitudinal Control System Design and Design Processes, Hardened Stability Augmentation Design. Rept. No. FAA-SS-73-1 (Boeing Co. Document No. D6-60285), June 1973

19. The General Electric Company: Preliminary Study Data GE 21/J1 Study A1 Turbojet Propulsion System for Use in Advanced Supersonic Propulsion System Technology Study. Report No. R72AEG329 (Contract NAS3-16950), Nov. 1972

20. Society of Automotive Engineers: Jet Noise Prediction. Aerospace Information Report SAE AIR 876, July 1965

21. Dunn, D. G.; and Peart, N. A.: Aircraft Noise Source and Contour Estimation. NASA CR-114649, July 1973

22. Carlson, Harry W.; and Miller, David S.: Numerical Method for the Design and Analysis of Wings at Supersonic Speeds. NASA TN D-7713, 1974

23. Carlson, Harry W.: Correlation of Sonic Boom Theory with Wind Tunnel and Flight Measurements. NASA TR R-213, 1964

24. Middleton, Wilbur D.; and Carlson, Harry W.: A Numerical Method for Calculating Near-Field Sonic-Boom Pressure Signatures. NASA TN D-3082, 1965

25. Thomas, Charles L.: Extrapolation of Sonic Boom Pressure Signatures by the Wave Form Parameter Method. NASA TN D-6832, 1972

26. Haglund, George T.; and Kane, Edward J.: Effect of SST Operational Maneuvers on Sonic Boom. AIAA Paper No. 72-196, 1972

27. Air Transport Association of America: Standard Method of Estimating Comparative Direct Operating Costs of Turbine Powered Transport Airplanes. December 1967

TABLE I

Wing Thickness Study Wave Drag Comparison

MODEL	C_{D_W} M = 1.2	C_{D_W} M = 2.7	WING VOL. m^3 ($ft.^3$)
Ref. Conf. (Ref. 2)	.0034265	.0021767	585(20669)
509B (Ref. 5)	.0023222	.0017359	502(17725)
AST-100 (Initial)	.0049973	.0023747	549(19393)
509B (Modified)	.0028369	.0018969	510(17993)
AST-100 (Interim)	.0048792	.0023286	545(19262)
AST-100 (Final)	.0031298	.0020003	520(18378)

TABLE II
AST-100 GEOMETRY TABLE

GEOMETRY	WING	HORIZONTAL	VERTICAL	VERT FIN ON WING
AREA (GROSS) S, m^2 (ft^2)	1021.5639 (10996.0000)	55.7418 (600.0000)	15.7935 * (170.0000)	21.6720 (233.2750)
MAC (GROSS) $\bar{c}$, m (ft)	34.1139 (111.9224)	6.3868 (20.9540)	6.1679 (20.2360)	7.8638 (25.8000)
AREA (REF) S, m^2 (ft^2)	926.1523 (9969.0000)	- -	- -	- -
MAC (REF) $\bar{c}$, m (ft)	29.3335 (96.2385)	- -	- -	- -
AREA (EXPOSED) S, m^2 (ft^2)	- -	39.9483 (430.0000)	- -	- -
SPAN b, m (ft)	41.9947 (137.7778)	9.7468 (31.9780)	2.8854 (9.4660)	3.2766 (10.7500)
ASPECT RATIO (GROSS)	1.7263	1.707	.527	.495
ASPECT RATIO (REF)	1.9042	-	-	-
SWEEP Λ LE RAD (DEG)	1.2915, (74.0000) 1.2364, (70.8400) 1.0472 (60.0000)	1.0580 (60.6400)	1.1903 (68.2000)	1.2810 (73.4200)
ROOT CHORD m (ft)	55.8021 (183.0779)	9.1025 (29.8640)	8.8498 (29.0347	11.6434 (38.2000)
TIP CHORD m (ft)	5.3763 (17.6389)	2.3390 (7.6740)	2.0975 (6.8816)	1.5850 (5.2000)
ROOT T/C %	SEE FIG.	3.000	2.996	2.996
TIP T/C %	SEE FIG.	3.000	2.996	2.996
TAPER RATIO	-	.257	.237	.136
DIHEDRAL RAD (DEG)	-	-.2618 (-15.0000)	-	
VOL COEFF (GROSS), $\bar{V}$	-	.0672	.0167	.0126
VOL COEFF (REF), $\bar{V}$	-	.0620	.0185	.0140

* DOES NOT INCLUDE 20.2528 m^2 (218.0000 ft^2) VENTRAL

TABLE III

AST-100 Wing Control Surfaces

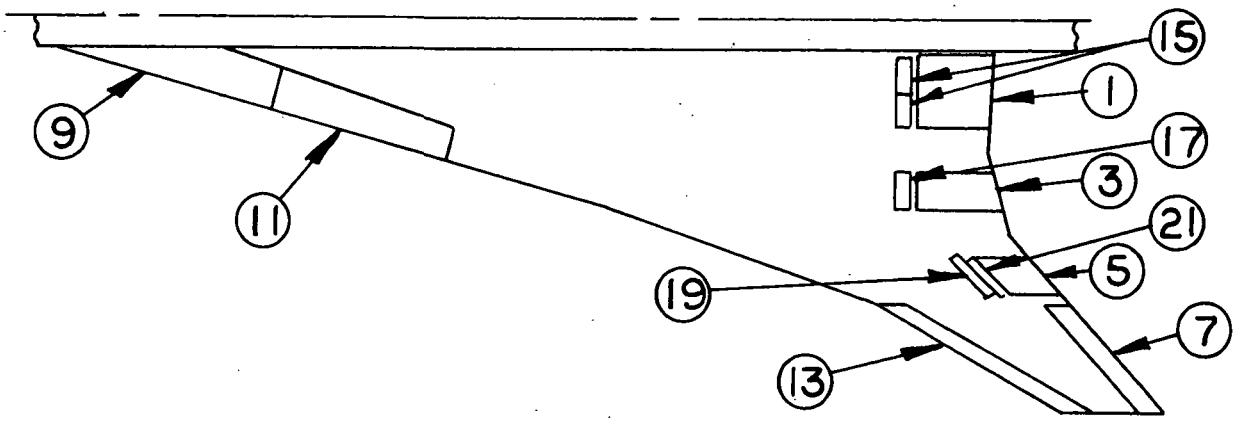

W.T. MODEL DESIGNATION	* NUMBER	AREA, m^2 (ft^2) EACH
t_1	1 AND 2	15.849 (170.600)
t_2	3 AND 4	9.290 (100.000)
t_3	5 AND 6	6.300 (67.800
t_4	7 AND 8	8.668 (93.300)
L_1	9 AND 10	18.307 (197.056)
L_2	11 AND 12	19.123 (205.833)
L_6	13 AND 14	9.935 (106.944)
	15 AND 16	4.258 (45.833)
	17 AND 18	2.385 (25.667)
	19 AND 20	1.432 (15.417)
	21 AND 22	.939 (10.111)

* ODD NUMBERS - LEFT WING
EVEN NUMBERS - RIGHT WING

TABLE IV

FIG.	FLIGHT CONDITION	CONFIG.	δf	LANDING GEAR	C_L	it/δe	GRD EFFECT	C.G.	L/D AT C_L	SOURCE	L/D
1	T. O. & INITIAL CLIMB	REF	20°	DN	.44	-8.7°/0°	IN	.575$\bar{c}$	6.70	REF. 2 FIG IV-1A-1	6.75
		100	20°	DN	.44	-2°/-3°	IN	.5375$\bar{c}$	7.52	REF. 6	8.09
2	CLIMBOUT	REF	5°	UP	.44	11.3°/0°	OUT	.575$\bar{c}$	7.80	REF. 2 FIG VI-1A-1	10.87
		100	5°	UP	.44	1°/1°	OUT	.5375$\bar{c}$	8.63	REF. 6	13.53
3	APPROACH	REF	20°	DN	.55	4.5°/0°	OUT	.597$\bar{c}$	5.75	REF. 2 FIG VI-1A-9	6.75
		100	20°	DN	.55	0°/0°	OUT	.560$\bar{c}$	5.91	REF. 6	8.00

TABLE V

Componet Wetted Areas and
Configuration Skin Friction Coefficient

$S_{W_{ref}} = 926.15\ m^2\ (9969\ ft^2)$

COMPONENT	WETTED AREA, $m^2(ft^2)$	
WING	1719.87	(18512.52)
FUSELAGE	785.03	(8449.99)
NACELLES (4)	307.36	(3308.41)
WING FINS (2)	92.16	(991.95)
VERTICAL TAIL	31.69	(341.12)
HORIZONTAL TAIL	84.09	(905.13)
VENTRAL FIN	40.51	(436.00)
TOTAL	3060.71	(32945.12)

MACH NUMBER	ALTITUDE, m(ft)		C_{D_F} (TOTAL)
0.6	2134	(7000)	.005592
1.2	10455	(34300)	.005247
2.62	18288	(60000)	.004137

TABLE VI
Configuration Drag Polars
$S_{W_{ref}}$ = 926.15 m^2 (9969 ft^2)

C_L	C_D					
MACH NO.	.6	.8	.95	1.05	1.2	1.4
ALTITUDE, m (ft)	2,134 (7,000)	6,248 (20,500)	8,992 (29,500)	9,601 (31,500)	10,455 (34,300)	11,491 (37,700)
0.	.011337	.012019	.015074	.018740	.019133	.016657
.02	.010283	.010832	.013456	.016783	.017231	.014980
.04	.009535	.009967	.012206	.015252	.015788	.013772
.06	.009095	.009424	.011326	.014149	.014802	.013033
.08	.008963	.009203	.010815	.013473	.014275	.012763
.10	.009138	.009305	.010672	.013223	.014205	.012962
.12	.009620	.009729	.010899	.013401	.014583	.013630
.14	.010410	.010476	.011495	.014006	.015438	.014767
.16	.011508	.011544	.012460	.015038	.016742	.016373
.18	.012912	.012935	.013794	.016497	.018503	.018448
.20	.014625	.014648	.015496	.018383	.020723	.020991
.22	.016645	.016684	.017568	.020696	.023400	.024004
.24	.018972	.019042	.020009	.023436	.026535	.027486
.26	.021607	.021722	.022819	.026603	.030128	.031436
.28	.024549	.024724	.025998	.030197	.034179	
.30	.027799	.028049	.029546	.034218	.038687	
.32	.031356	.031696	.033463	.038667		

TABLE VI Concluded

C_L	C_D				
MACH NO.	1.6	1.8	2.2	2.4	2.62
ALTITUDE, m (ft)	12,588 (41,300)	13,594 (44,600)	15,728 (51,600)	16,764 (55,000)	18,288 (60,000)
0	.014160	.012656	.010687	.009830	.009694
.02	.012718	.011424	.009731	.008891	.008689
.04	.011754	.010677	.009298	.008521	.008324
.06	.011266	.010417	.009388	.008718	.008597
.08	.011255	.010641	.010001	.009484	.009509
.10	.011722	.011352	.011136	.010817	.011061
.12	.012665	.012549	.012795	.012719	.013251
.14	.014085	.014231	.014976	.015189	.016080
.16	.015983	.016400	.017681	.018226	.019548
.18	.018357	.019054	.020908	.021832	.023655
.20	.021208	.022194	.024658	.026006	.028401
.22	.024537	.025820	.028932	.030748	.033786
.24	.028342	.029932	.033728	.036058	.039810

TABLE VII

STABILITY MODE	DUTCH-ROLL			ROLL	SPIRAL
Symbols	ζ_{min}	$(\zeta\omega_n)_{min}$ RAD/SEC	$\omega_{n_{min}}$ RAD/SEC	$\tau_{R_{max}}$ SEC	$T_{2_{min}}$ SEC
Requirement	.08	.15	.4	1.4	20
Inherent Characteristics MLW	-.1937	-.1476	.762	1.65	-15.58*
Inherent Characteristics NLW	-.1943	-.1391	.716	1.74	-15.58*

*Negative sign signifies the time taken to half the amplitude of oscillation (spiral stability).

TABLE VIII

WEIGHT SUMMARY

	KILOGRAMS	POUNDS
STRUCTURE	87576	193073
PROPULSION	27016	59561
SYSTEMS	27064	59665
WEIGHT EMPTY	141656	312299
OPERATING ITEMS	7791	17177
OPERATING WEIGHT	149448	329476
PAYLOAD	27682	61028
ZERO FUEL WEIGHT	177130	390504
MISSION FUEL	148550	327496
TAKE-OFF GROSS WEIGHT	325679	718000

TABLE IX

GROUP WEIGHT SUMMARY

ITEM	KILOGRAMS	POUNDS
WING	38970	85913
HORIZONTAL TAIL	2160	4763
VERTICAL TAIL	2673	5892
CANARD	0	0
FUSELAGE	23773	52410
LANDING GEAR	12380	27293
NACELLE	7622	16803
STRUCTURE TOTAL	(87577)	(193073)
ENGINES	23587	52000
THRUST REVERSERS	0	0
MISCELLANEOUS SYSTEMS	807	1780
FUEL SYSTEM-TANKS AND PLUMBING	2622	5781
-INSULATION	0	0
PROPULSION TOTAL	(27016)	(59561)
SURFACE CONTROLS	4266	9405
AUXILIARY POWER	0	0
INSTRUMENTS	1542	3400
HYDRAULICS	2540	5600
ELECTRICAL	2291	5050
AVIONICS	1220	2690
FURNISHINGS AND EQUIPMENT	11390	25110
AIR CONDITIONING	3719	8200
ANTI-ICING	95	210
SYSTEMS AND EQUIPMENT TOTAL	(27064)	(59665)
MFG AND CERTIF TOLERANCE	0	0
WEIGHT EMPTY	141657	312299
CREW AND BAGGAGE - FLIGHT, 3	306	675
- CABIN, 10	744	1640
UNUSABLE FUEL	1059	2335
ENGINE OIL	324	715
PASSENGER SERVICE	4015	8852
CARGO CONTAINERS, 7	1343	2960
OPERATING WEIGHT	149448	329476
PASSENGERS, 292	21854	48180
PASSENGER BAGGAGE	5828	12848
CARGO	0	0
ZERO FUEL WEIGHT	177130	390504
MISSION FUEL	148549	327496
TAKEOFF GROSS WEIGHT	325679	718000

TABLE X

Mass Data Summary

ITEM	CONDITION		
DESCRIPTION	TAKEOFF GROSS WEIGHT	MAXIMUM DESIGN LANDING WEIGHT	NORMAL LANDING WEIGHT
MASS, kg	325679	251404	205931
lbm	718000	554250	454000
HORIZONTAL c.g. m	54.605	53.680	54.559
LOCATION, in.	2149.8	2113.4	2148.0
percent of M.A.C.	55.97	52.90	55.90
ROLL INERTIA, I_x, kg-m^2	23.282×10^6	20.082×10^6	19.366×10^6
slug-ft^2	17.17×10^6	14.81×10^6	14.28×10^6
PITCH INERTIA, I_y, kg-m^2	81.841×10^6	80.385×10^6	78.947×10^6
slug-ft^2	60.36×10^6	59.29×10^6	58.23×10^6
YAW INERTIA, I_z, kg-m^2	103.418×10^6	98.912×10^6	96.762×10^6
slug-ft^2	76.28×10^6	72.95×10^6	71.37×10^6
PRODUCT OF INERTIA, I_{xz}, kg-m^2	-2.015×10^6	-2.023×10^6	-2.028×10^6
slug-ft^2	-1.49×10^6	-1.49×10^6	-1.50×10^6
PRINCIPAL AXIS ANGLE OF INCLINATION, θ deg	-1.44	-2.05	-1.50

TABLE XI (a)

CONDITIONS FOR SONIC BOOM CALCULATIONS
FOR
AST-100

Mach No.	Weight lbm	Altitude, ft	Flight Path Angle, deg	Acceleration Along Flight Path, ft/sec^2	Angle-of-Attack, deg
1.15	683,500	33,200	1.86	2.75	.617
1.175	683,000	33,700	1.79	2.70	.541
1.2	682,500	34,200	1.70	2.67	.510
1.3	680,000	36,000	1.45	2.60	.353
1.4	678,000	37,800	1.30	2.55	.235
1.6	673,000	41,300	1.15	2.55	.003
1.8	668,000	45,000	1.00	2.35	-.103
2.0	663,000	48,400	.80	2.10	-.167
2.2	657,000	51,700	.70	1.90	-.180
2.4	652,000	55,000	.55	1.80	-.123
2.62	646,000	58,400	0.	1.80	-.028
2.62*	644,000	62,000	0.	0.	.448
2.62**	458,433	69,000	0.	0.	.430

Atmosphere - Standard + 8°C Day

*Start of Cruise

**End of Cruise

TABLE XI (b)

CONDITIONS FOR SONIC BOOM CALCULATIONS

FOR

REFERENCE CONFIGURATION

Mach No.	Weight, lbm	Altitude, ft	Flight Path Angle, deg	Acceleration Along Flight Path, ft/sec^2	Angle-of-Attack, deg
1.175	726,500	34,200	2.31	3.48	.769
1.2	726,000	34,700	2.25	3.48	.743
1.3	724,000	36,500	1.95	3.38	.583
1.4	722,000	38,100	1.80	3.38	.441
1.6	717,000	41,300	1.70	3.38	.150
1.8	713,000	45,000	1.45	3.28	.038
2.0	709,000	48,300	1.30	3.09	-.036
2.2	705,000	51,600	1.05	2.83	-.045
2.4	700,000	55,000	.90	2.54	.022
2.7	693,000	60,000	.70	2.0	.222
2.7*	692,000	61,500	0.	0.	.432
2.7**	487,586	68,800	0.	0.	.428

Atmosphere - Standard

*Start of Cruise

**End of Cruise

TABLE XII

MISSION PERFORMANCE

MISSION: Design Supersonic Cruise Mach 2.62

MODEL NO: AST-100

AIRCRAFT CHARACTERISTICS

Takeoff gross weight - kg (lbm)	325679	(718000)	
Operating weight empty - kg (lbm)	149448	(329476)	
Payload-No. Passengers -	292		
Cargo -	0		
Total Weight - kg (lbm)	27682	(61028)	
Wing area - reference - m^2 (ft^2)	926	(9969)	
- actual - m^2 (ft^2)	1022	(10996)	
S.L. static Installed thrust per engine (std. day +8°C), N (lbf)	293485	(65978)	
Initial installed thrust to weight ratio	.37		
Initial wing loading - reference, kg/m^2 (lbm/ft^2)	353	(72.0)	
- actual, kg/m^2 (lbm/ft^2)	319	(65.3)	

Design Mission

	OPERATING WEIGHTS, kg (lbm)	Δ FUEL kg (lbm)	Δ RANGE km (n. m.)	Δ TIME minute
Takeoff	325679 (718000)			
		4354 (9600)	0	11
Start Climb	321325 (708400)			
		28925 (63769)	624 (337)	22
Start Cruise	292400 (644631)			
		84405 (186081)	6354 (3431)	134
End Cruise	207995 (458550)			
		1610 (3550)	370 (200)	20
End Descent	206385 (455000)			
		1169 (2578)	0	5
Taxi-in				
Block Fuel and Time		120463 (265578)		192
Trip Range			7349 (3968)	

NOTES: 1. Taxi-in fuel taken out of reserves at destination

2. C.A.B. range corresponding to block time and fuel equals trip range minus traffic allowances as will be specified for supersonic aircraft.

TABLE XII Concluded

Model No.: AST-100

Reserve Fuel Breakdown, kg (lbm):

1. 7% Trip Fuel	8351	(18410)
2. Missed Approach	4037	(8900)
3. 482 km (260 n. m.) to alternate airport	10482	(23108)
4. 30 min. holding at 457 m. (15,000 ft.)	6383	(14073)
Total Reserve	29253	(64491)

Initial Cruise Conditions:

Lift Coefficient	.0980	
Drag Coefficient	.0110	
Lift/Drag	8.91	
TSFC, kg/hr/N (lbm/hr/lbf)	0.138	(1.355)
Altitude, m(ft)	18898	(62000)

TABLE XIII

BASELINE DATA FOR AST-100 DIRECT OPERATING COST ANALYSIS

Gross takeoff weight, kg (lbm)	325,679 (718,000)
Range, km (n.mi.)	7,349 (3968)
Cruise speed, Mach number	2.62
Number of engines	4
Thrust per engine, N(lbf)	293,485 (65,978)
Seats (passengers)	292
Load factor, %	100
Fuel cost, cents/liter (cents/gal)	7.93 (30)
Insurance rate, % of purchase price	1.0
Year dollars	Jan. 1, 1975
Depreciation period, years	14
Residual value, %	0
Utilization rate, hrs/yr	3600
Crew	3
Purchase price:	
Aircraft (complete), millions of dollars	55.44
Airframe, millions of dollars	46.74
Engines, millions of dollars	8.70
Crew pay relative to subsonic flight, %	117

TABLE XIV

AST-100 DIRECT OPERATING COST (DOC)

Cost Element	Dollars/km	Dollars/n.mi.	Percent of Total
Crew	.207	.384	7.8
Fuel and oil	1.651	3.058	61.4
Hull insurance	.068	.125	2.5
Maintenance	.231	.427	8.6
Airframe			
Labor	(.025)	(.047)	
Materials	(.045)	(.084)	
Engine			
Labor	(.017)	(.032)	
Materials	(.098)	(.182)	
Burden	(.044)	(.081)	
Depreciation	.529	.980	19.7
Total DOC per aircraft	2.686	4.974	100

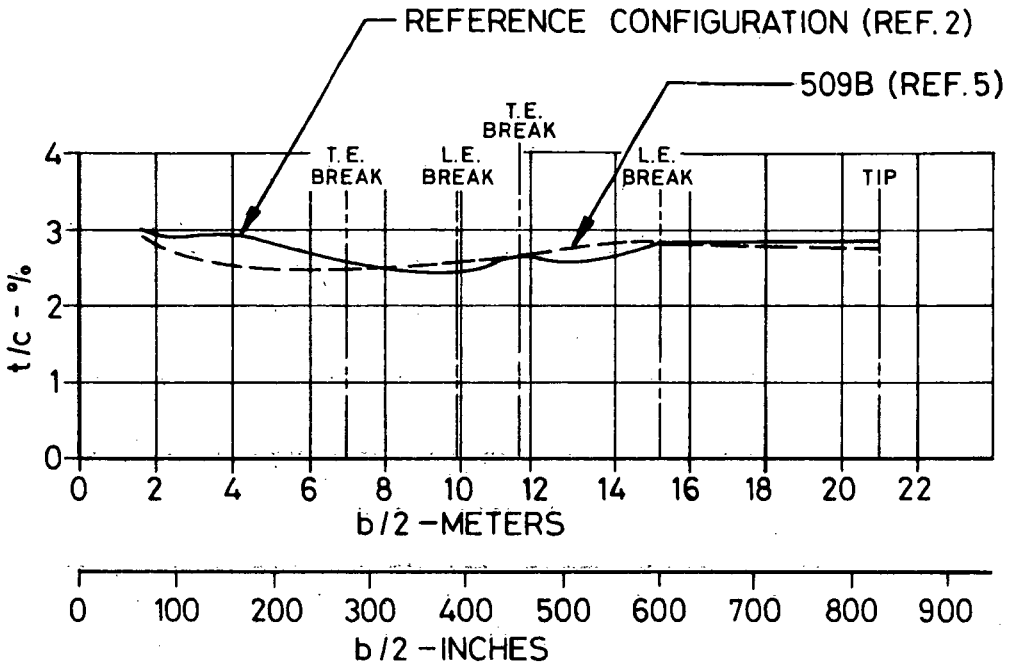

Figure 1 Wing Spanwise Thickness Distribution

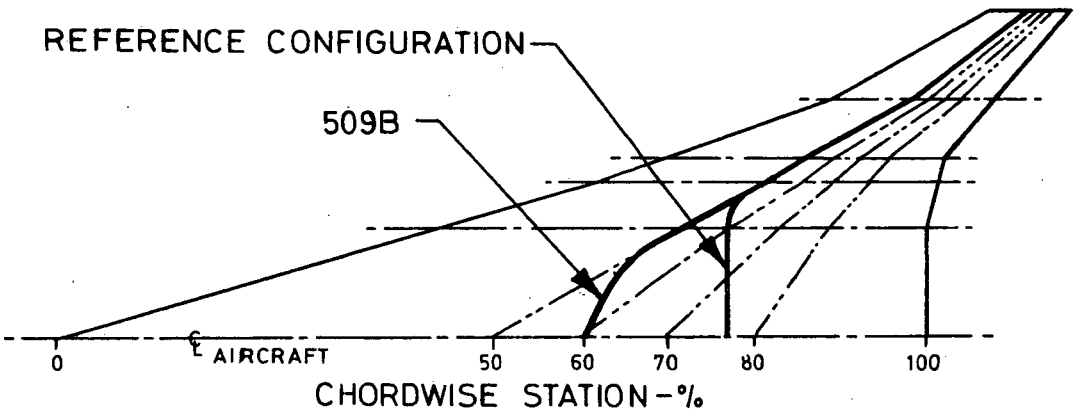

Figure 2 Maximum Thickness Location

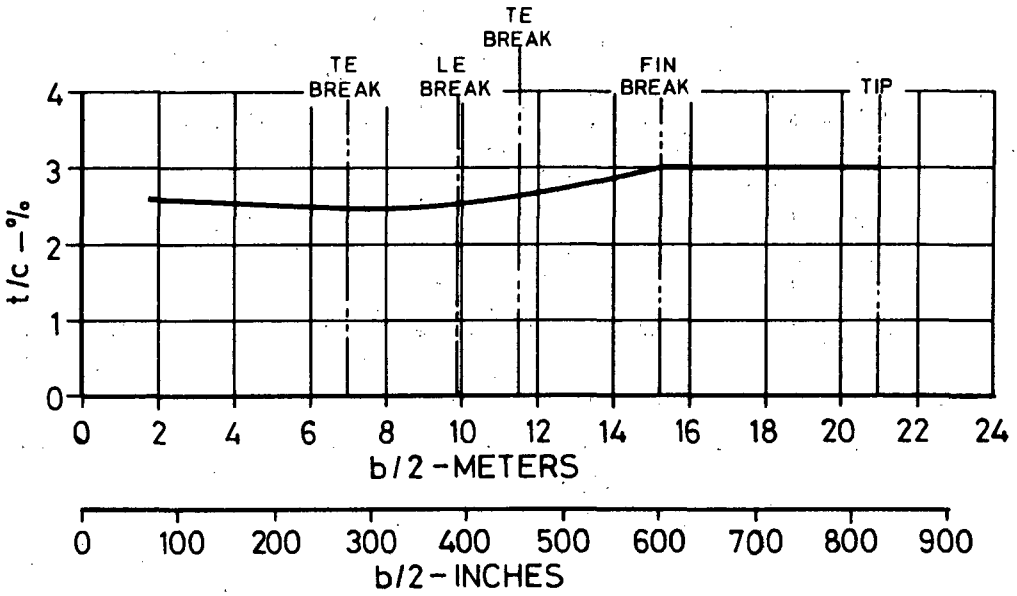

Figure 3 AST-100 (Initial) Spanwise Thickness Distribution

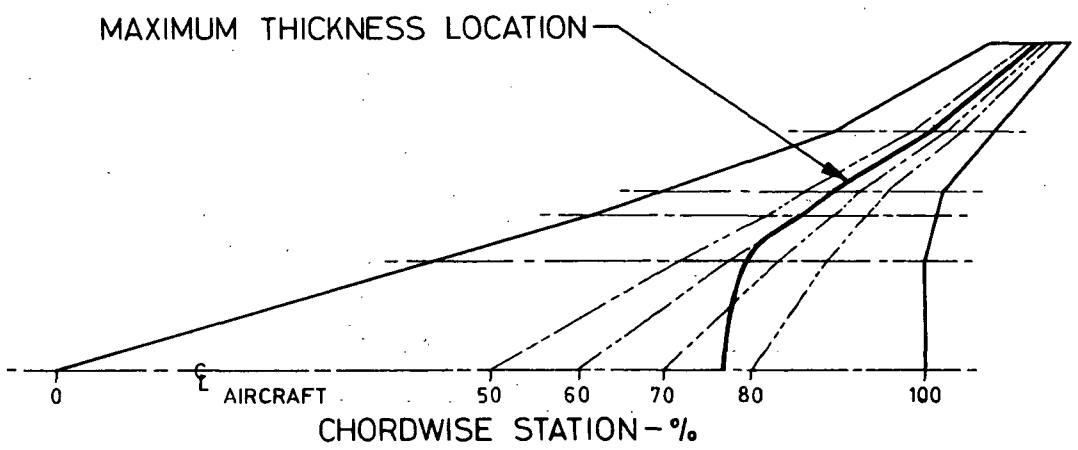

Figure 4 AST-100 (Initial) Wing Maximum Thickness Location

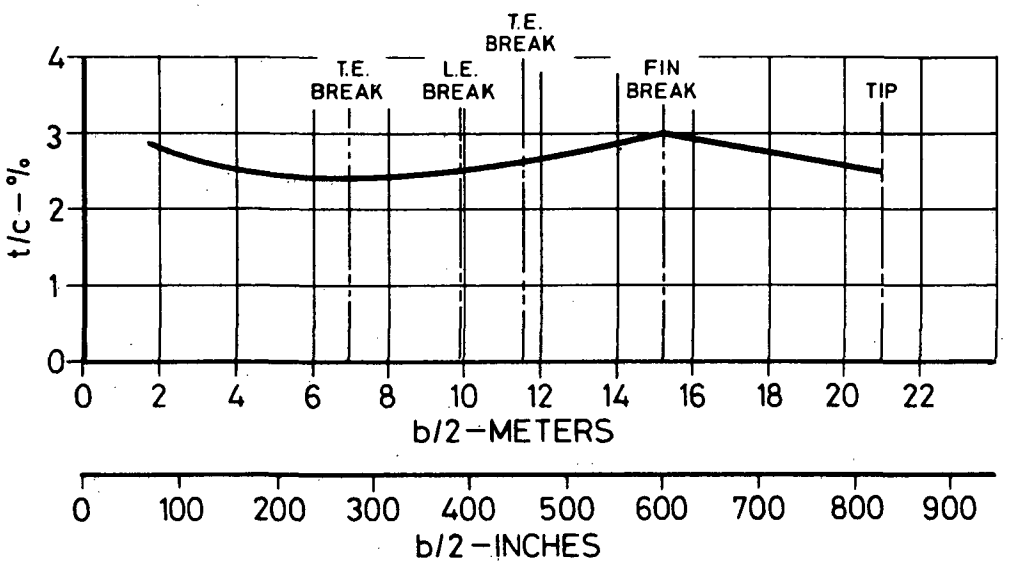

Figure 5 AST-100 (Final) Wing Spanwise Thickness Distribution

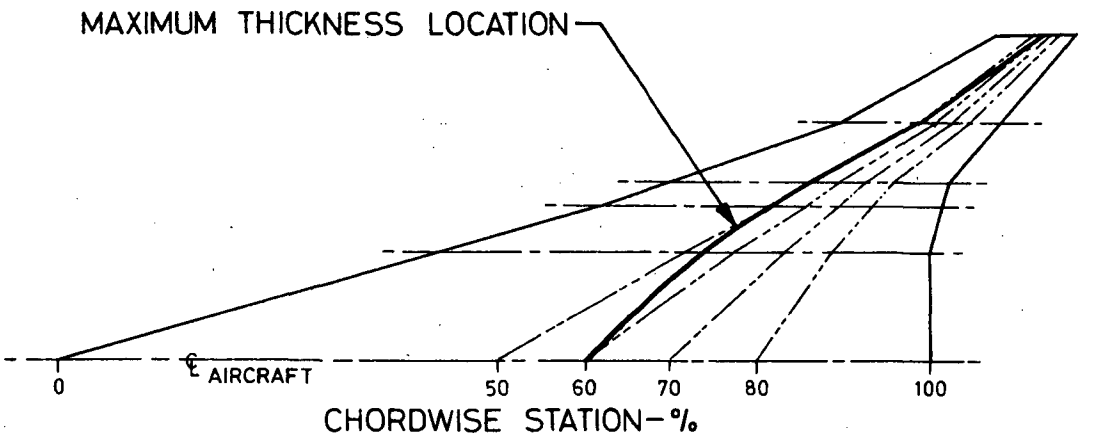

Figure 6 AST-100 (Final) Wing Maximum Thickness Location

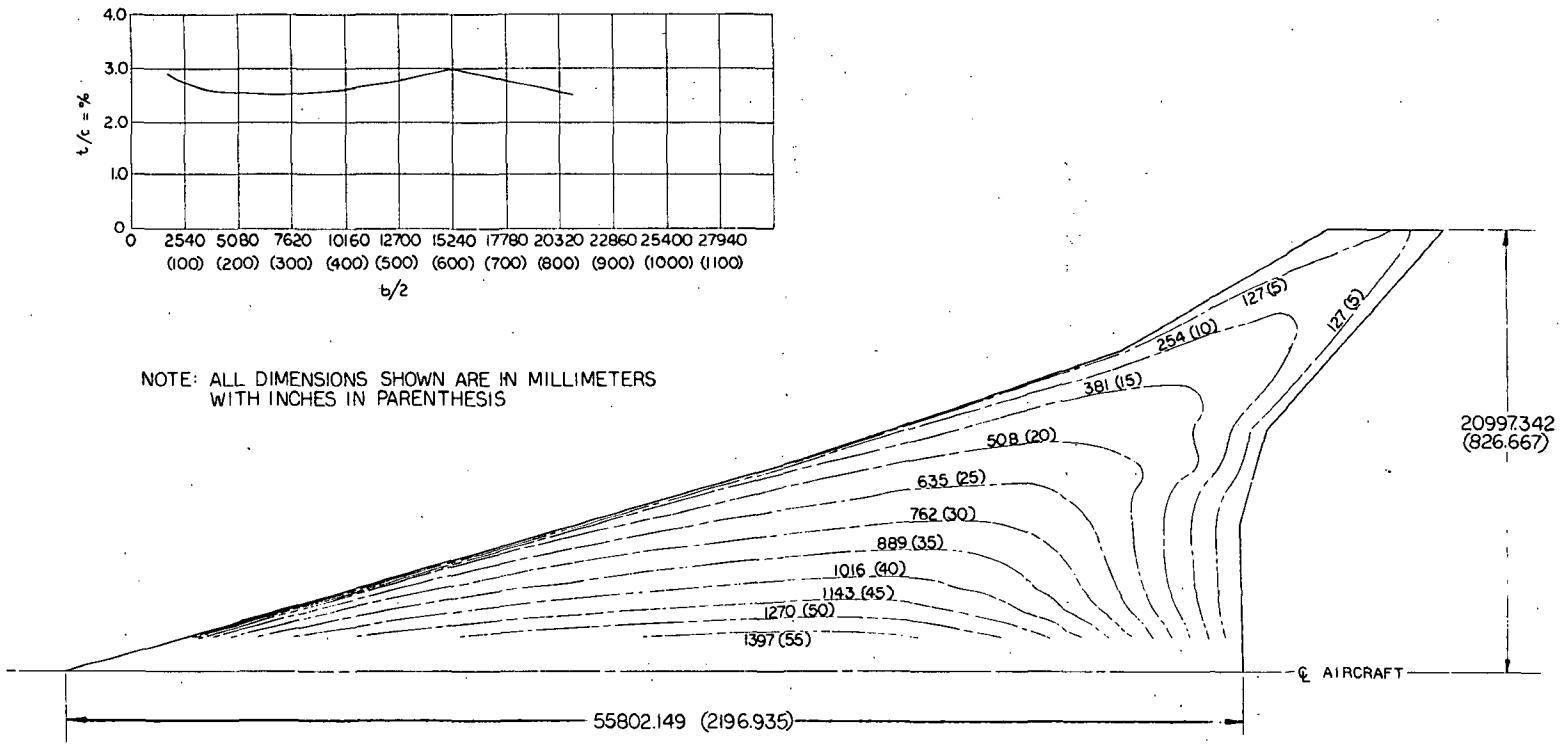

Figure 7 AST-100 Wing Thickness Map

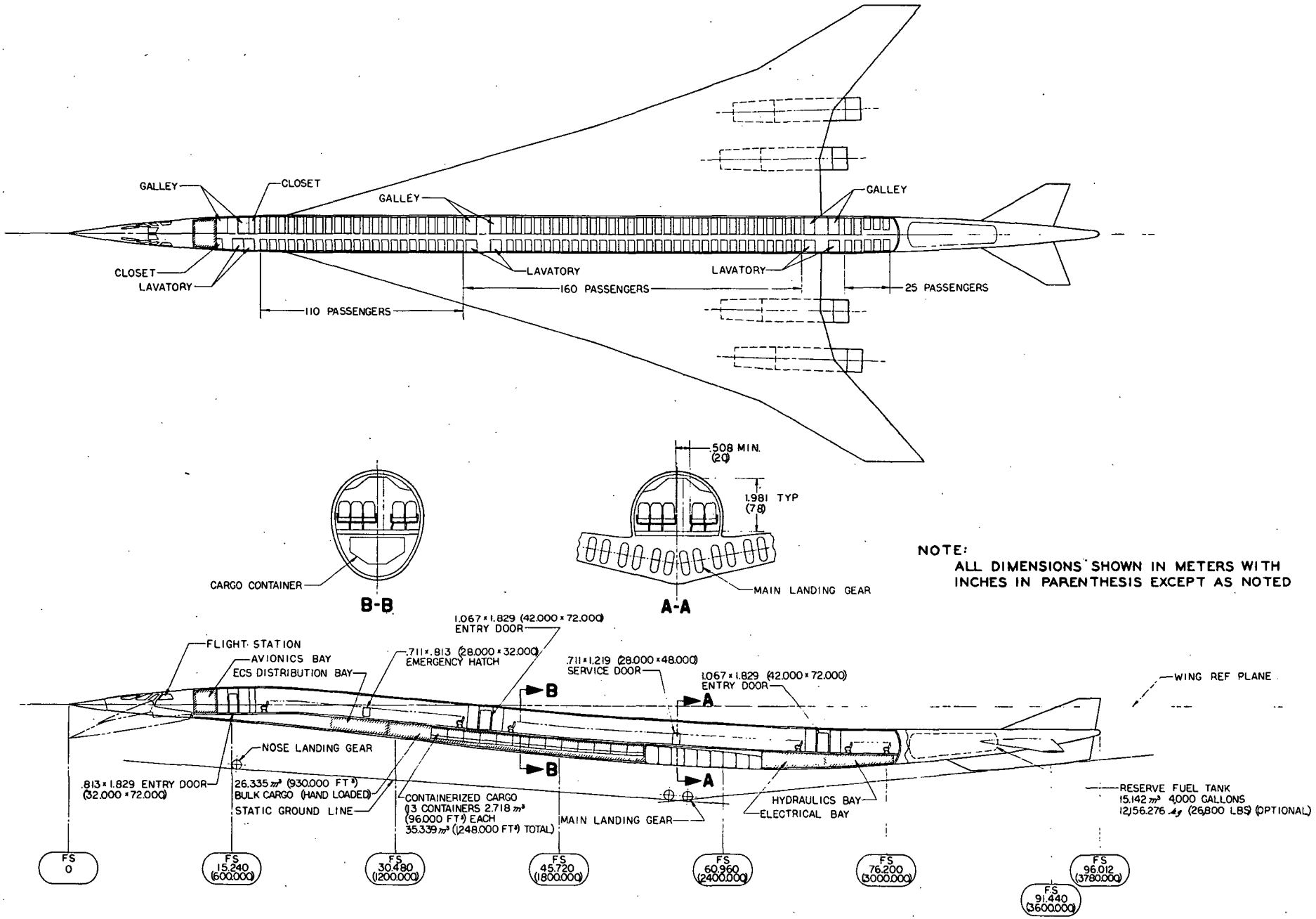

Figure 8 Inboard Profile

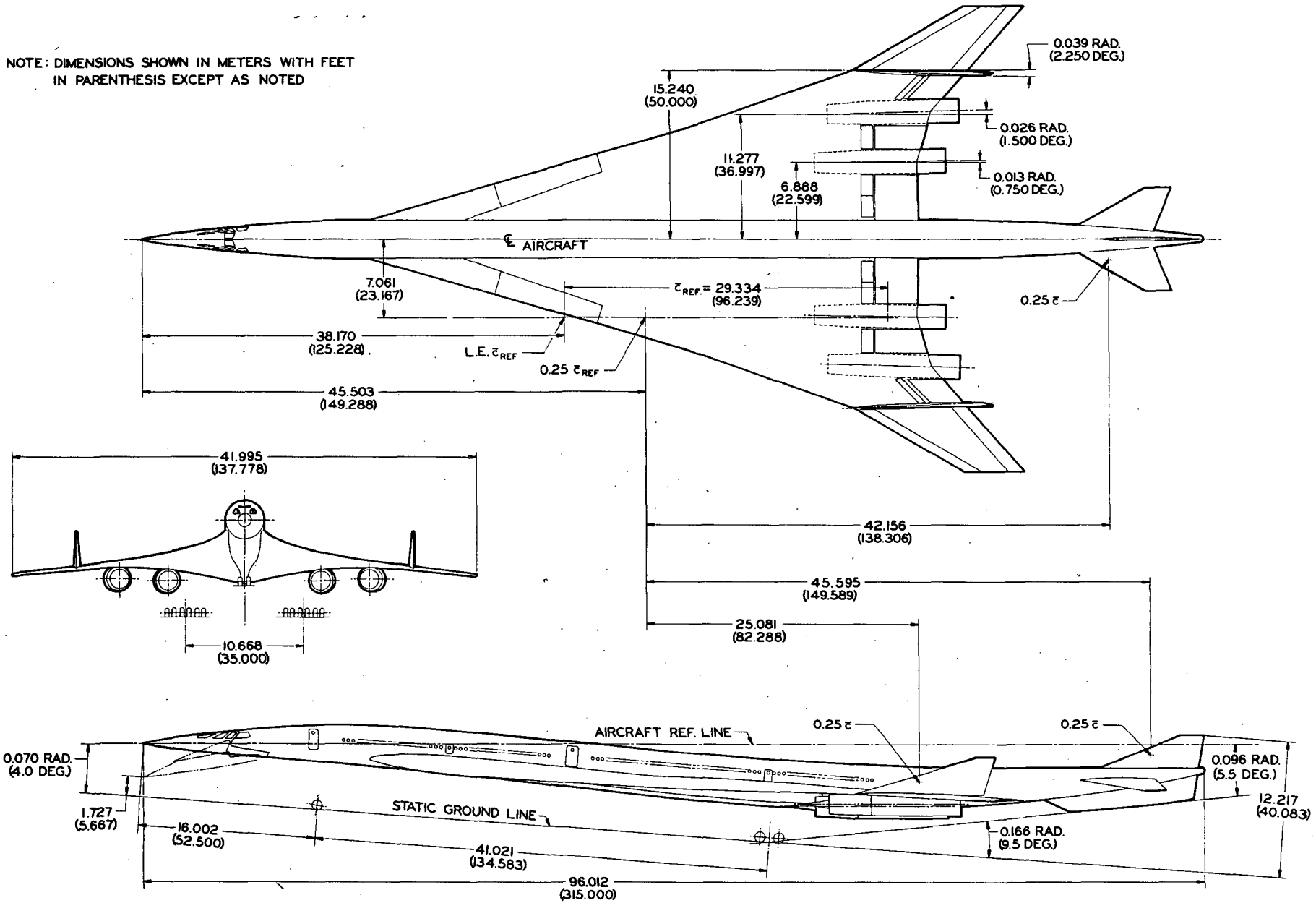

Figure 9 General Arrangement

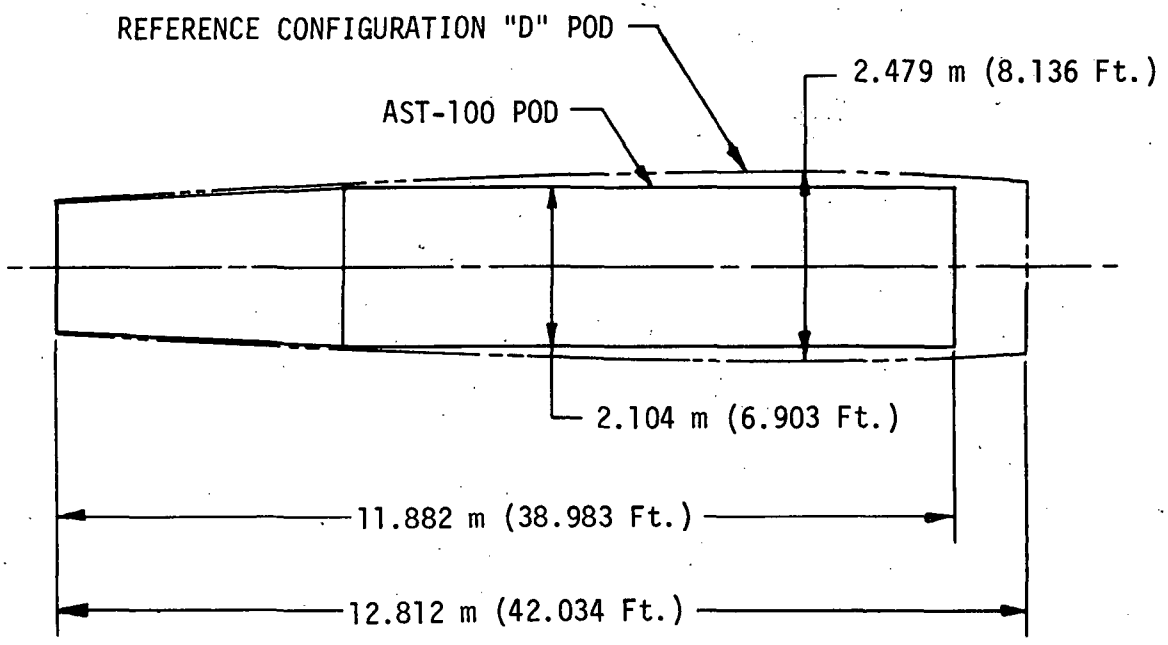

Figure 10 Nacelle Pod Comparison

NOTE: ALL DIMENSIONS SHOWN ARE IN
METERS WITH FEET IN PARENTHESIS

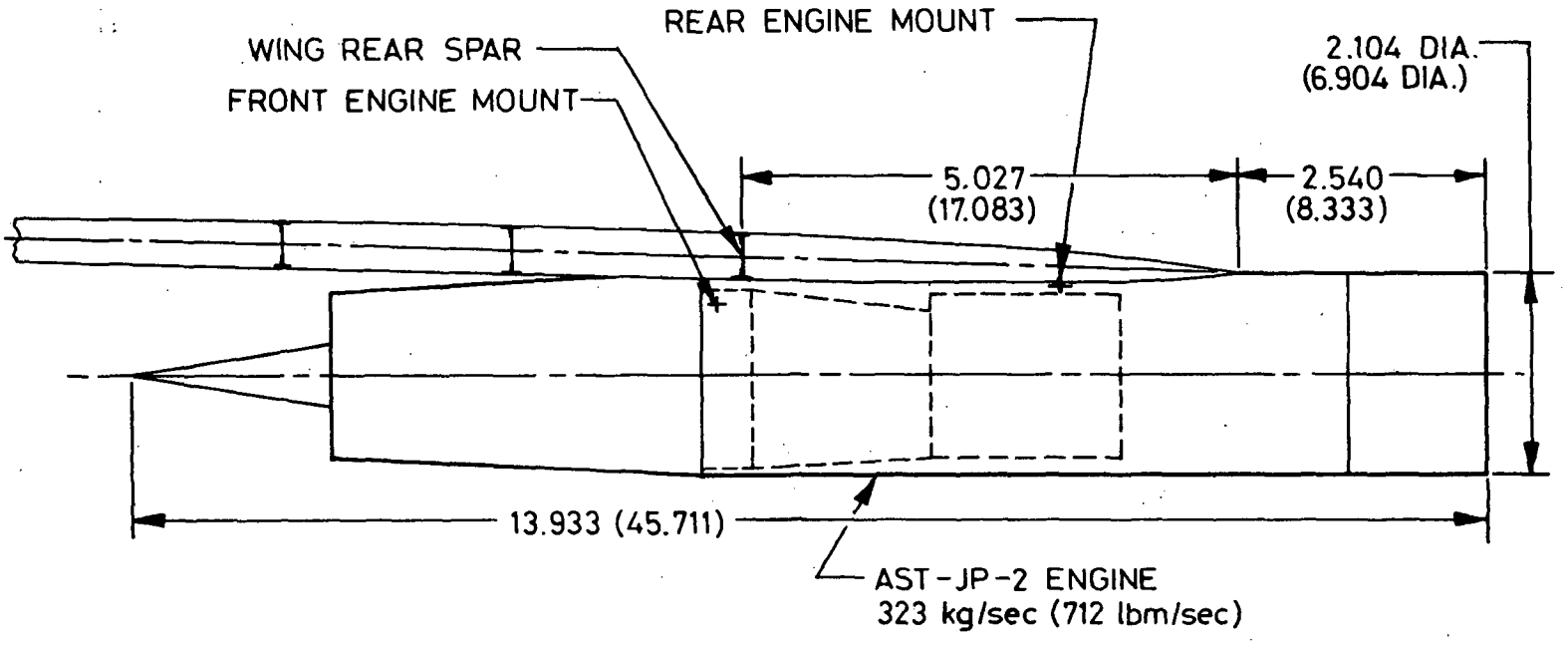

Figure 11 Typical Engine Installation

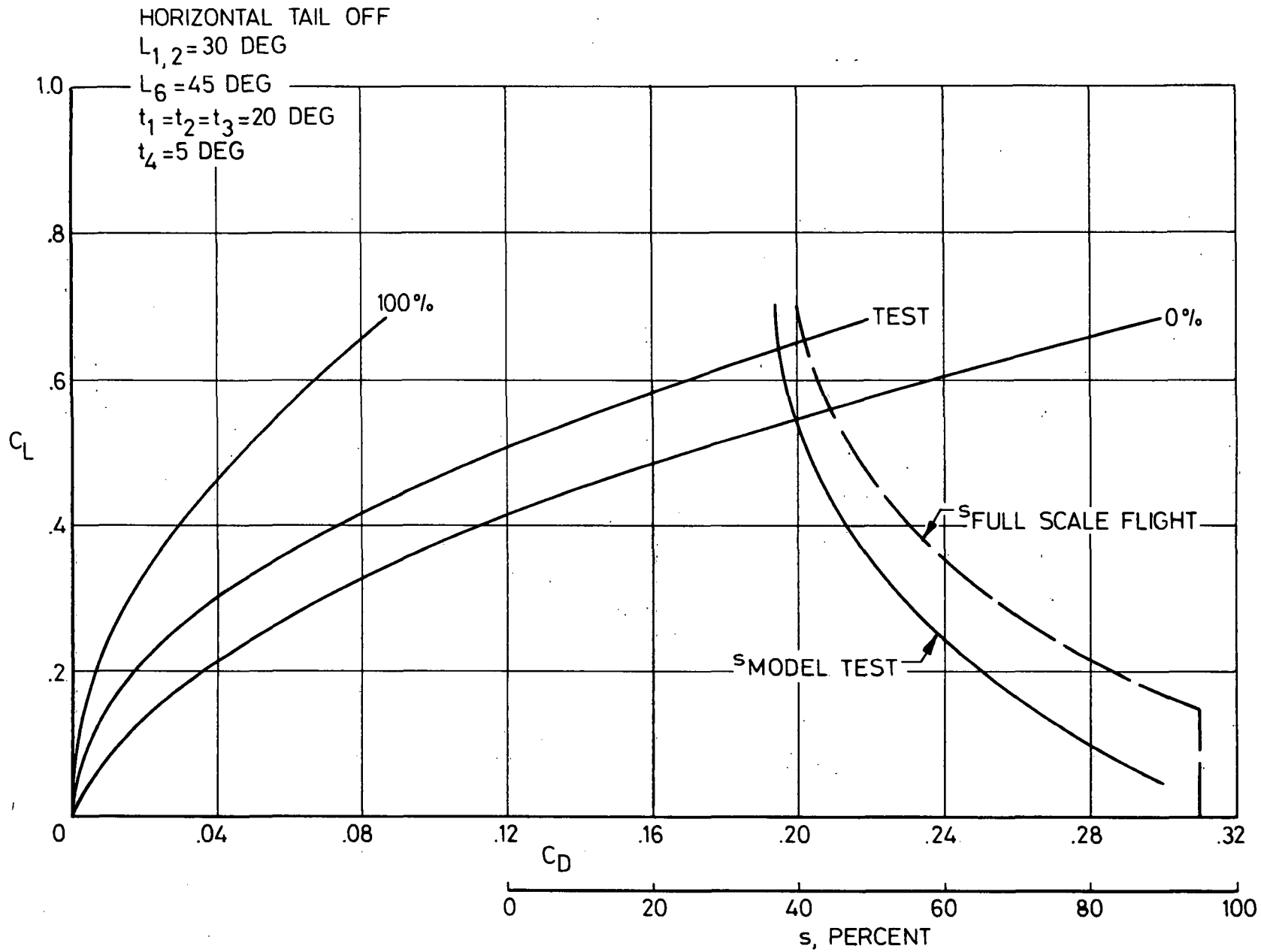

Figure 12(a) Drag Polars For Test (Ref. 6), 100 Percent and 0 Percent Suction Levels and Leading Edge Suction Percentage for Test and Full Scale.

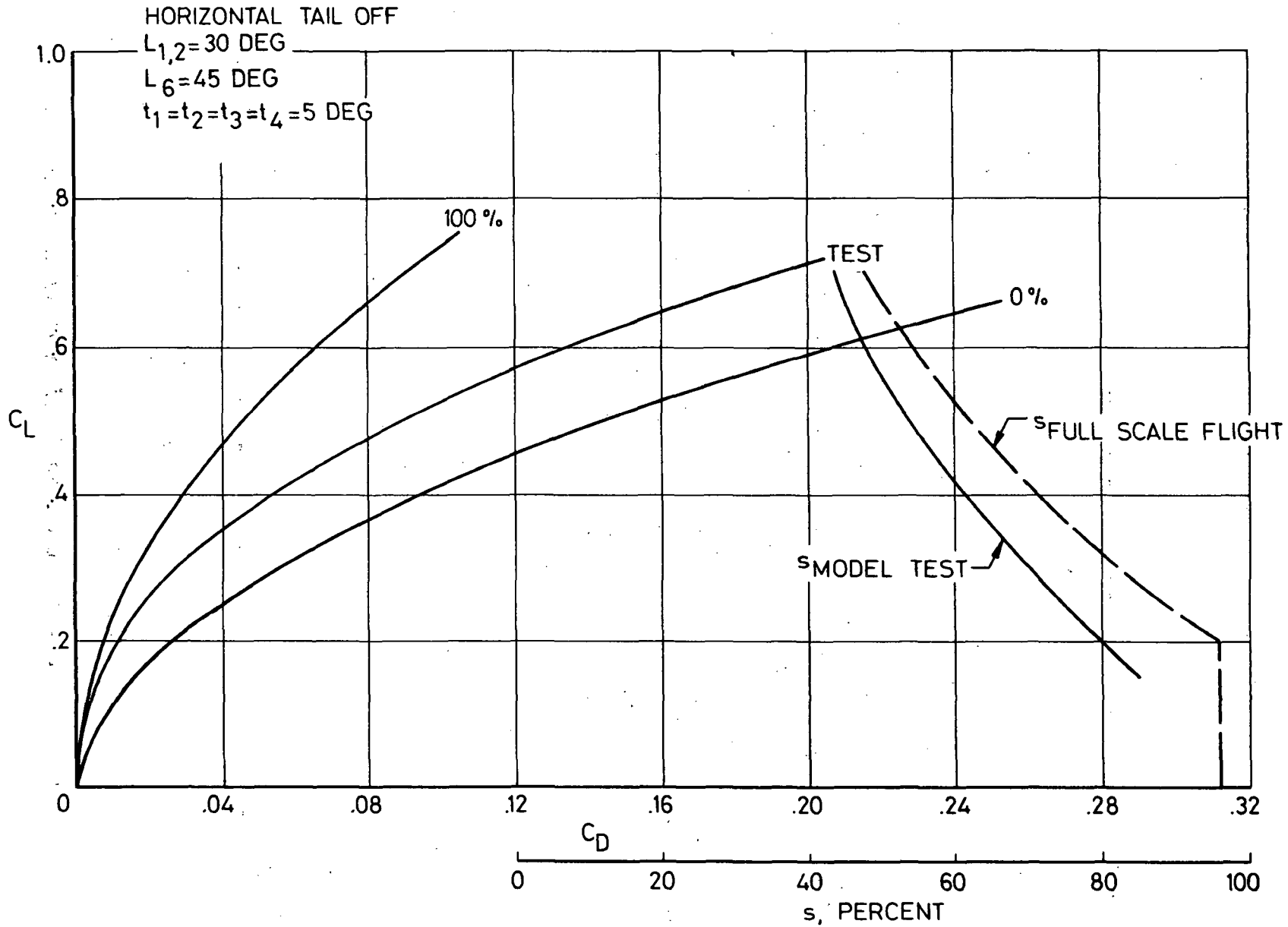

Figure 12(b) Drag Polars for Test (Ref. 6), 100 Percent and 0 Percent Suction Levels and Leading Edge Suction Percentage for Test and Full Scale.

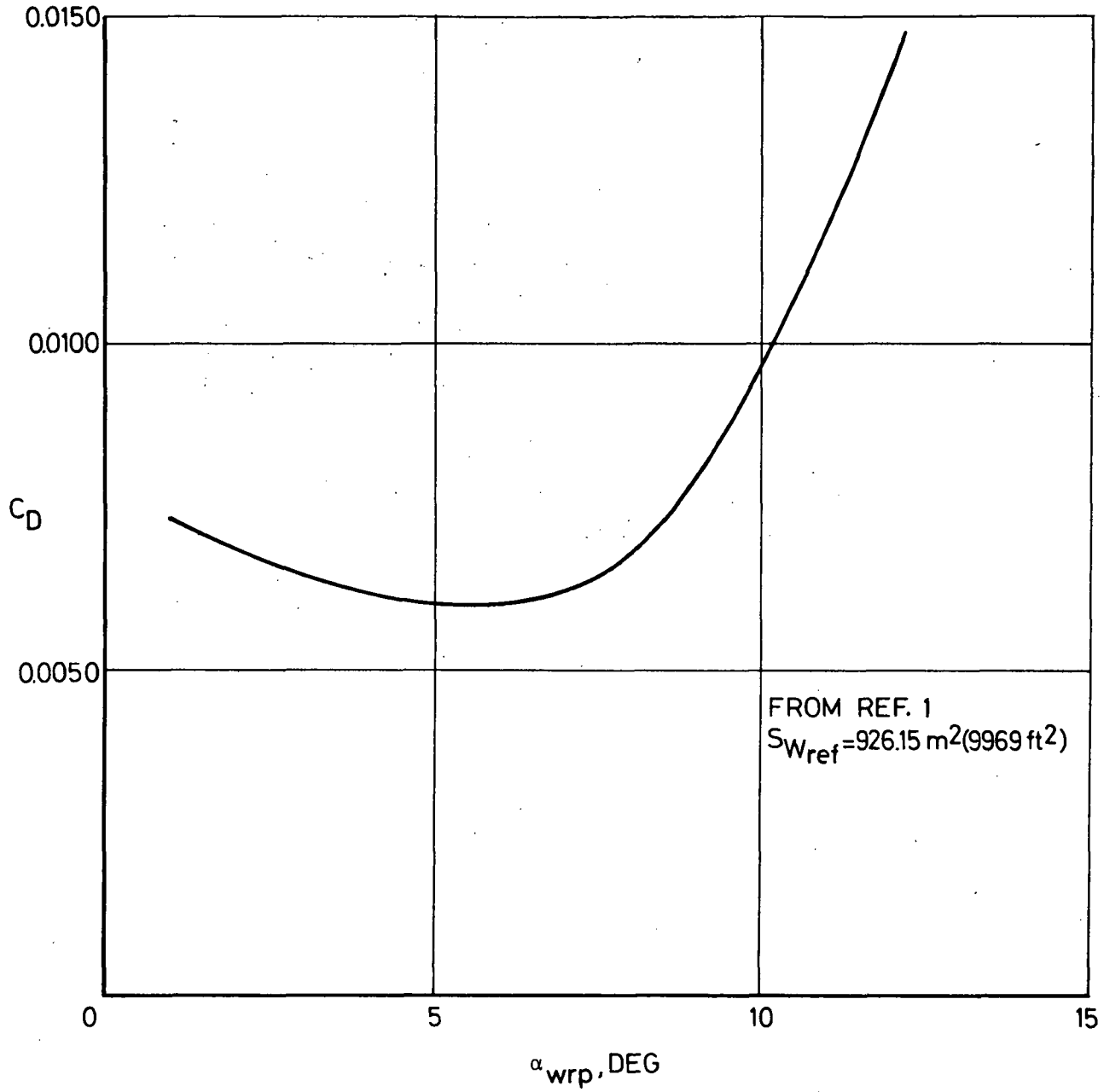

Figure 13 Landing Gear Drag Coefficient Variation with Angle-of-Attack.

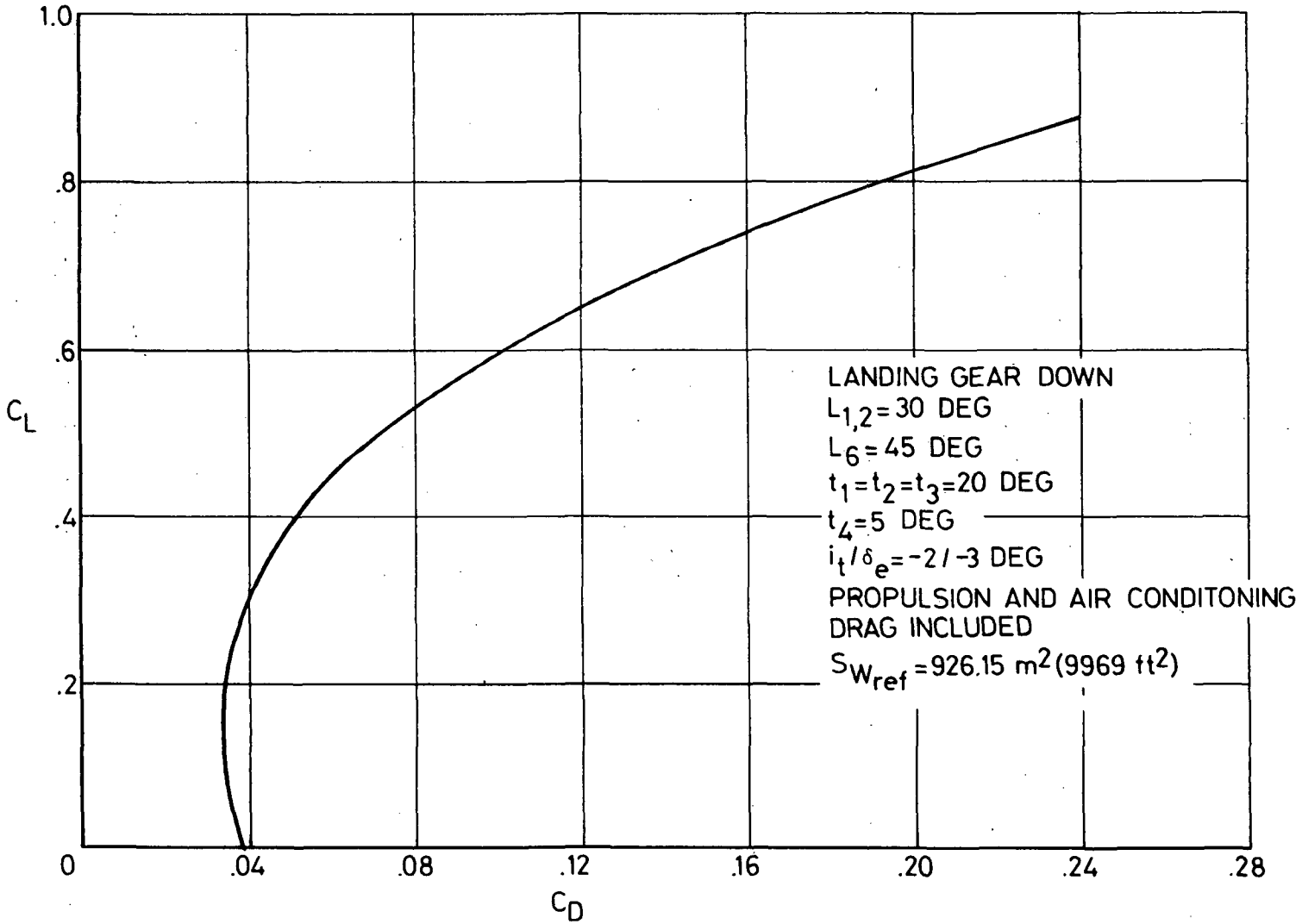

Figure 14 Takeoff and Initial Climb Polar (Aircraft Trimmed in Ground Effect)

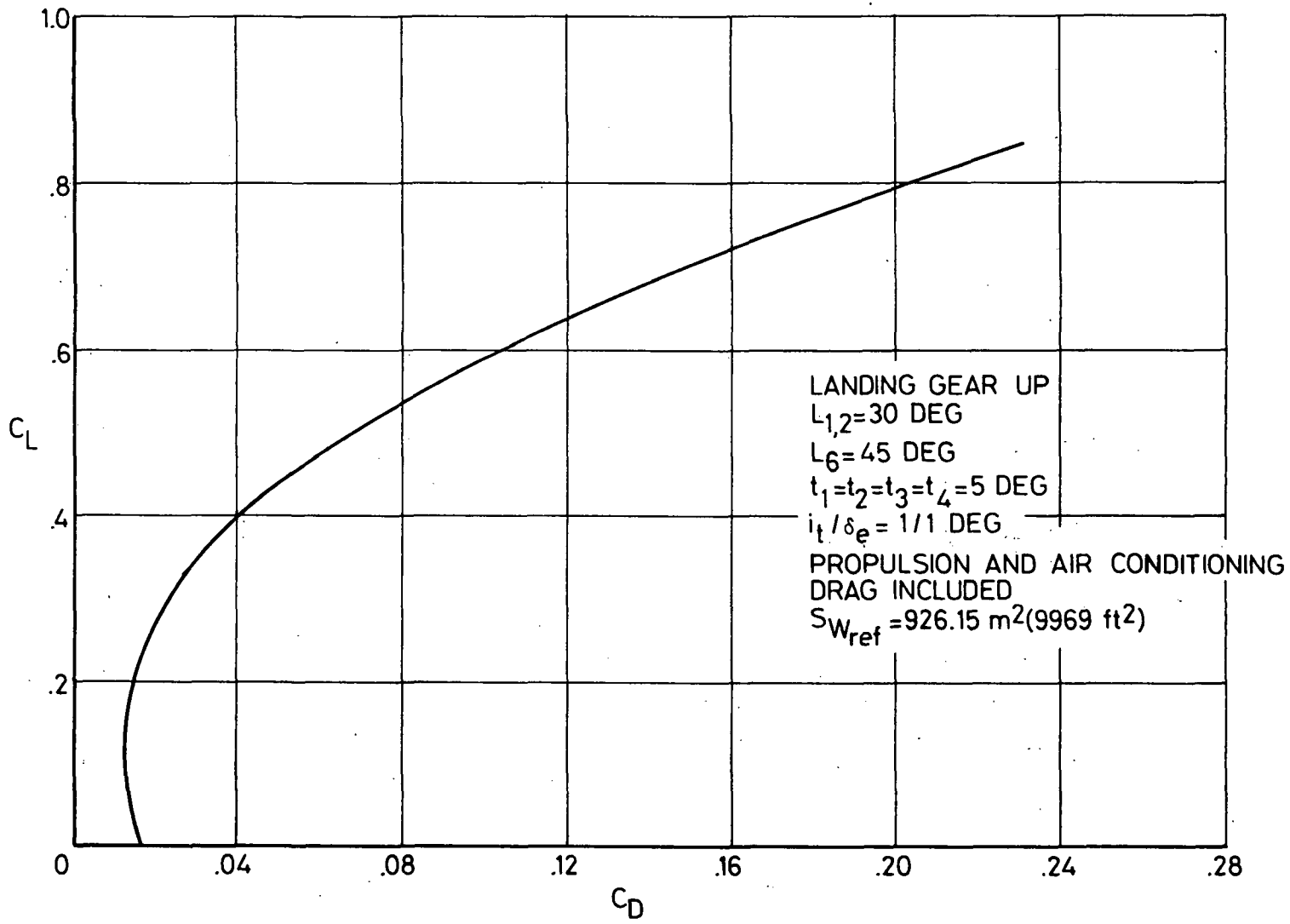

Figure 15 Climb Configuration Polar (Aircraft Trimmed)

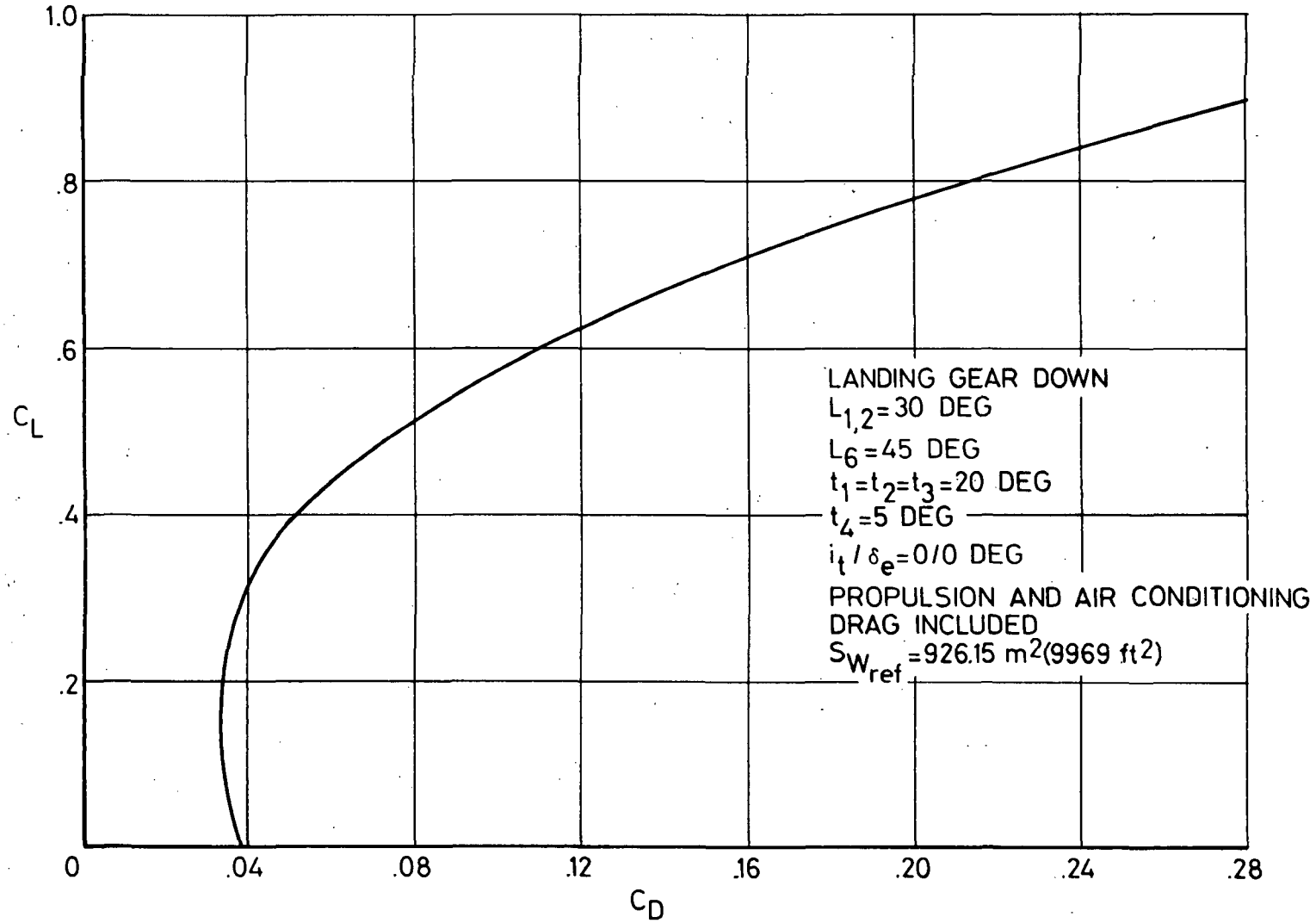

Figure 16 Approach Polar (Aircraft Trimmed)

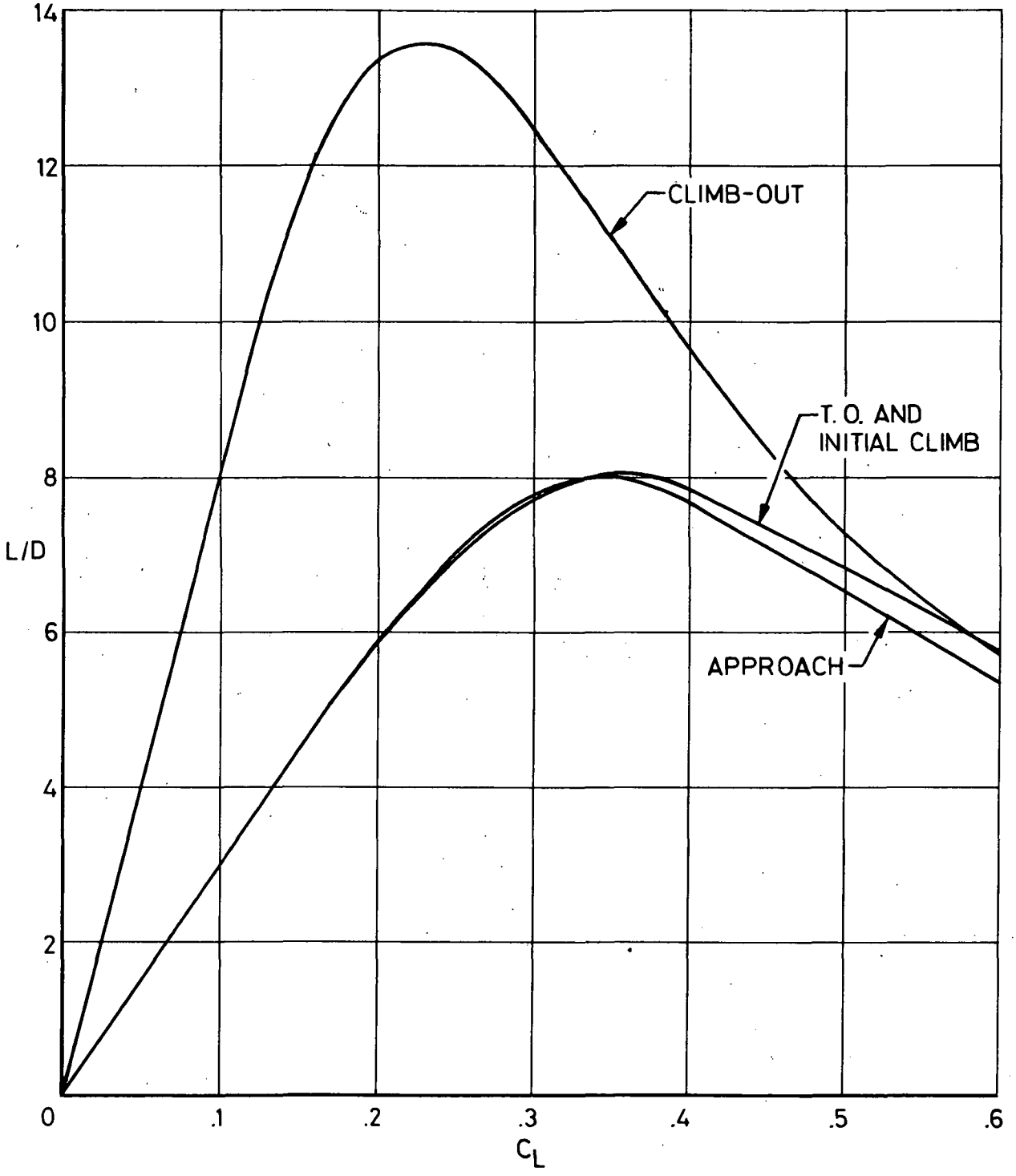

Figure 17 Lift to Drag Ratio Variation with Lift Coefficient (Aircraft Trimmed).

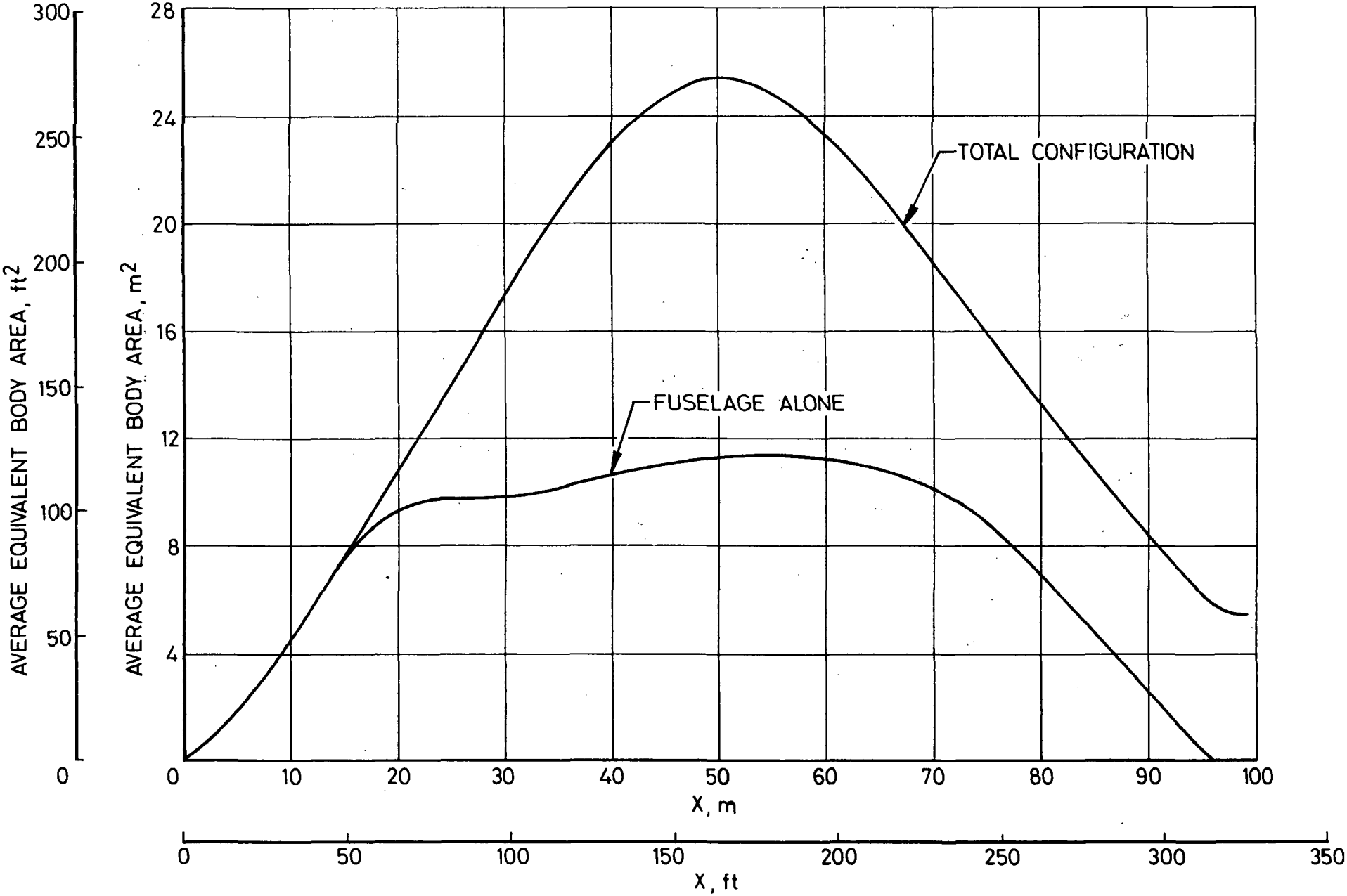

Figure 18 Equavalent Area Distribution at M = 2.62

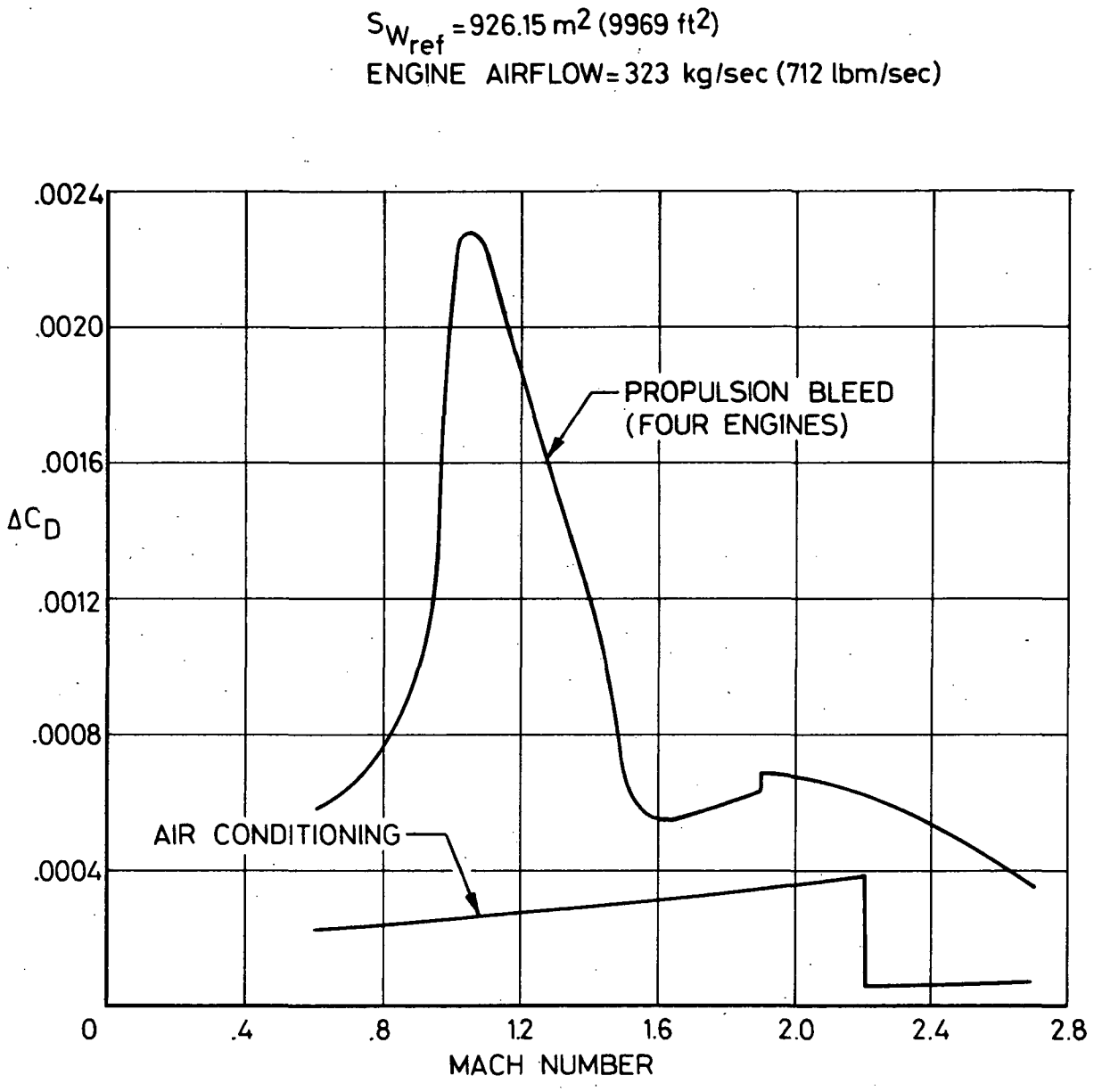

Figure 19 Propulsion Bleed and Airconditioning Drag Increments

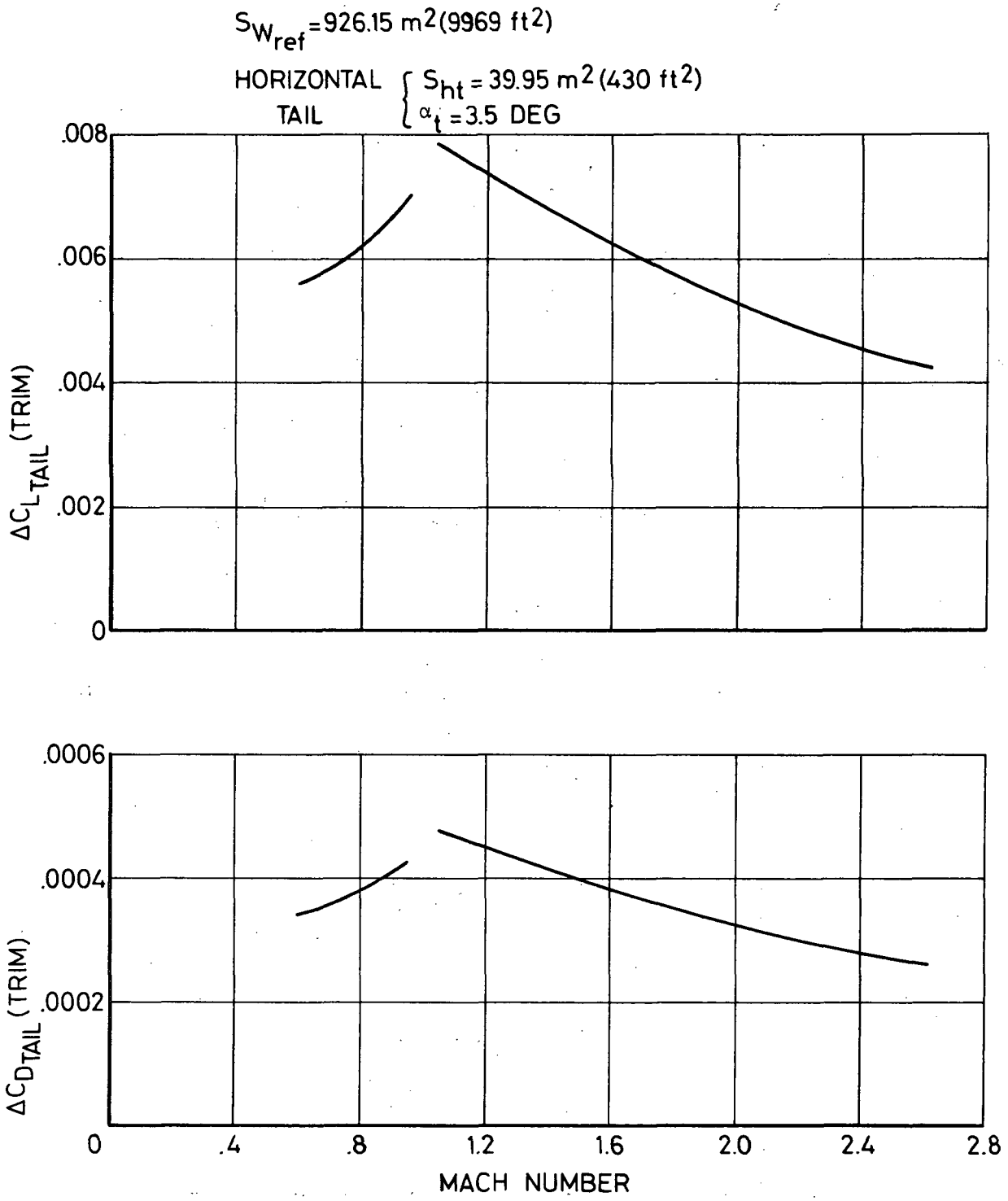

Figure 20 Lift and Drag Increments Due to Lifting Horizontal Tail

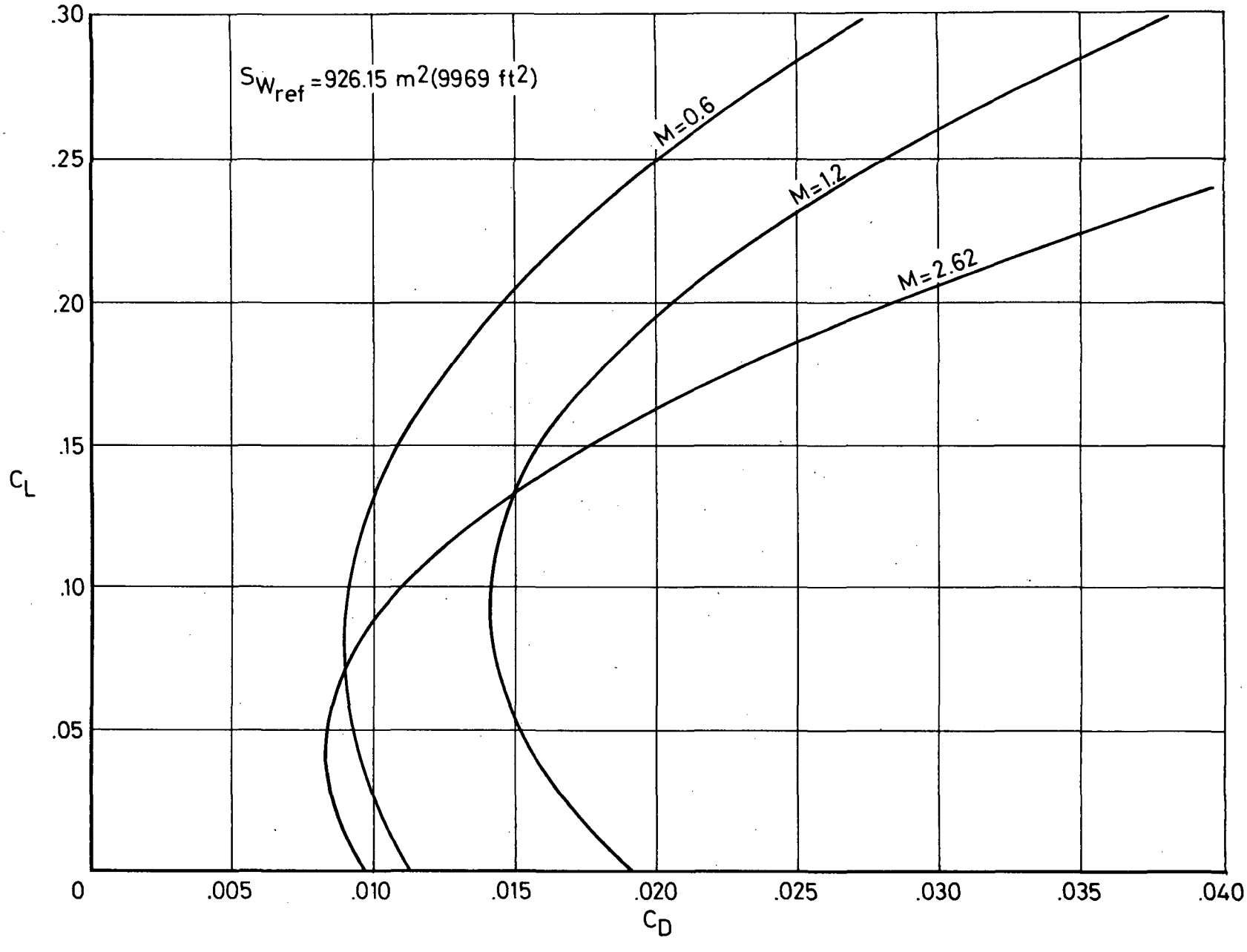

Figure 21 Typical Drag Polars

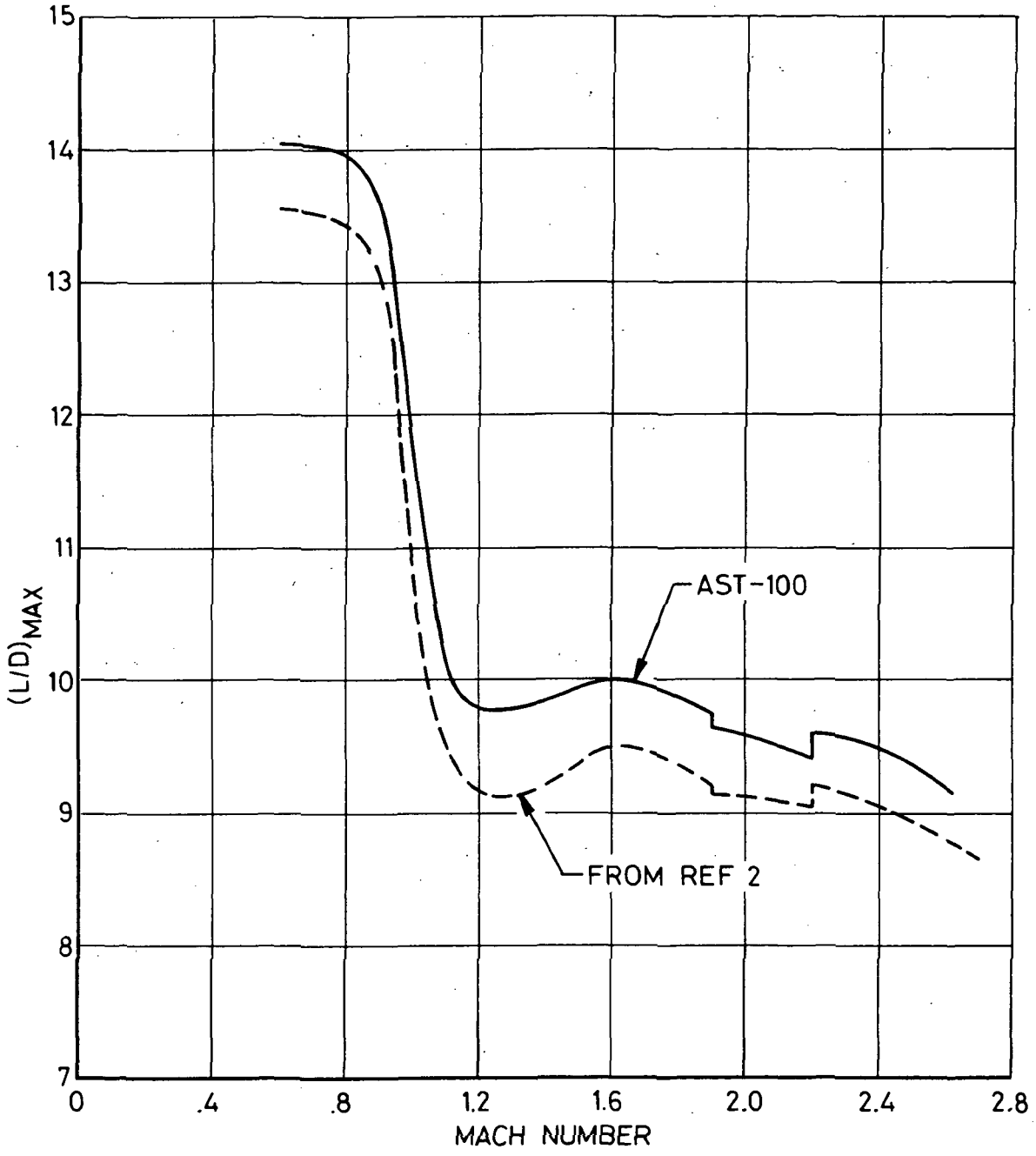

Figure 22 Maximum Lift-to-Drag Ratio Variation with Mach Number

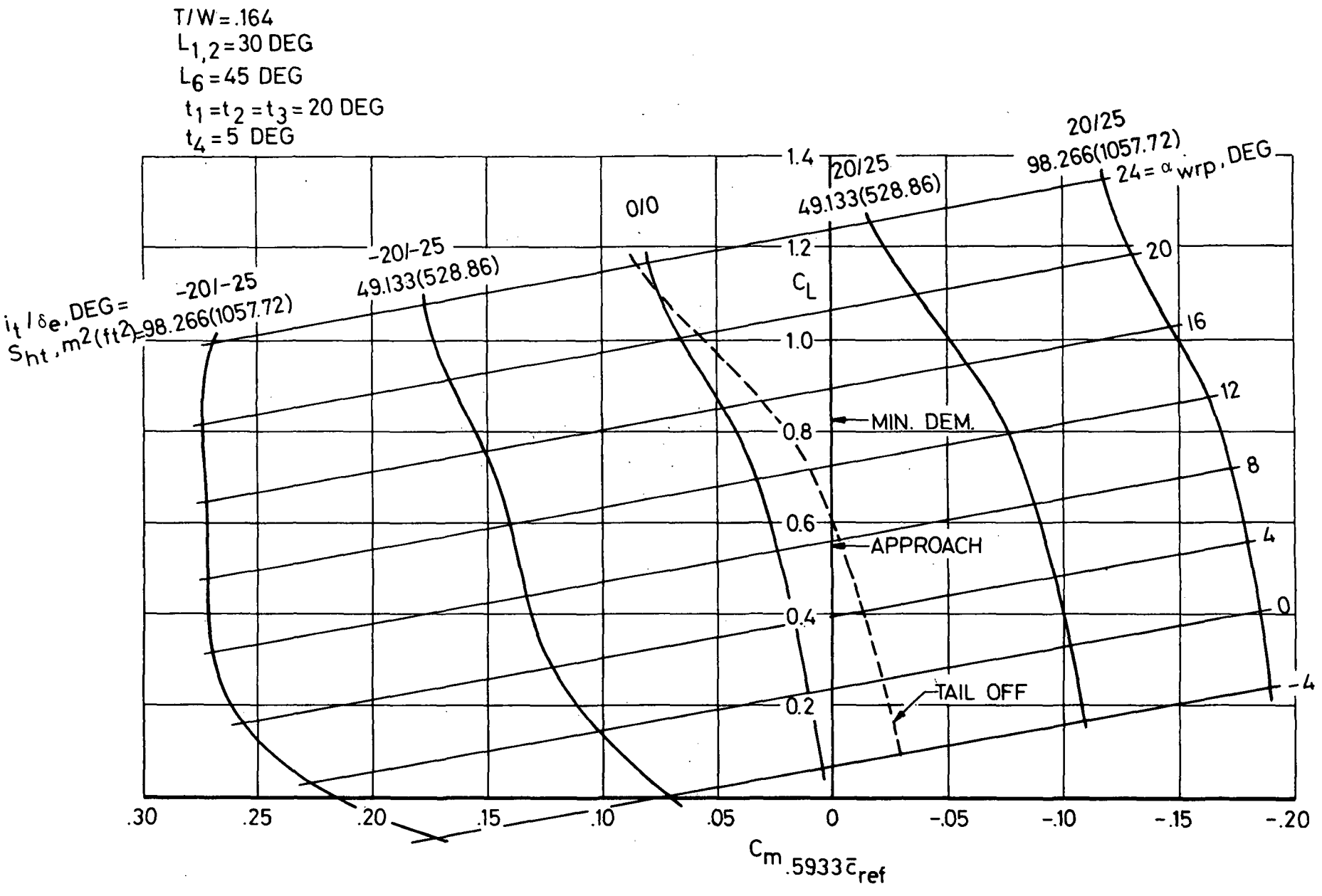

Figure 23 Effect of Horizontal Tail Size and Maximum Control Deflection on Stability and Trim, Out of Ground Effect.

$S_{ht} = 49.133\ m^2 (528.86\ ft^2)$

$l_t / \bar{c}_{ref} = 1.0934$

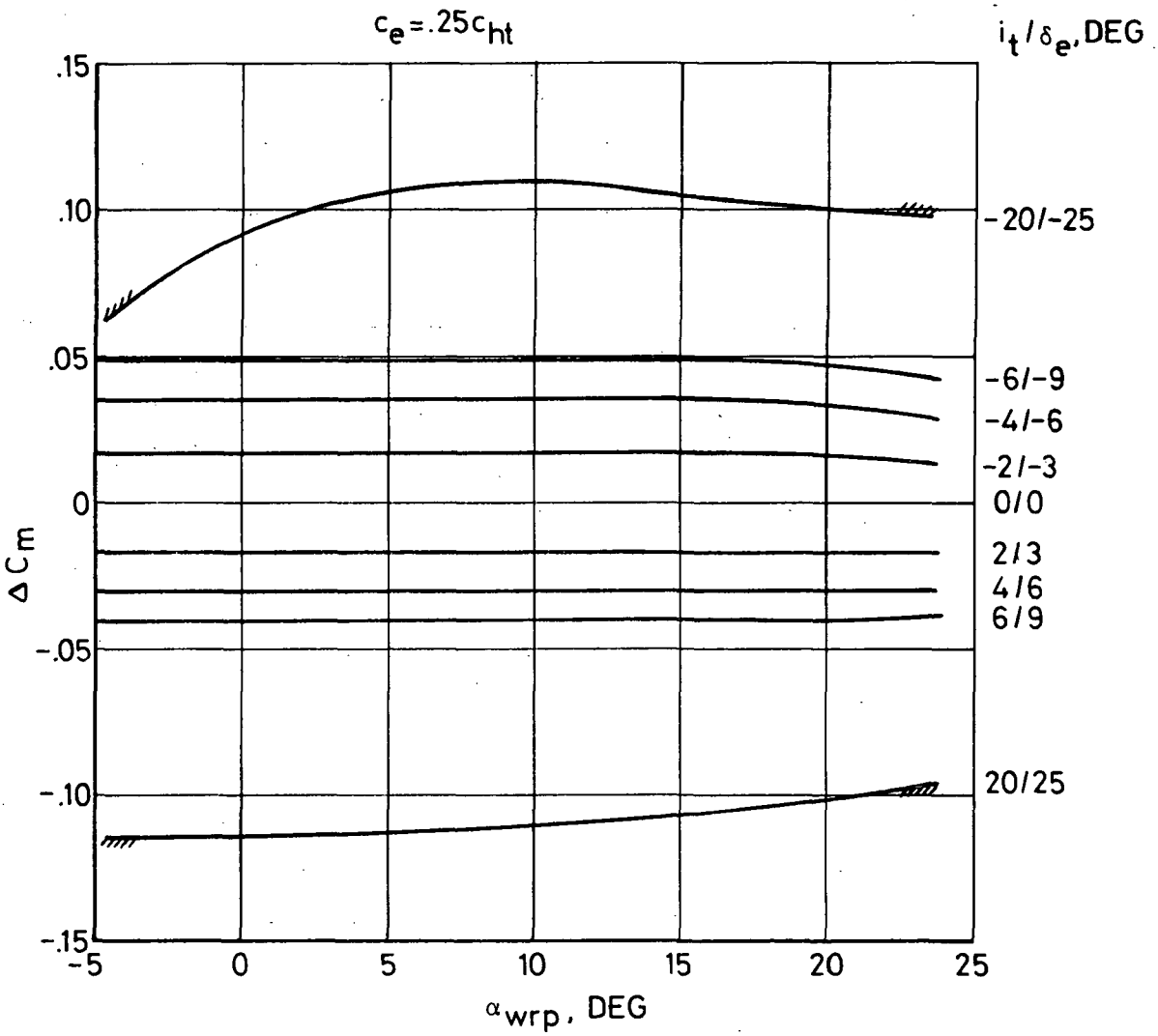

Figure 24 Horizontal Tail Moment Control Capability

$S_{wref} = 926.150\ m^2\ (9969\ ft^2)$
$S_{ht} = 39.948\ m^2\ (430\ ft^2)$

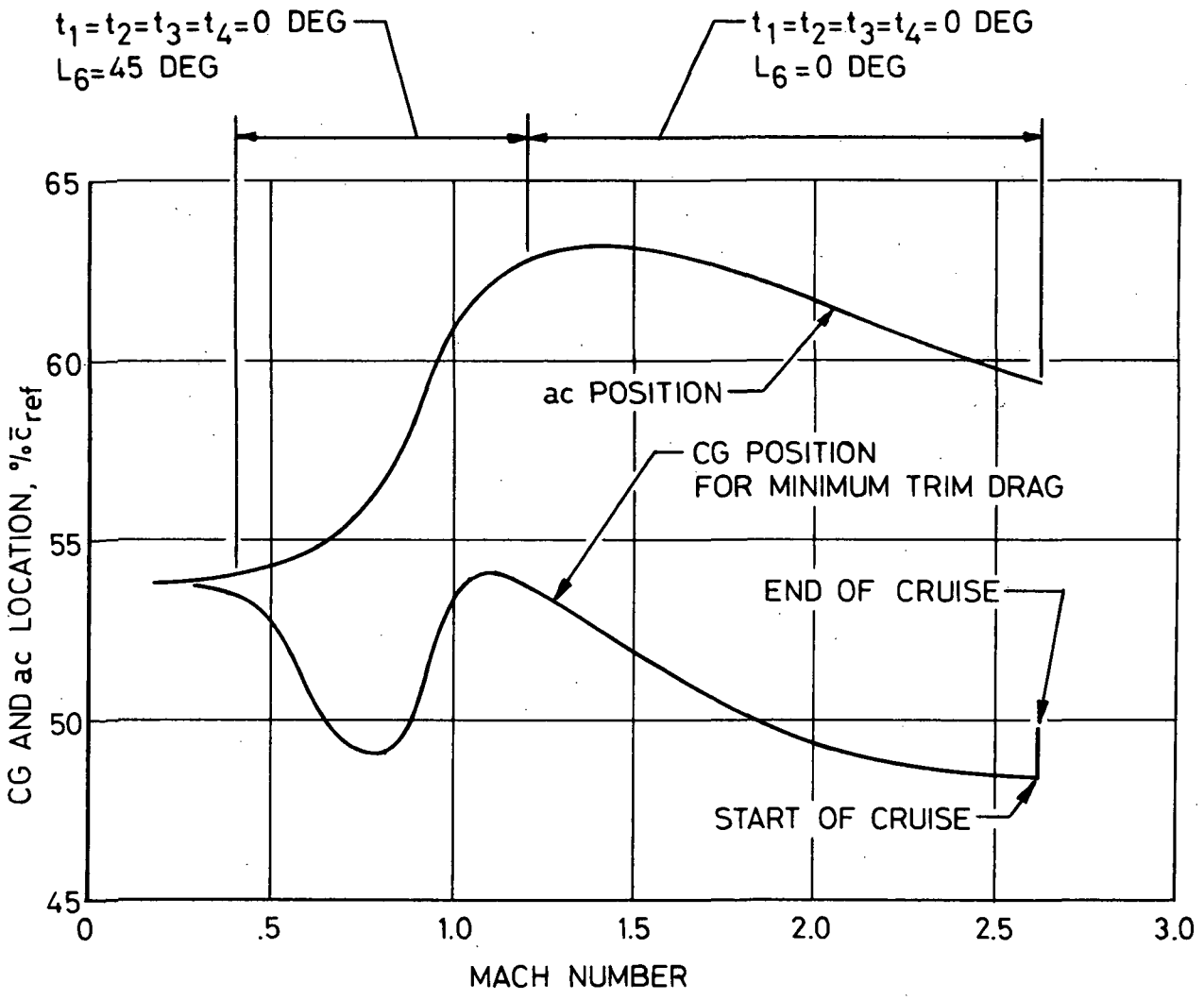

Figure 25 Aerodynamic Center Location and Required Center-of-Gravity Position for Maximum Performance

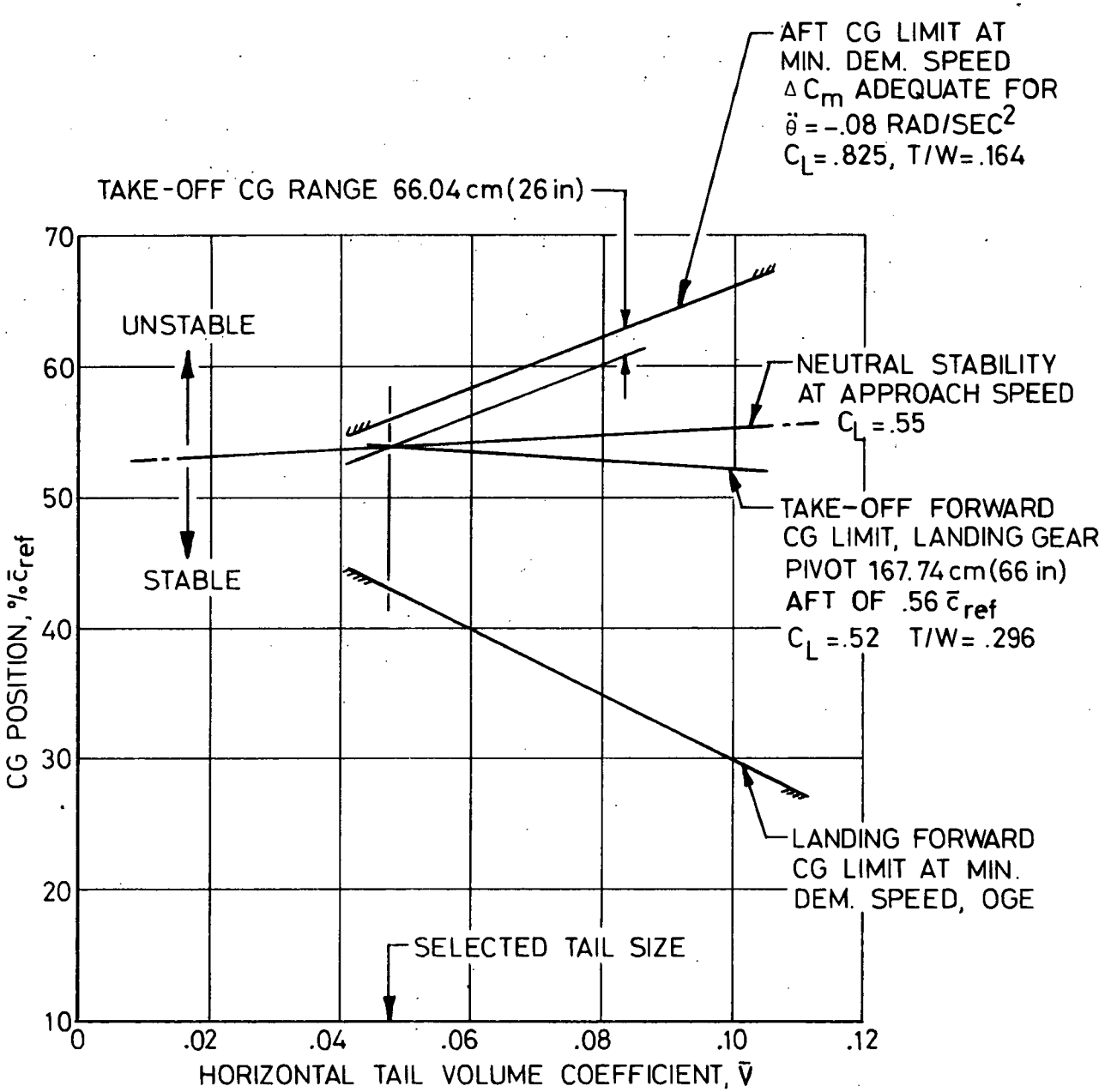

Figure 26 Center-of-Gravity Limits for Takeoff and Landing

T/W=.296
$L_{1,2}$ = 30 DEG
L_6 = 45 DEG
$t_1 = t_2 = t_3$ = 20 DEG
t_4 = 5 DEG
S_{ht} = 39.948 m^2 (430 ft^2)

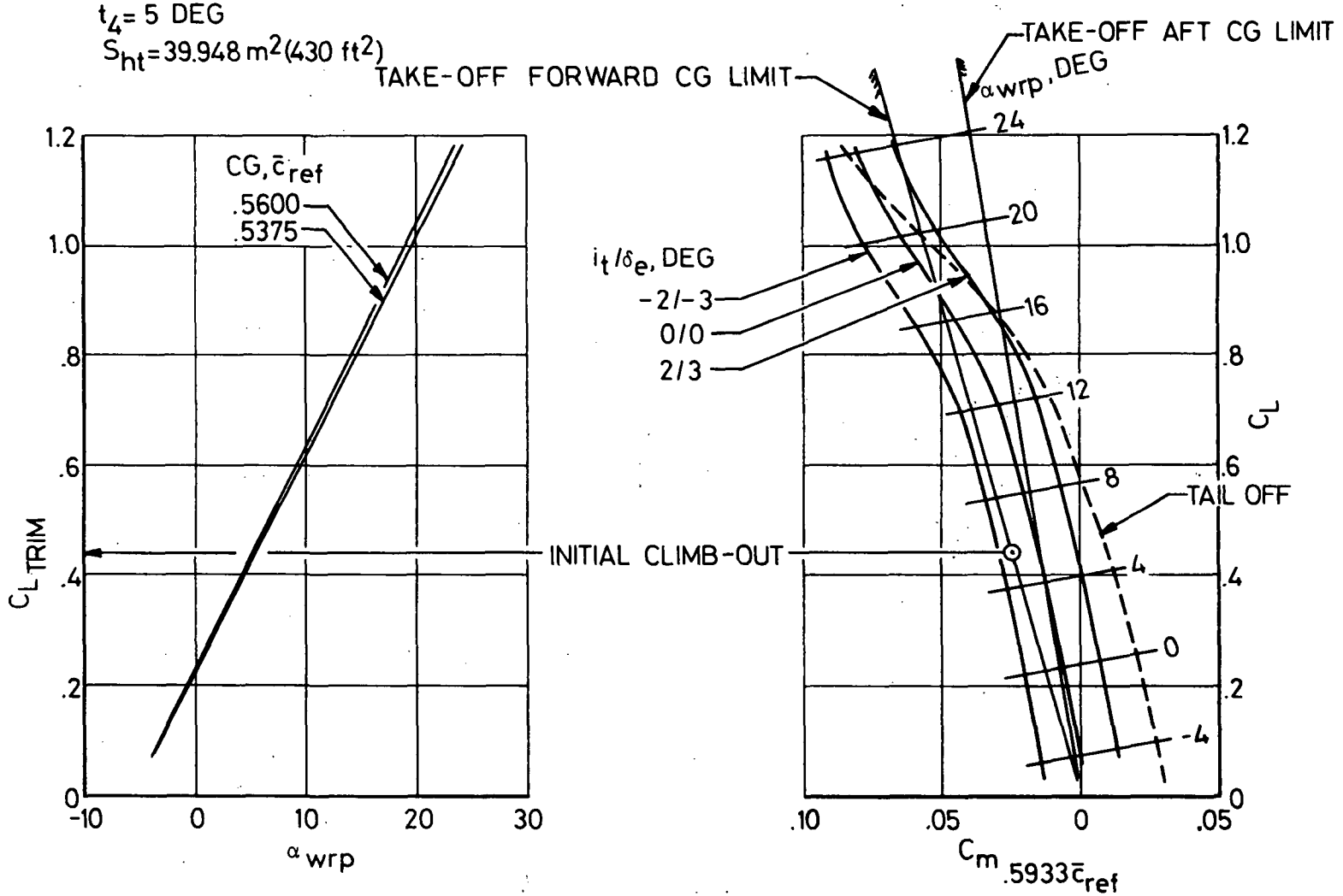

Figure 27 Initial Climb-out Trim and Stability, Out of Ground Effect.

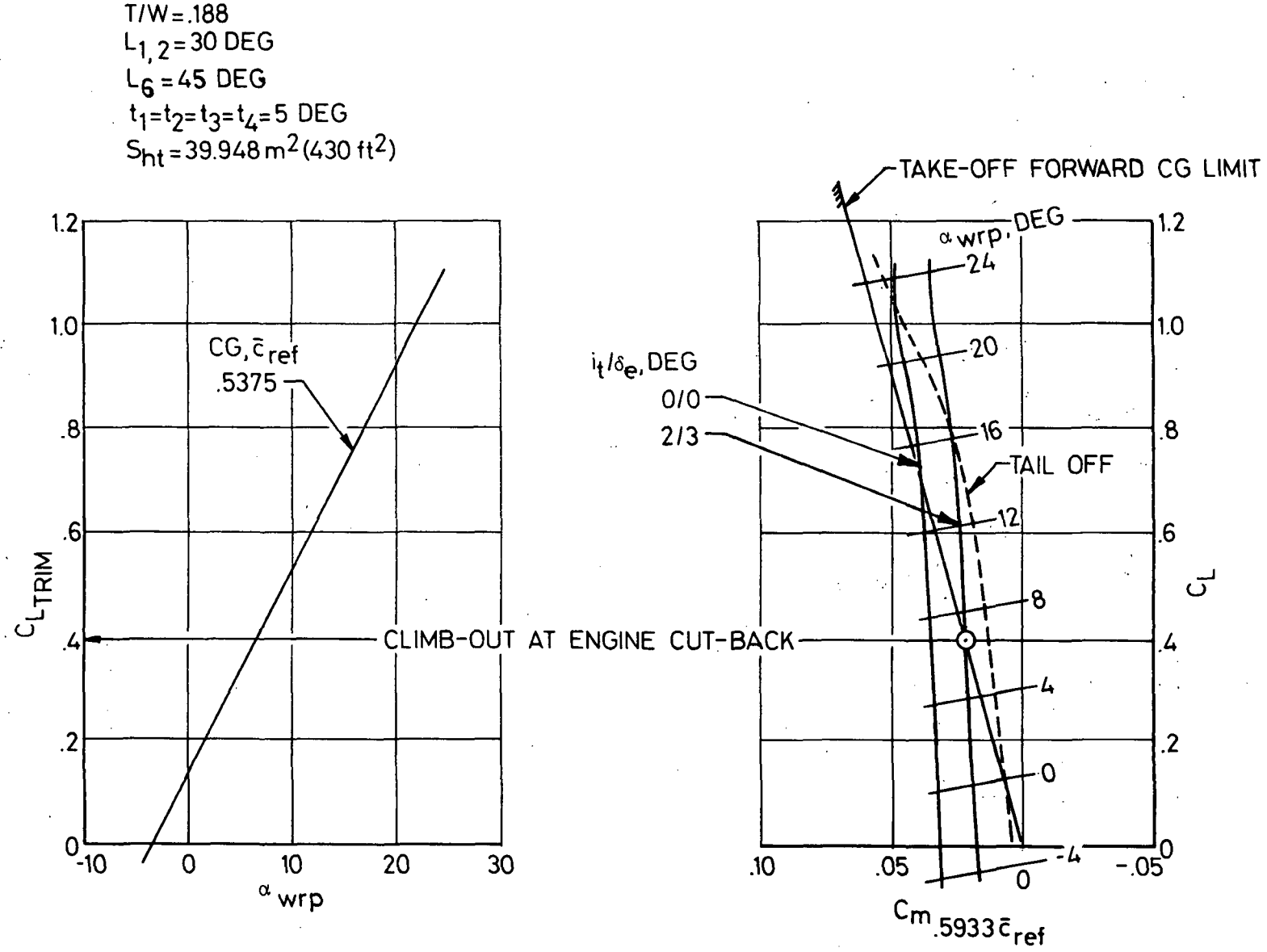

Figure 28 Climb-out Trim and Stability at Engine Cut-back, Out of Ground Effect.

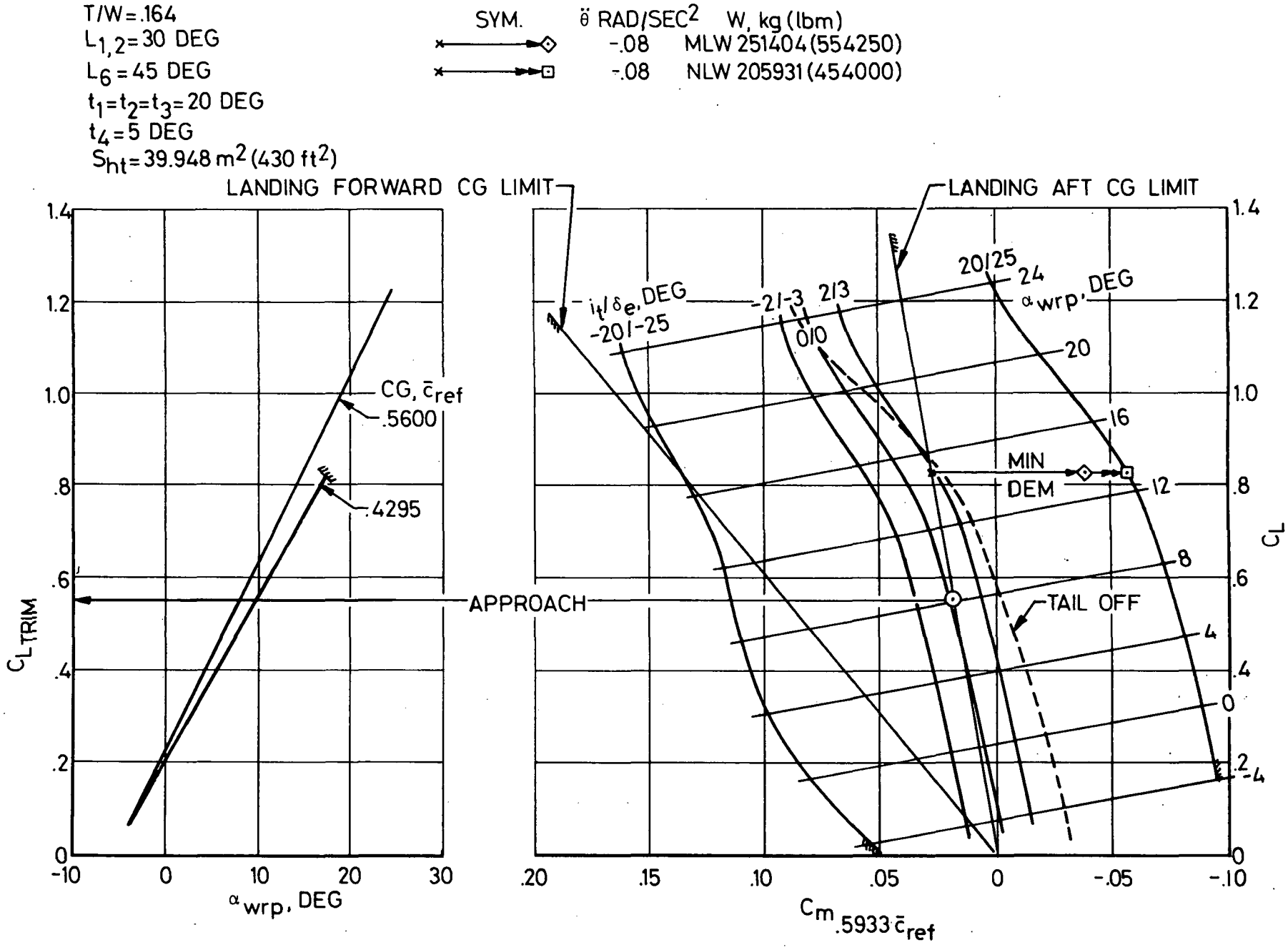

Figure 29 Approach Trim and Stability, Out of Ground Effect (3° glide slope)

$S_{vt} = 15.794\ m^2\ (170\ ft^2)$
$S_v = 20.253\ m^2\ (218\ ft^2)$
$S_{wf/SIDE} = 21.672\ m^2\ (233.275\ ft^2)$
$CG = .498\ \bar{c}_{ref}$

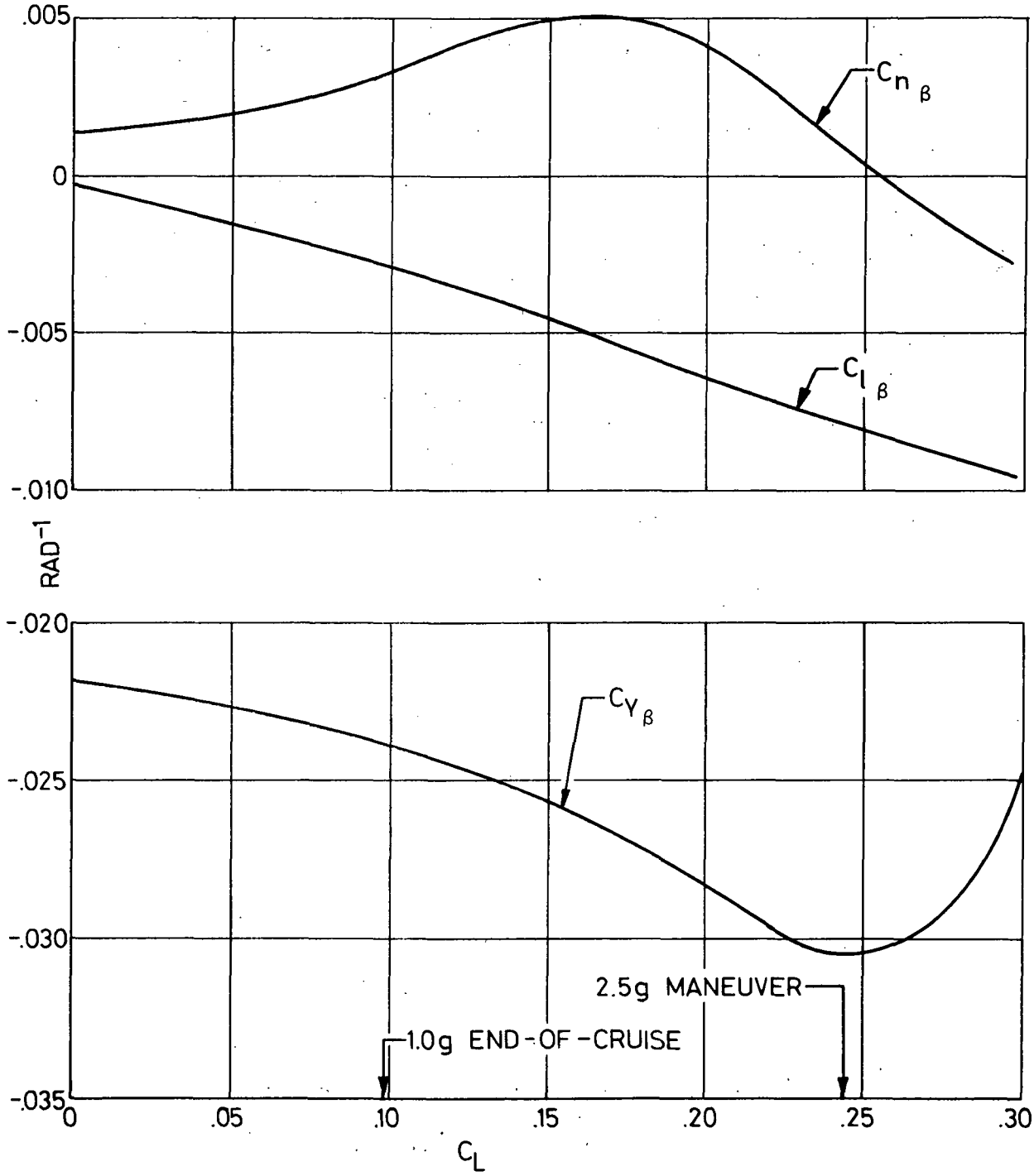

Figure 30 Estimated Flexible Static Lateral-Directional Stability at M = 2.7

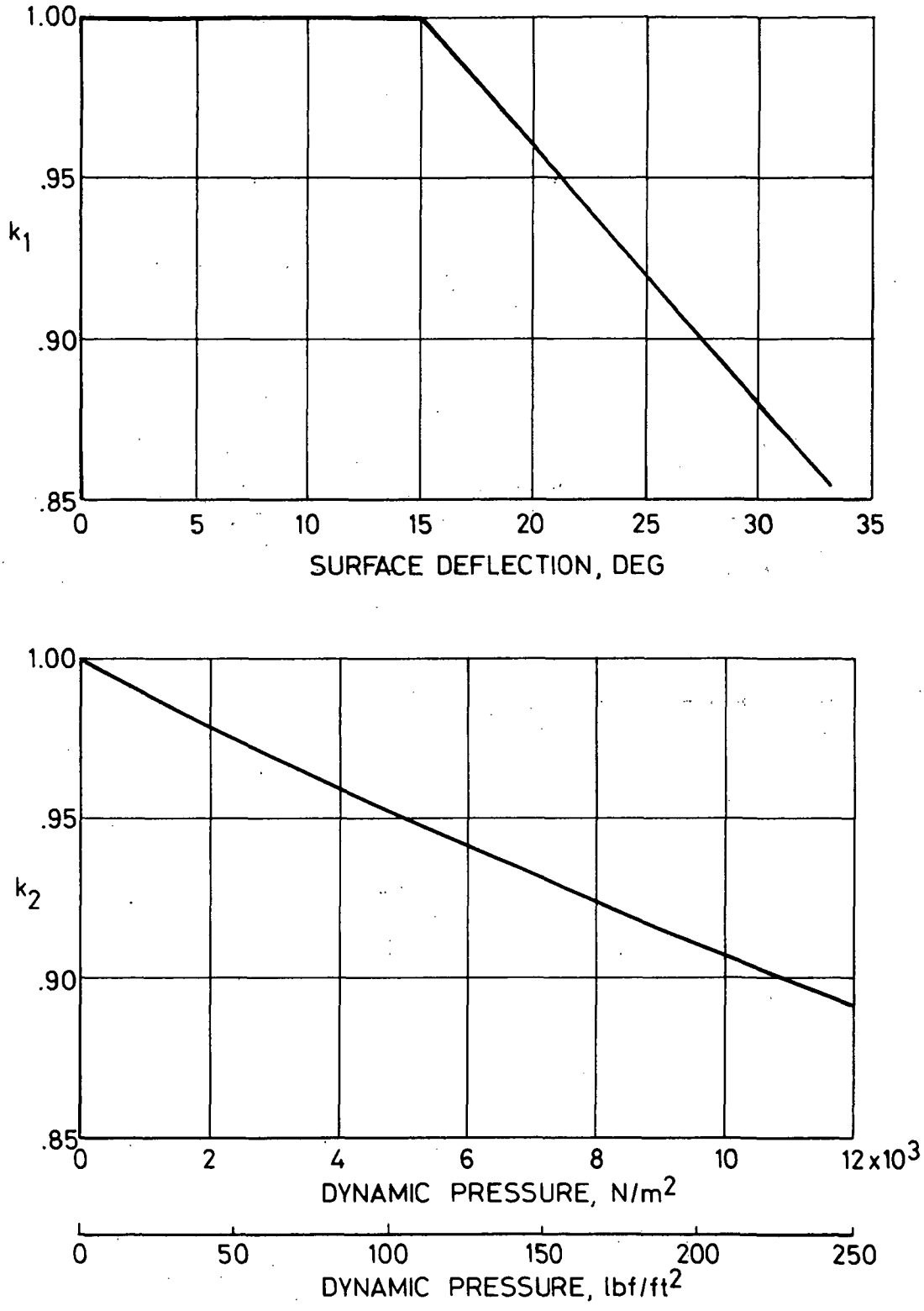

Figure 31 Estimated Rudder Effectiveness and Flexibility Parameters

$CG = .5600\,\bar{c}_{ref}$

$S_{W_{ref}} = 926.152\ m^2\ (9969\ ft^2)$

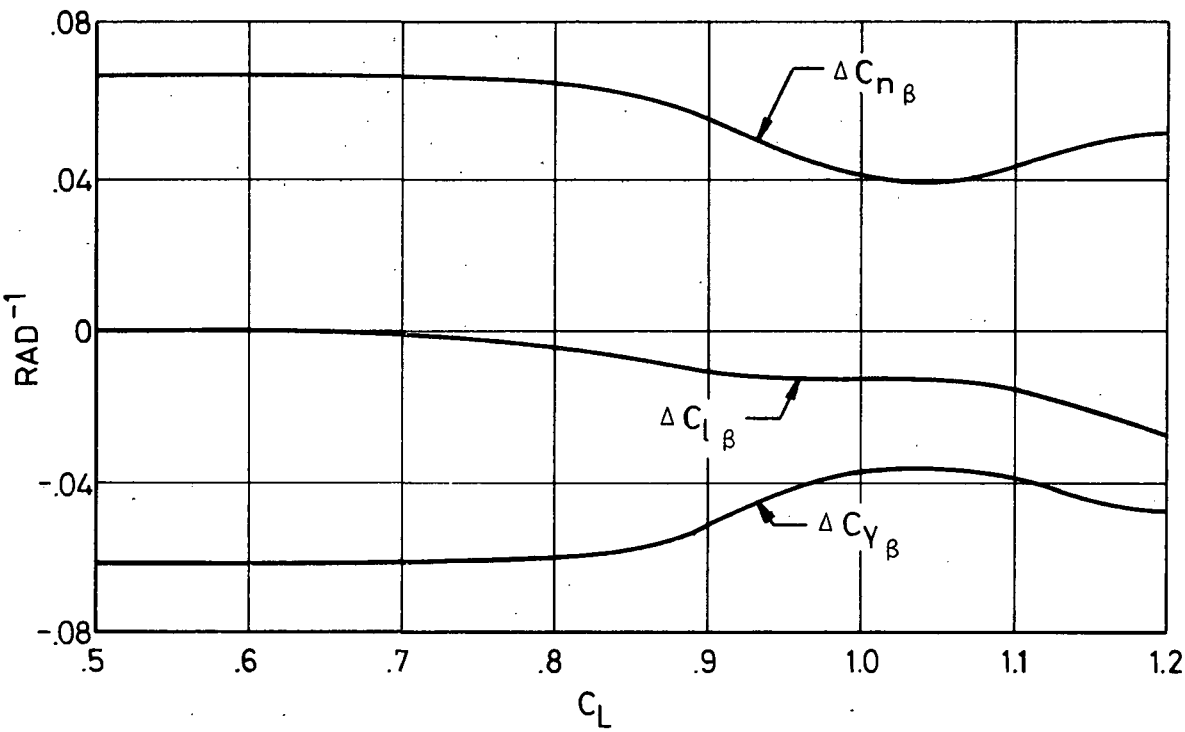

Figure 32 Estimated Vertical Tail Contribution to High-Lift Configuration Static Lateral-Directional Stability

W=325679 kg (718000 lbm)
MAXIMUM THRUST ON THREE OPERATING ENGINES

V=97.230 m/sec (189 kts) EAS

S_{vt} =15.794 m^2 (170 ft^2)

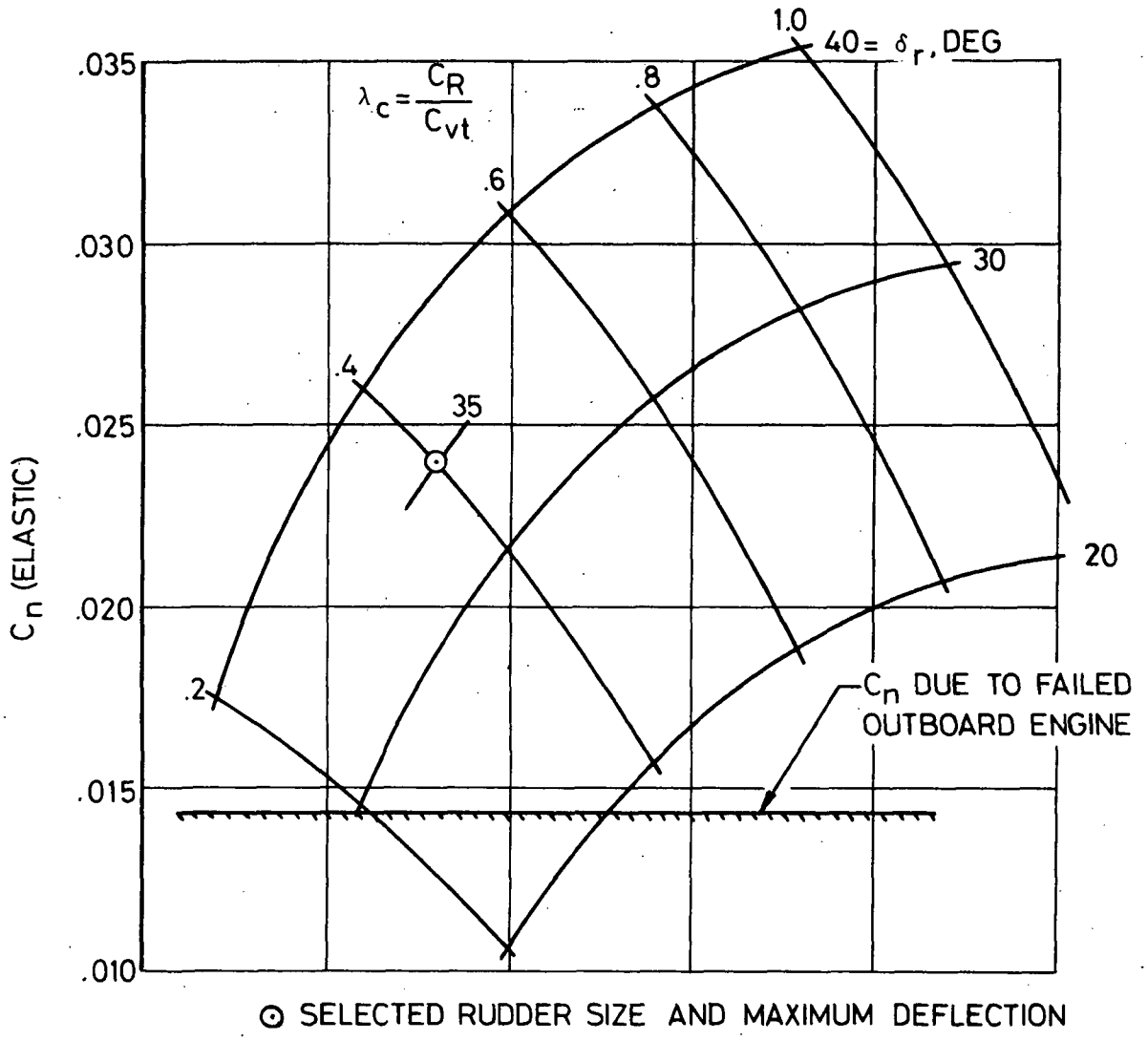

Figure 33 Estimated Directional Control Capability Assumming an Outboard Engine Failure

$L_{1,2} = 30$ DEG
$L_6 = 45$ DEG
$t_1 = t_2 = t_3 = 20$ DEG
$t_4 = 5$ DEG

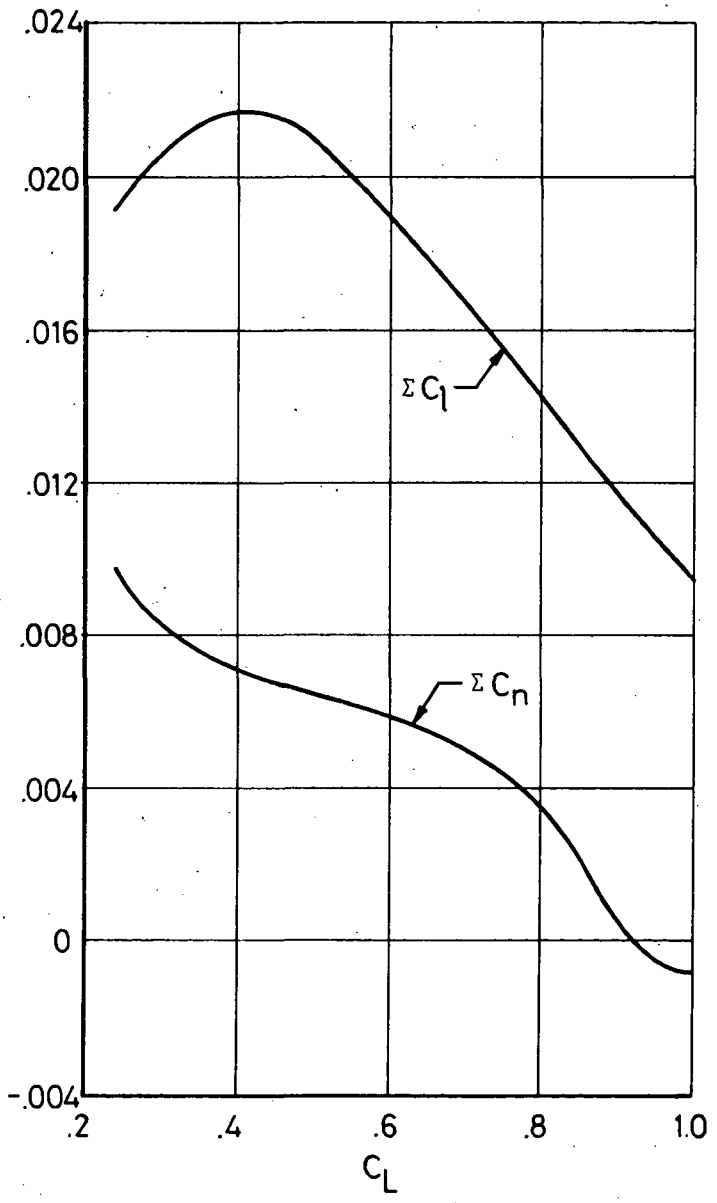

Figure 34 Estimated Flexible Maximum Lateral Control Characteristics

W = 325679 kg (718000 lbm)
$L_{1,2}$ = 30 DEG
L_6 = 45 DEG
$t_1 = t_2 = t_3$ = 20 DEG
t_4 = 5 DEG

MAXIMUM LATERAL CONTROL INPUT IN .25 sec

CLASS III, CATEGORY C (REF. 16)

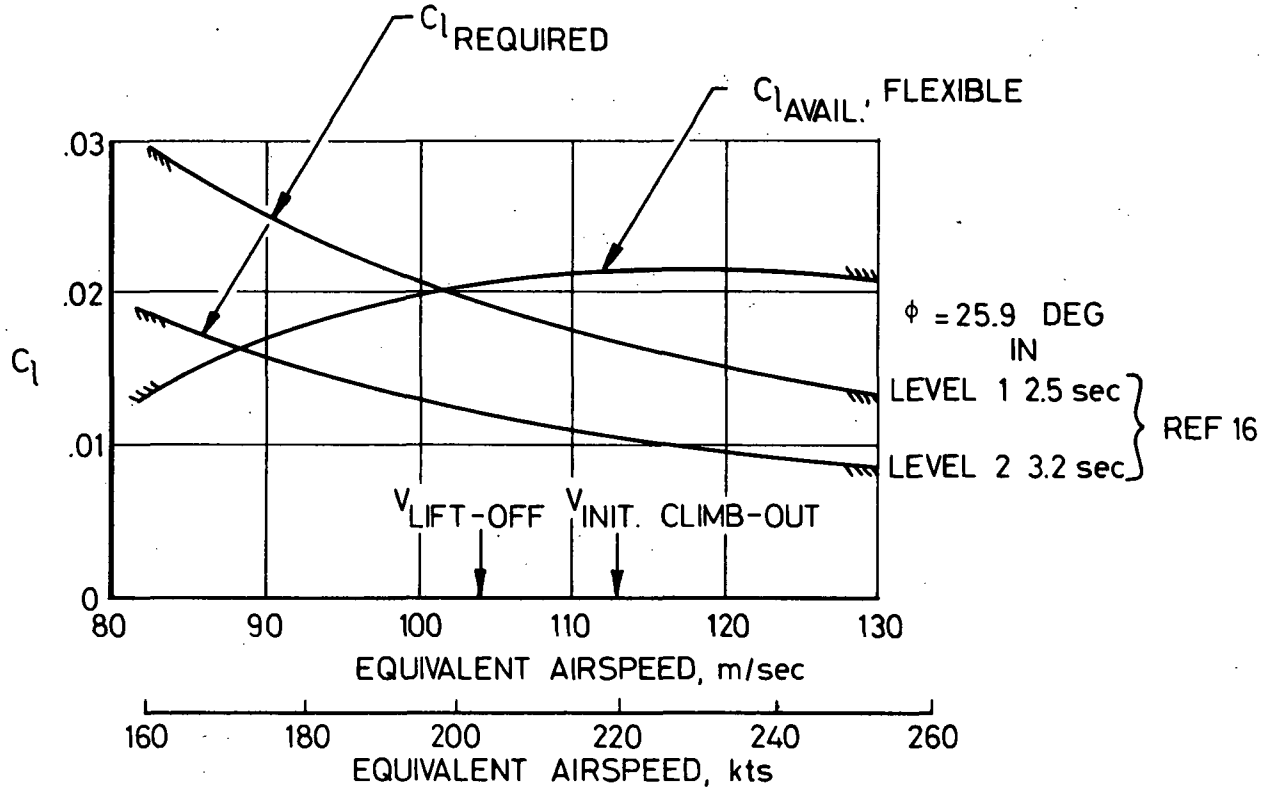

Figure 35 Estimated Roll Control Capability in the High-Lift Configuration, Takeoff

W = 205931 kg (454000 lbm)
$L_{1,2}$ = 30 DEG
L_6 = 45 DEG
$t_1 = t_2 = t_3$ = 20 DEG
t_4 = 5 DEG

MAXIMUM LATERAL CONTROL INPUT IN .25 sec

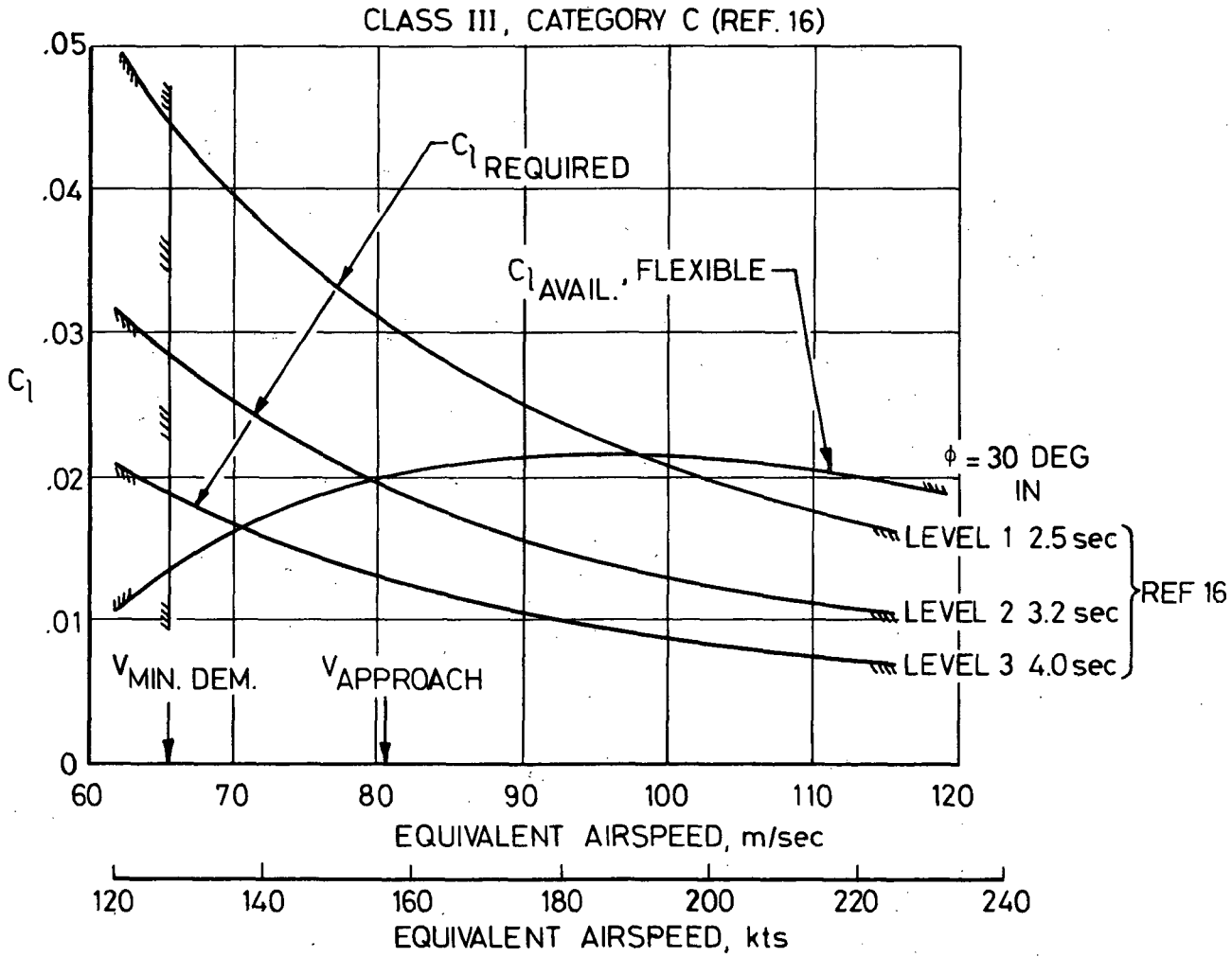

Figure 36 Estimated Roll Control Capability in the High-Lift Landing-Approach

W=205931 kg (454000 lbm)
$L_{1,2}$=30 DEG
L_6=45 DEG
$t_1=t_2=t_3$=20 DEG
t_4=5 DEG

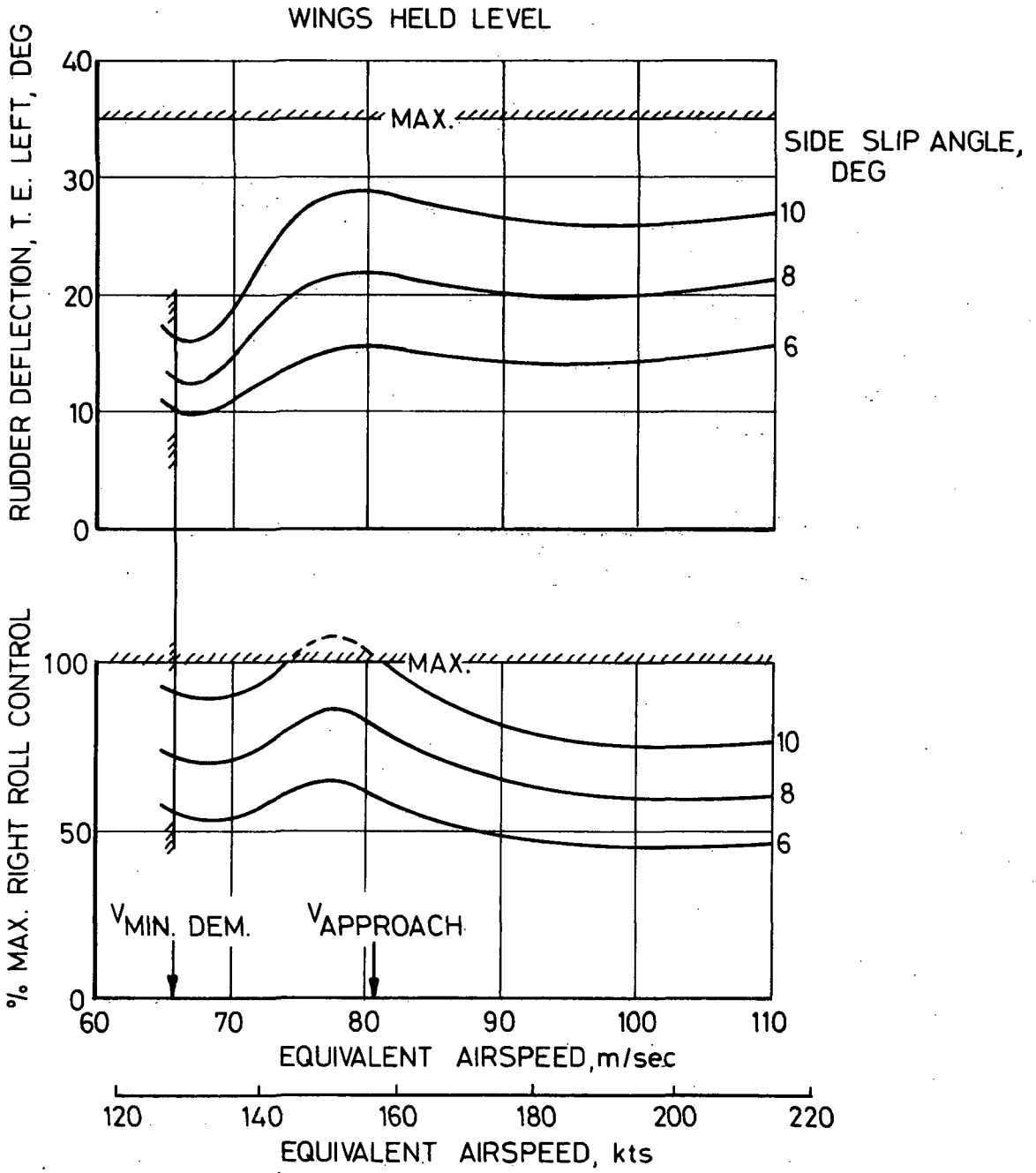

Figure 37 Estimated High-lift Configuration Lateral-directional Trim Characteristics in Steady Side-slip.

W=205931 kg (454000 lbm)

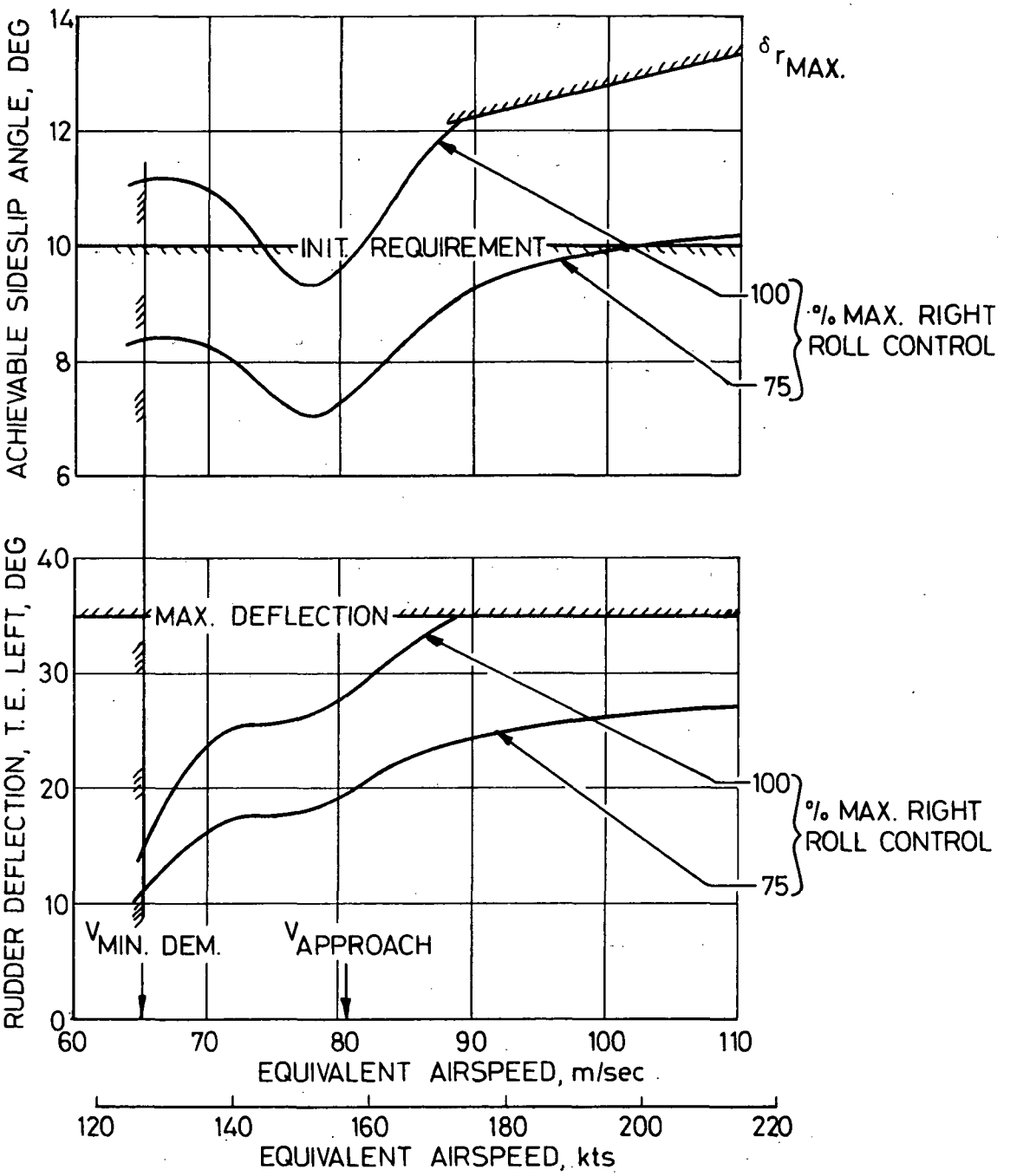

Figure 38 Estimated High-Lift Configuration Lateral-Directional Stability Characteristics for Given Levels of Lateral Control to Maintain Wings Level Flight.

W = 325679 kg (718000 lbm)
C_L = .11

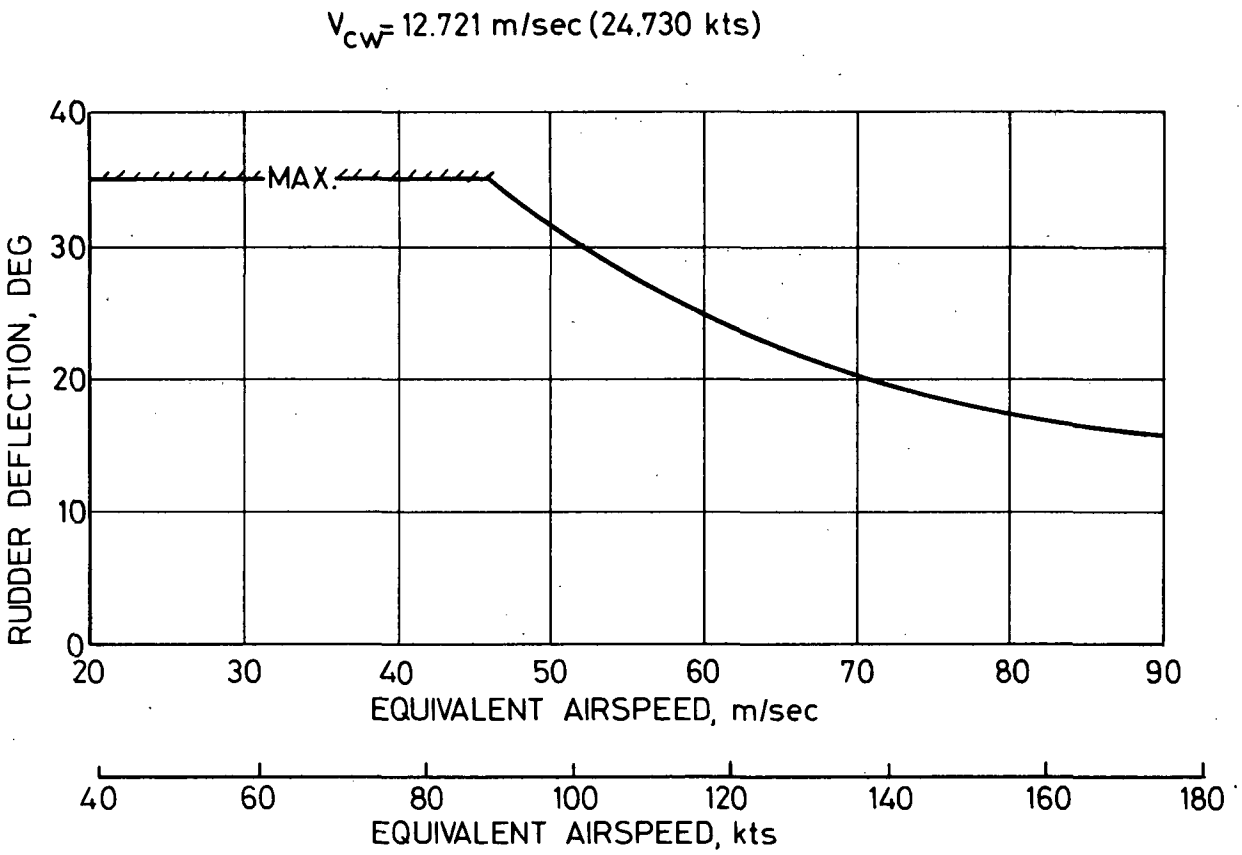

Figure 39 Estimated Directional Trim Requirements in a 90 Deg. Cross Wind

W=205931 kg (454000 lbm)
$C_{L_{TRIM}}$ = .55
GLIDE SLOPE = 3 DEG
CG = .5600 $\bar{c}_{ref}$
NEUTRAL POINT = .5375 $\bar{c}_{ref}$

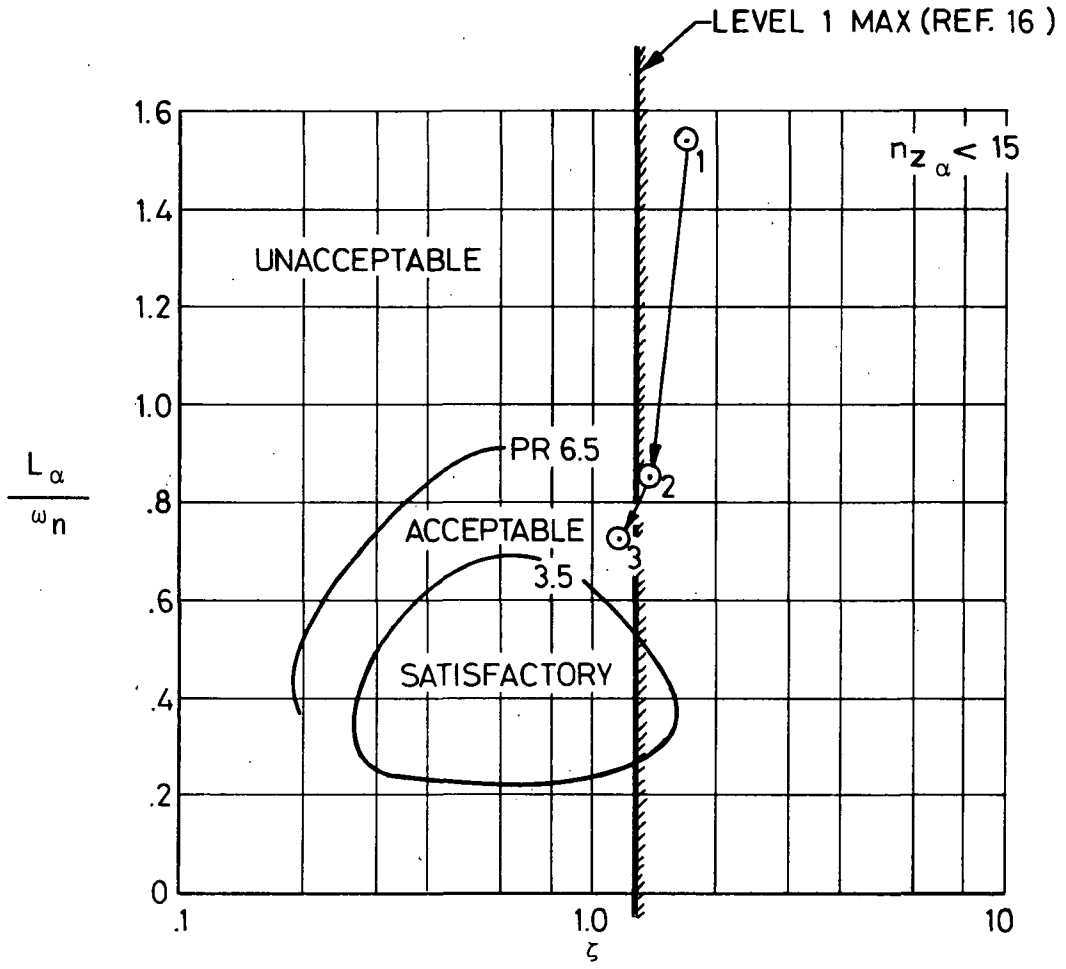

SUBSCRIPT	1	2	3
	INHERENT AIRFRAME CHARACTERISTICS	1 PLUS PITCH-RATE DAMPING	2 PLUS PITCH STIFFNESS

Figure 40 Longitudinal Short-Period Stability Characteristics in the Approach Mode of Flight

W=205931 kg(454000 lbm)
$C_{L_{TRIM}}$ = .55
GLIDE SLOPE = 3 DEG
CG = .5600 $\bar{c}_{ref}$
NEUTRAL POINT = .5375 $\bar{c}_{ref}$

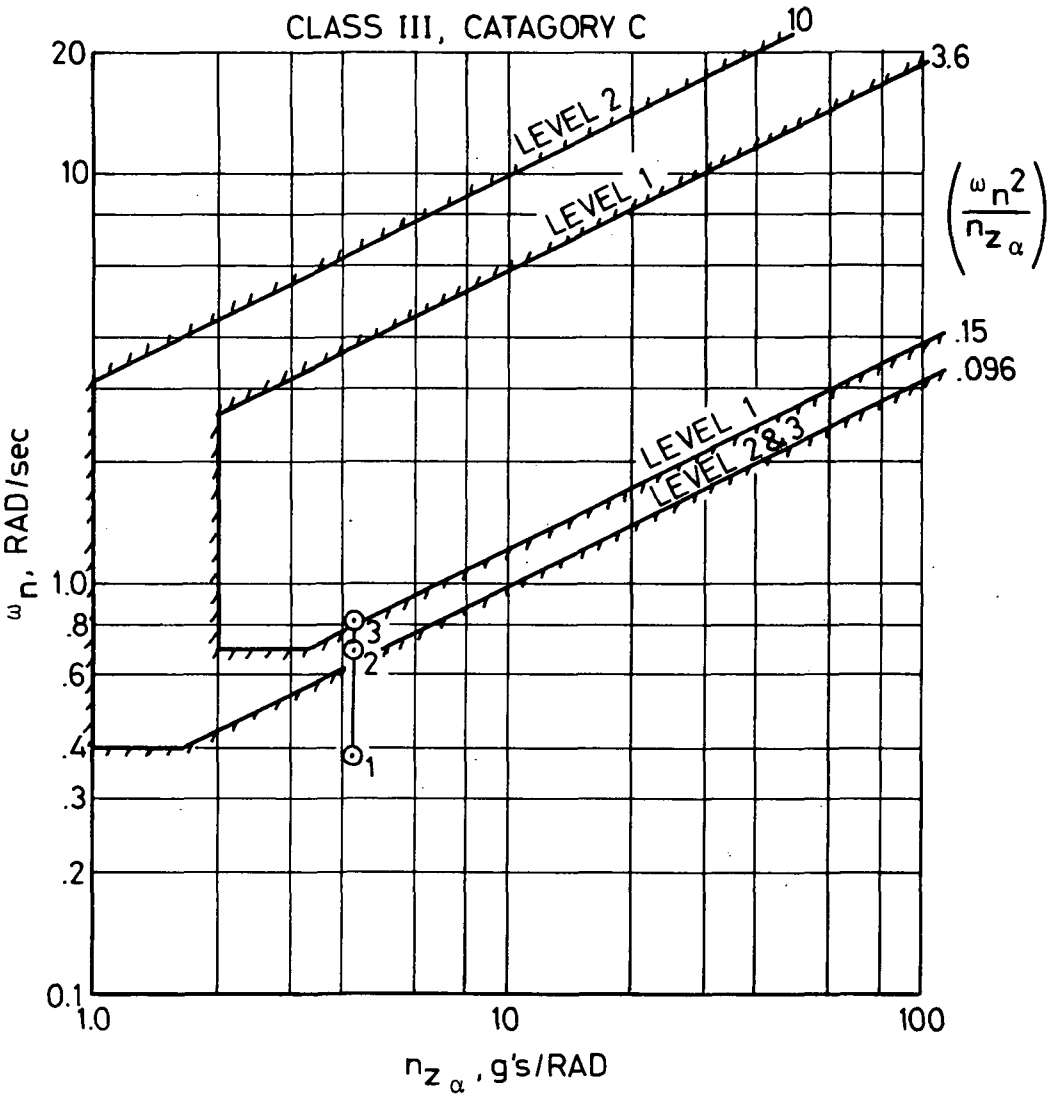

(FOR DEFINITON OF POINT NOTATION SEE FIGURE 40)

Figure 41 Longitudinal Short-Period Stability Characteristics in the Approach Mode of Flight

$C_{L_{TRIM}} = .55$
GLIDE SLOPE = 3 DEG
$CG = .5600\,\bar{c}_{ref}$

SYMBOL	W, kg (lbm)
⊙	251404 (554250)
△	205931 (454000)

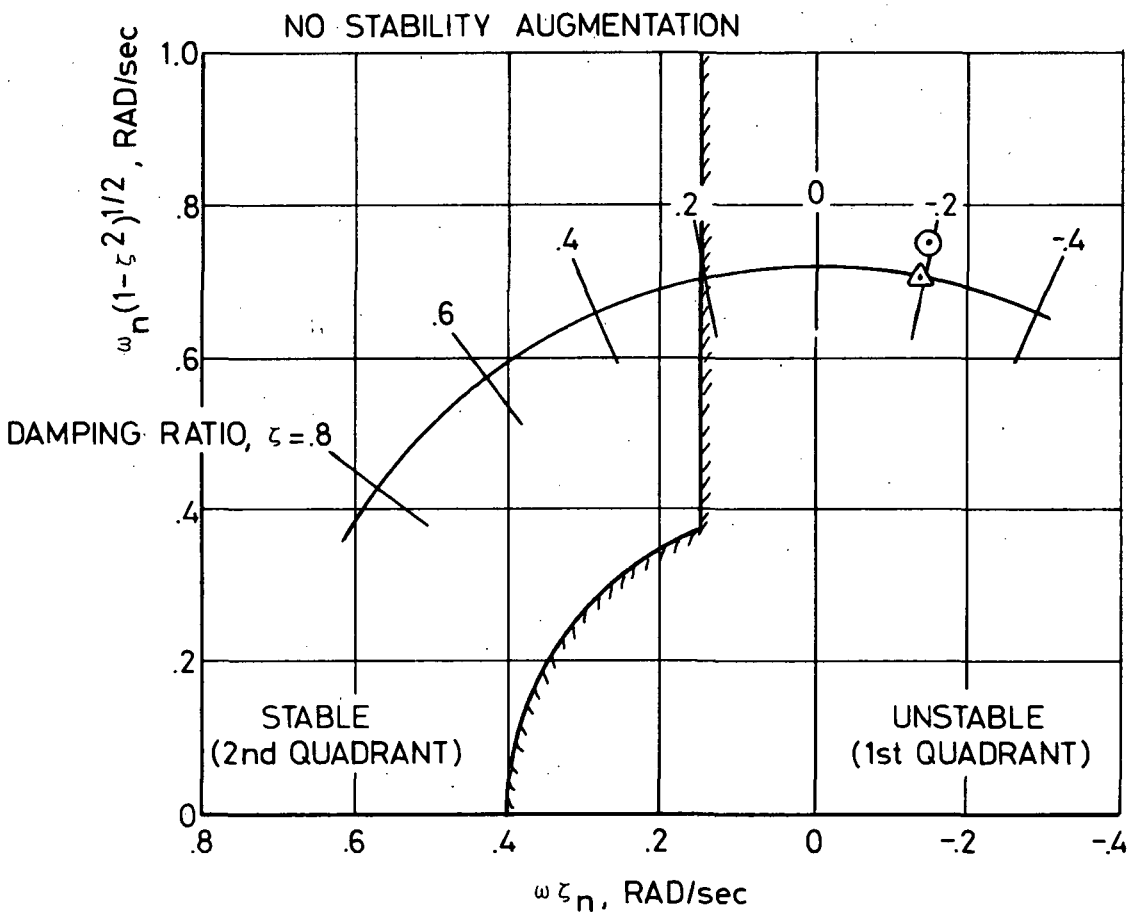

Figure 42 Dutch-roll Stability Characteristics in the Approach Mode of Flight

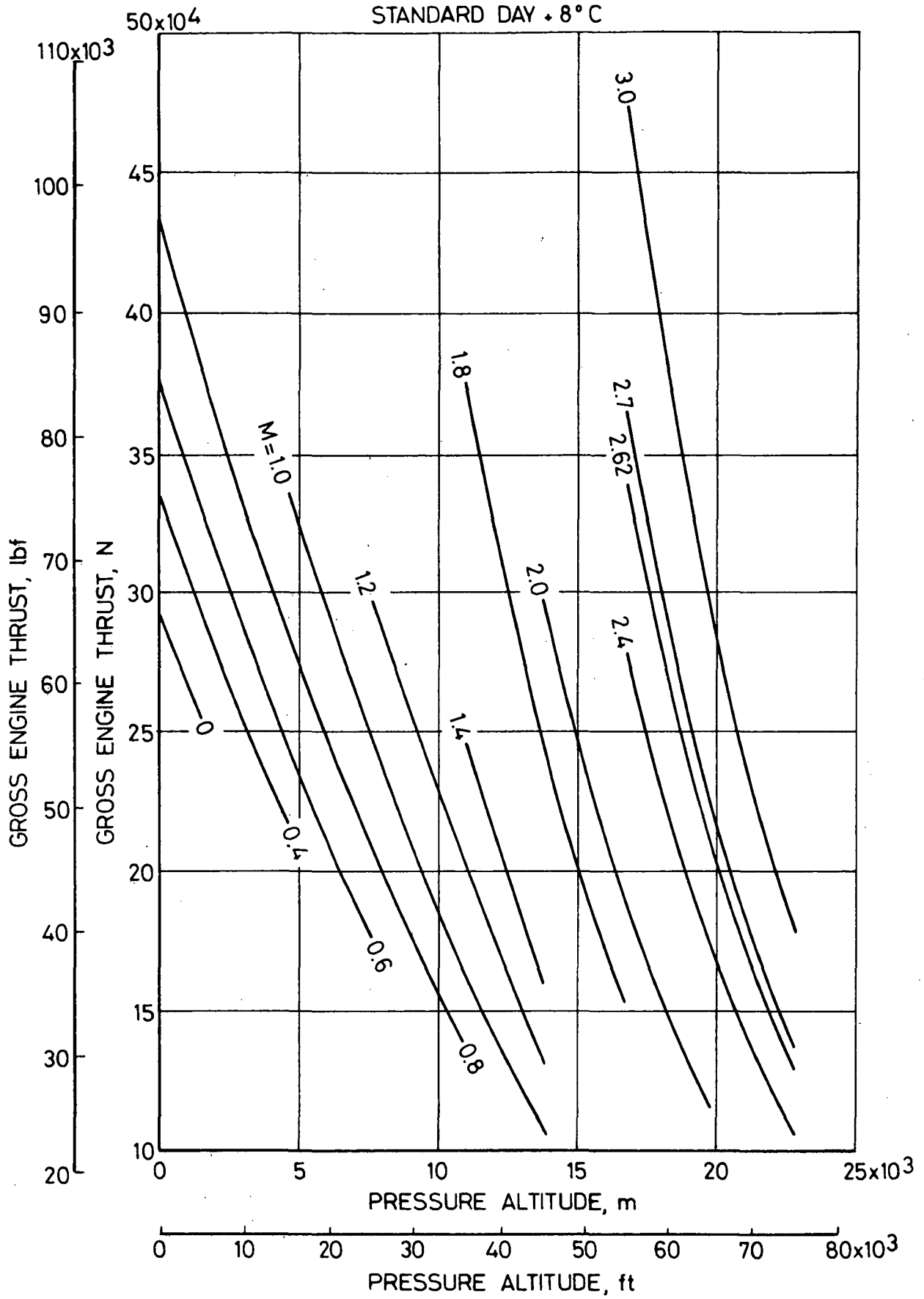

Figure 43 Installed Gross Thrust for Maximum Climb and Cruise

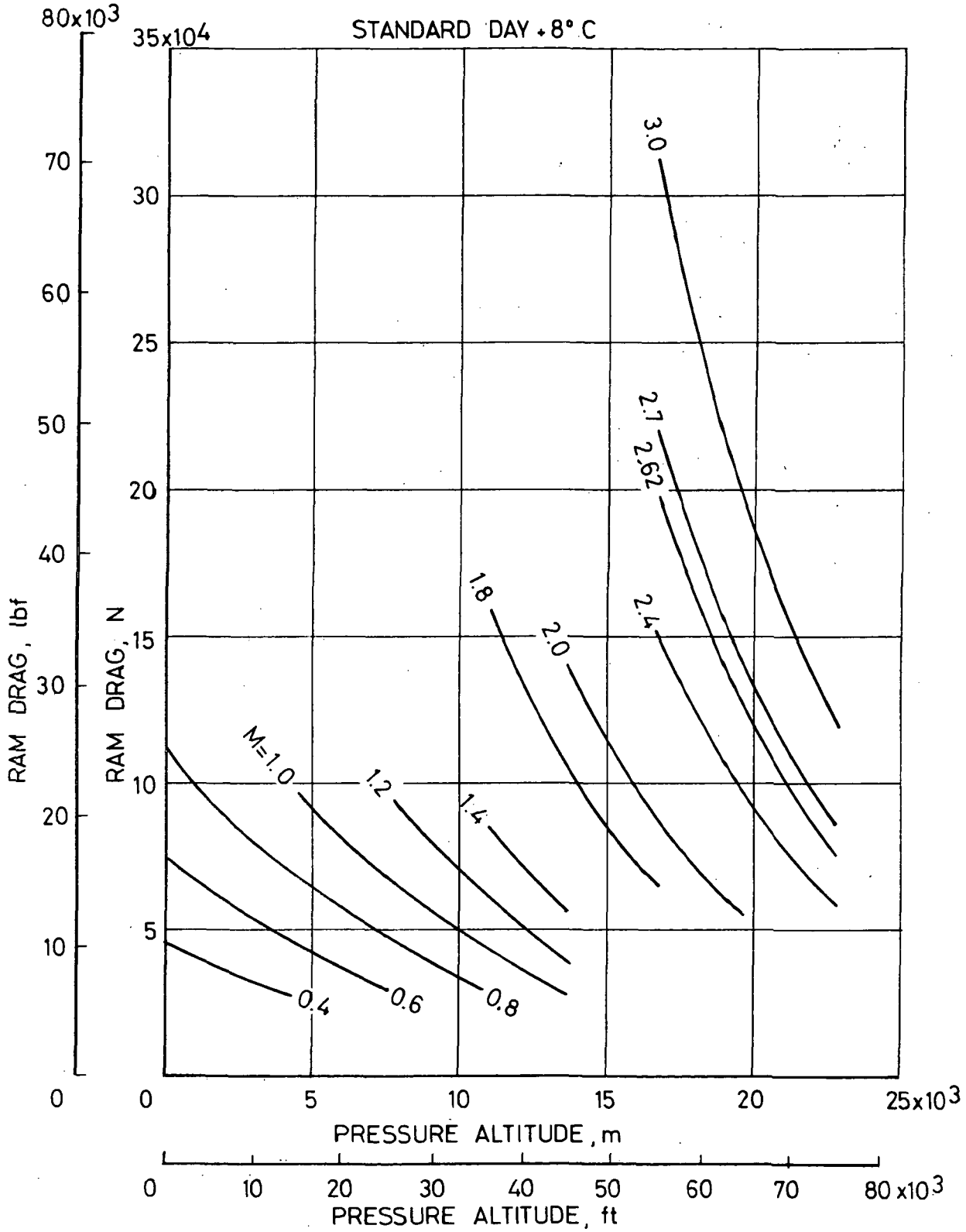

Figure 44 Installed Ram Drag for Maximum Climb and Cruise

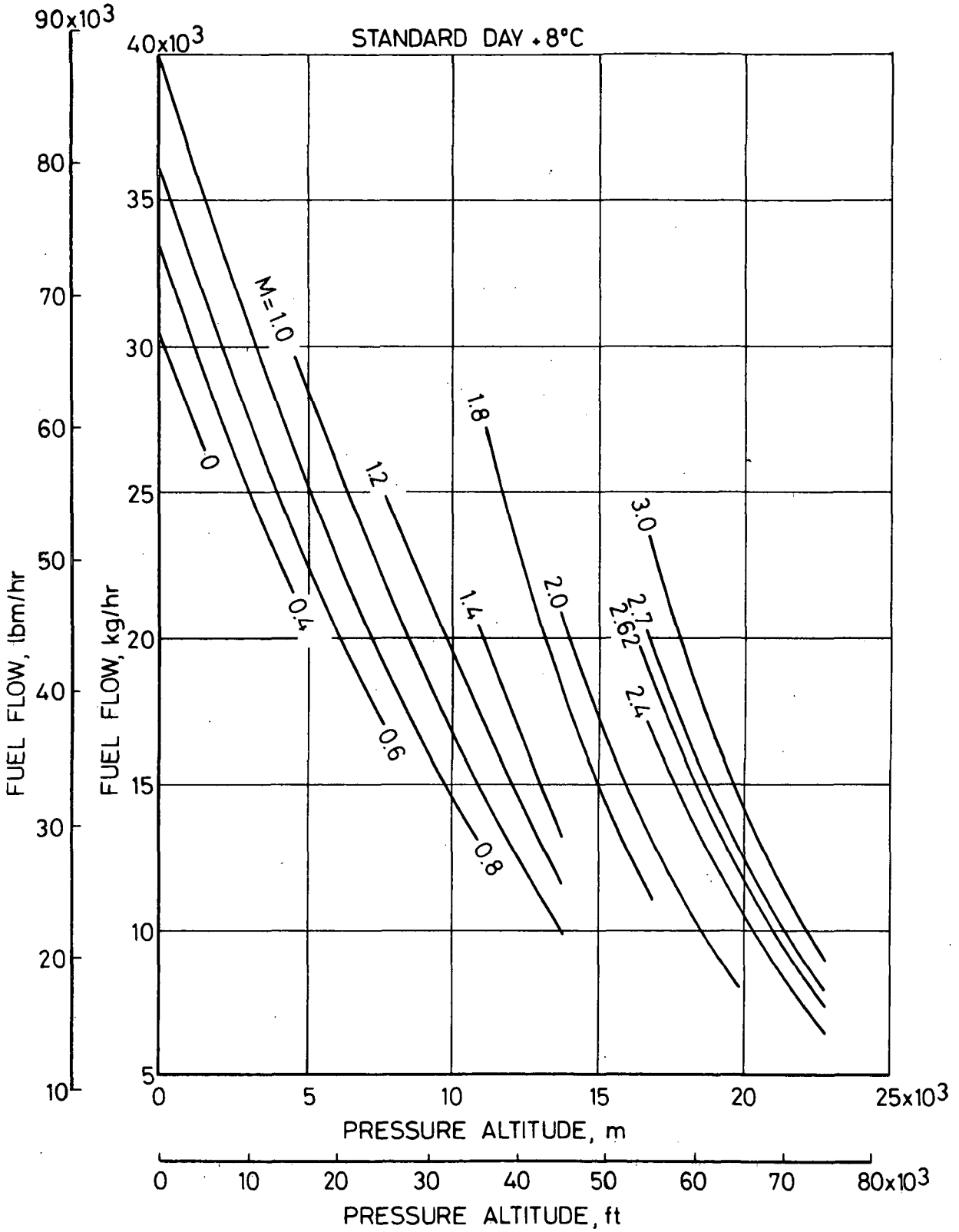

Figure 45 Installed Fuel Flow for Maximum Climb and Cruise

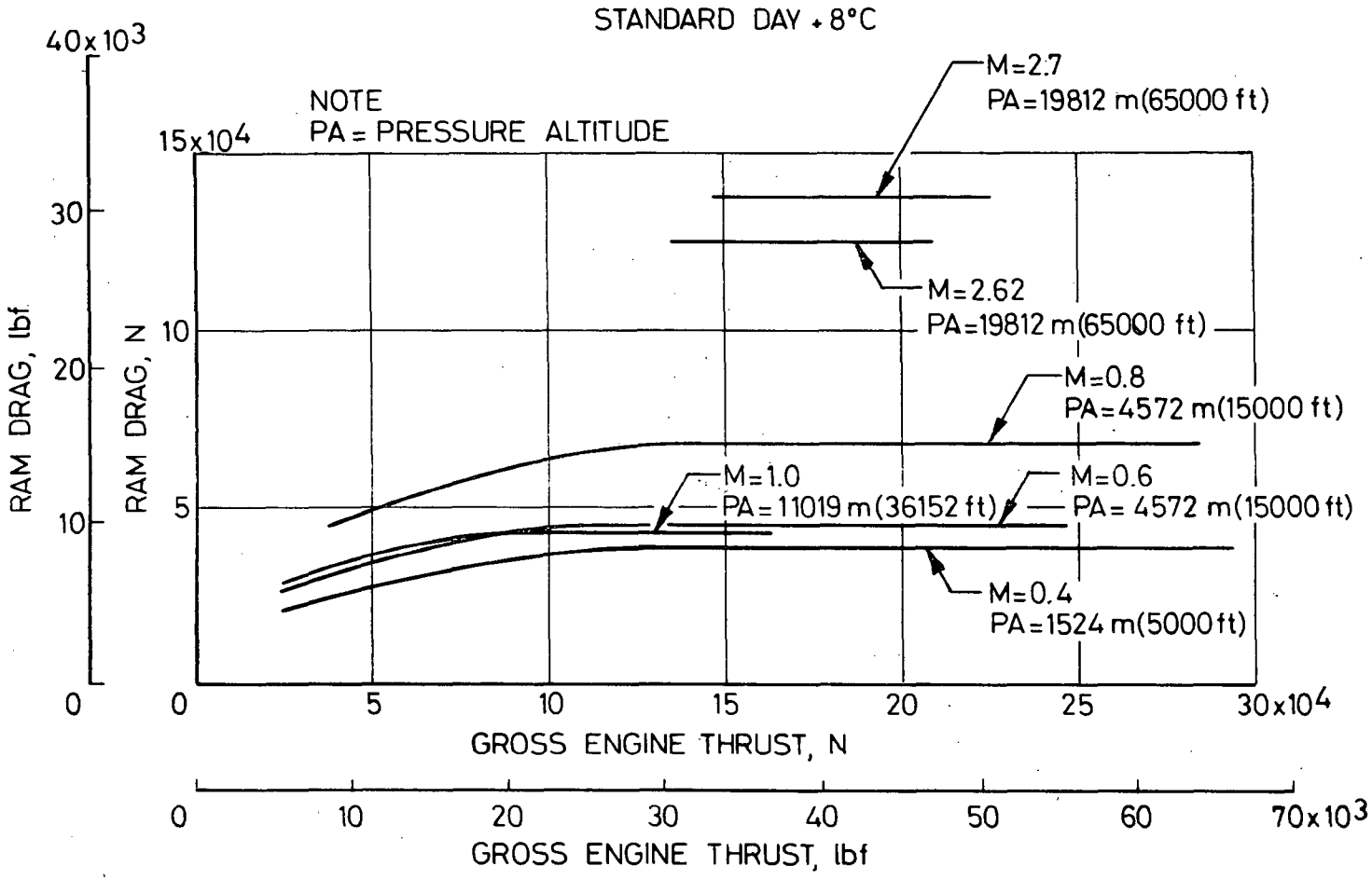

Figure 46 Installed Ram Drag for Maximum and Part Power Cruise

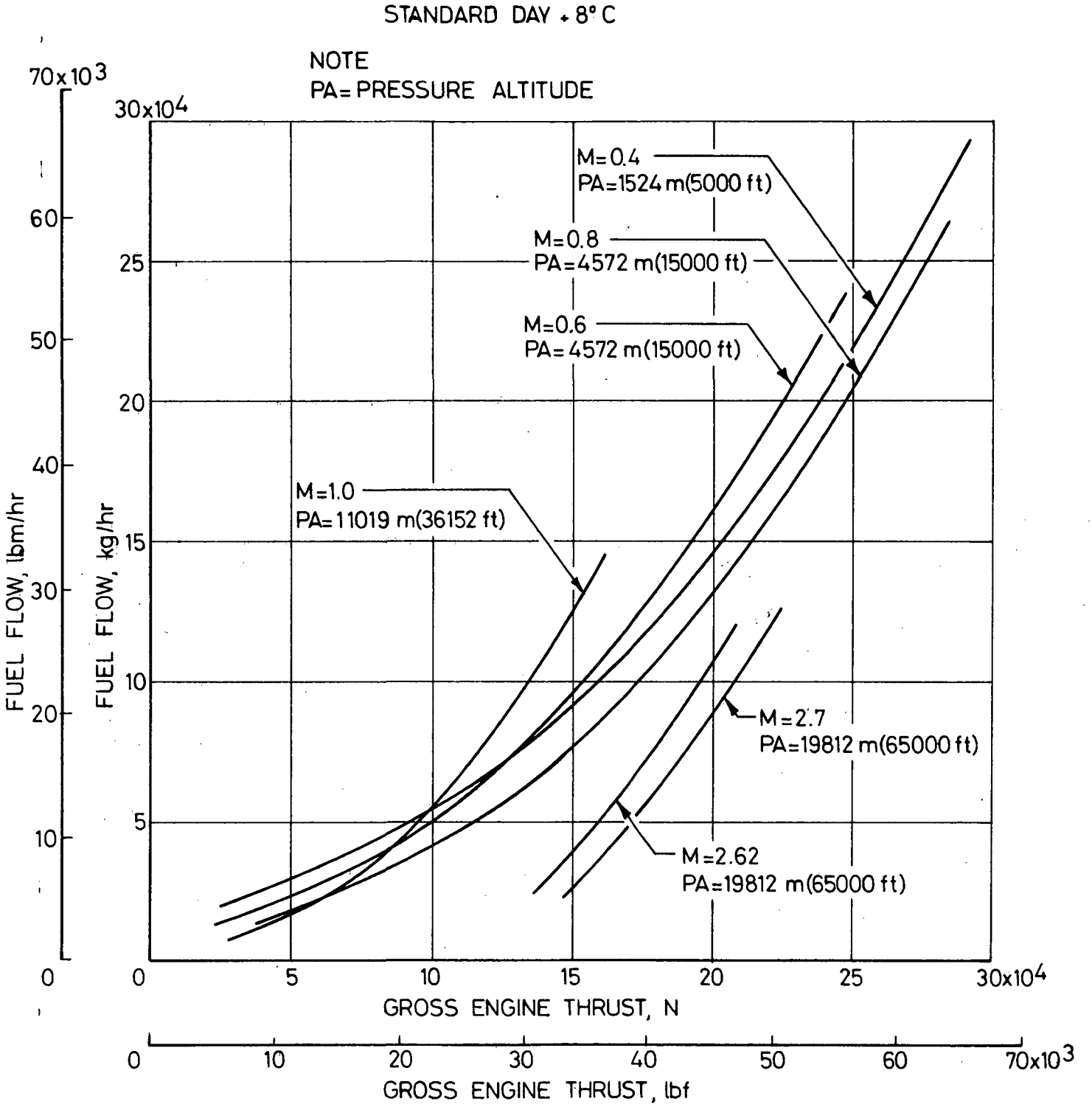

Figure 47 Installed Fuel Flow for Maximum and Part Power Cruise

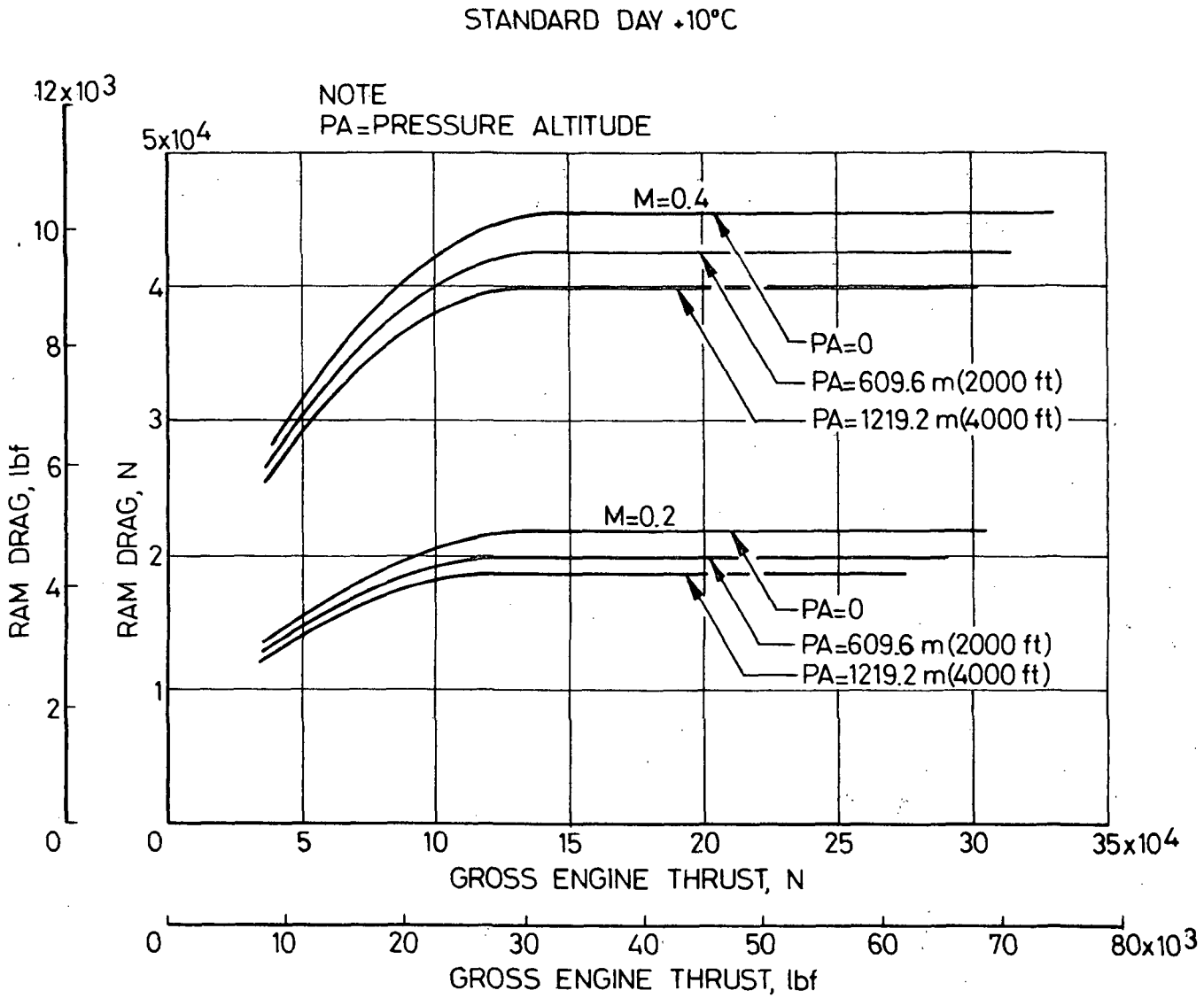

Figure 48 Installed Ram Drag for Takeoff and Part Power Cruise

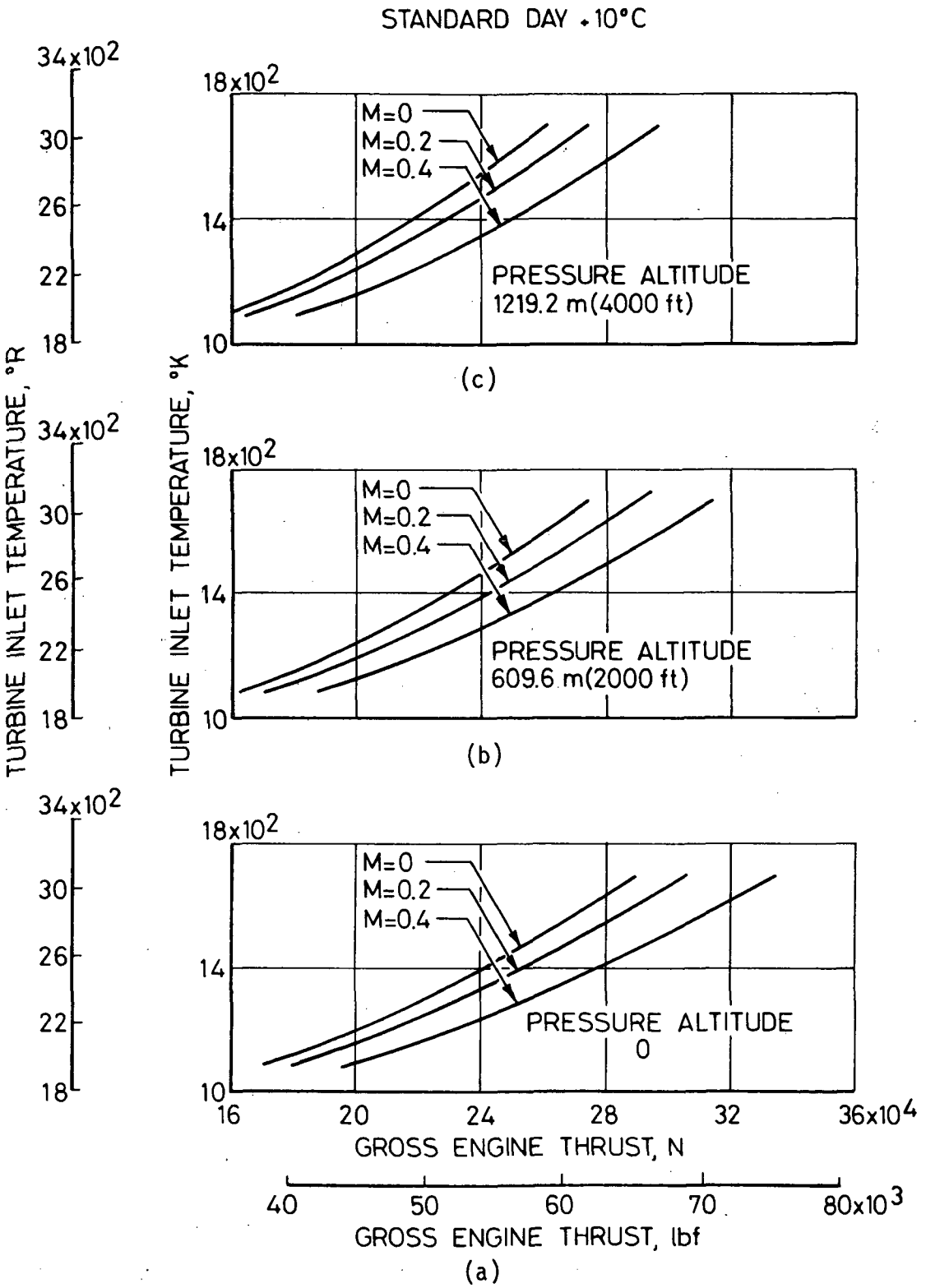

Figure 49 Installed Turbine Inlet Temperature For Takeoff and Part Power Cruise

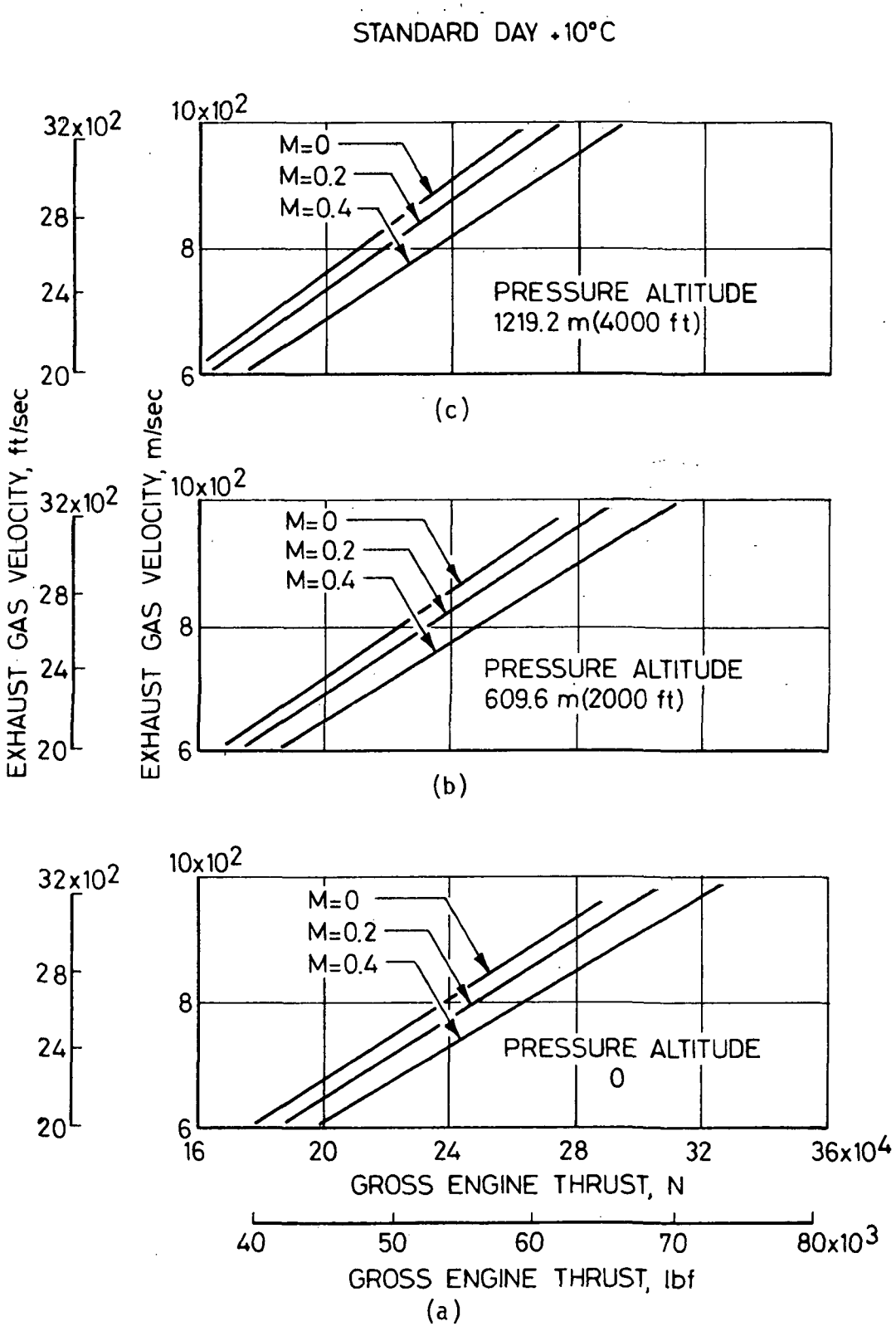

Figure 50 Installed Exhaust Gas Velocity For Takeoff and Part Power Cruise

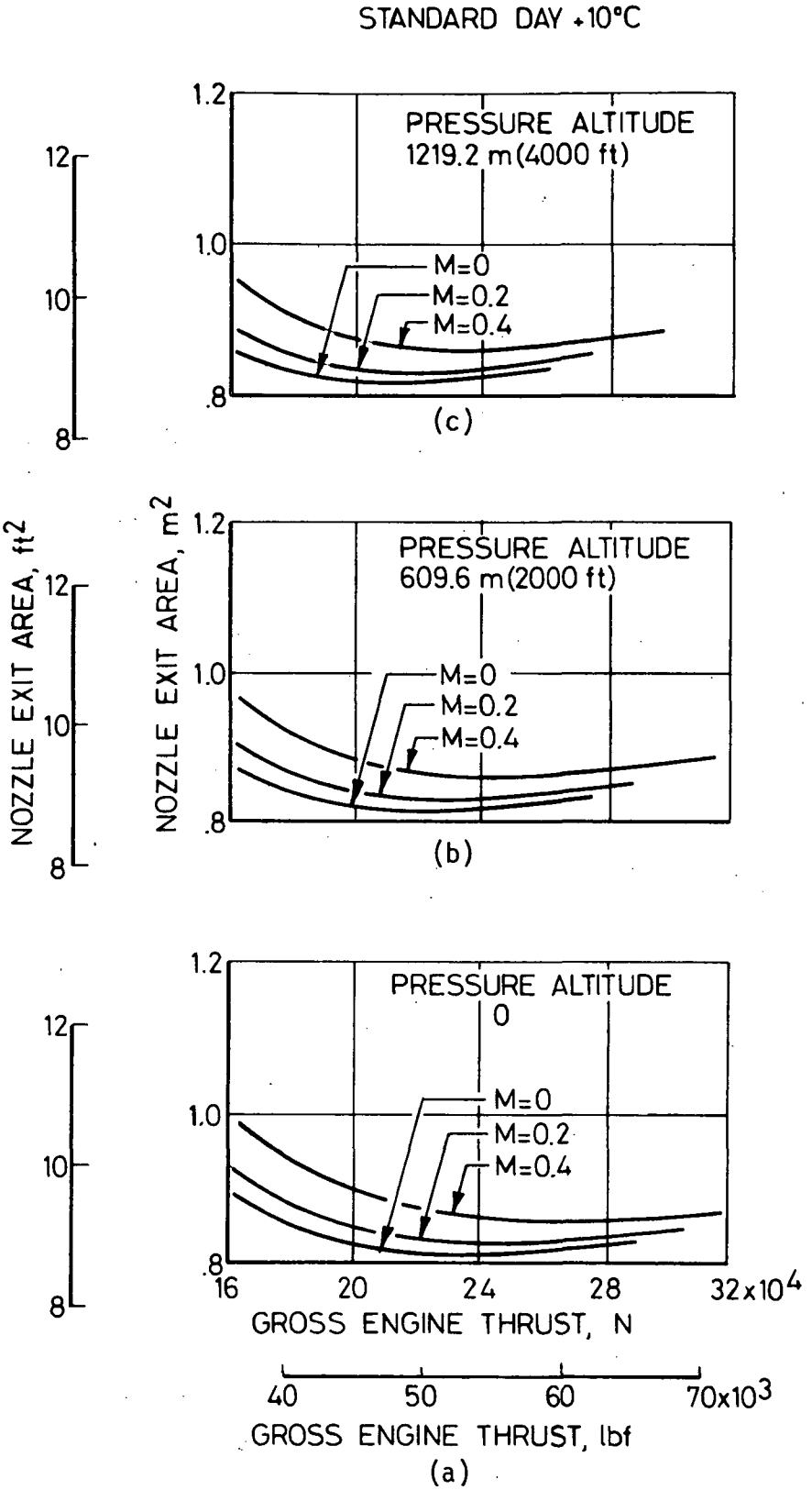

Figure 51 Installed Nozzle Exit Area for Takeoff and Part Power Cruise

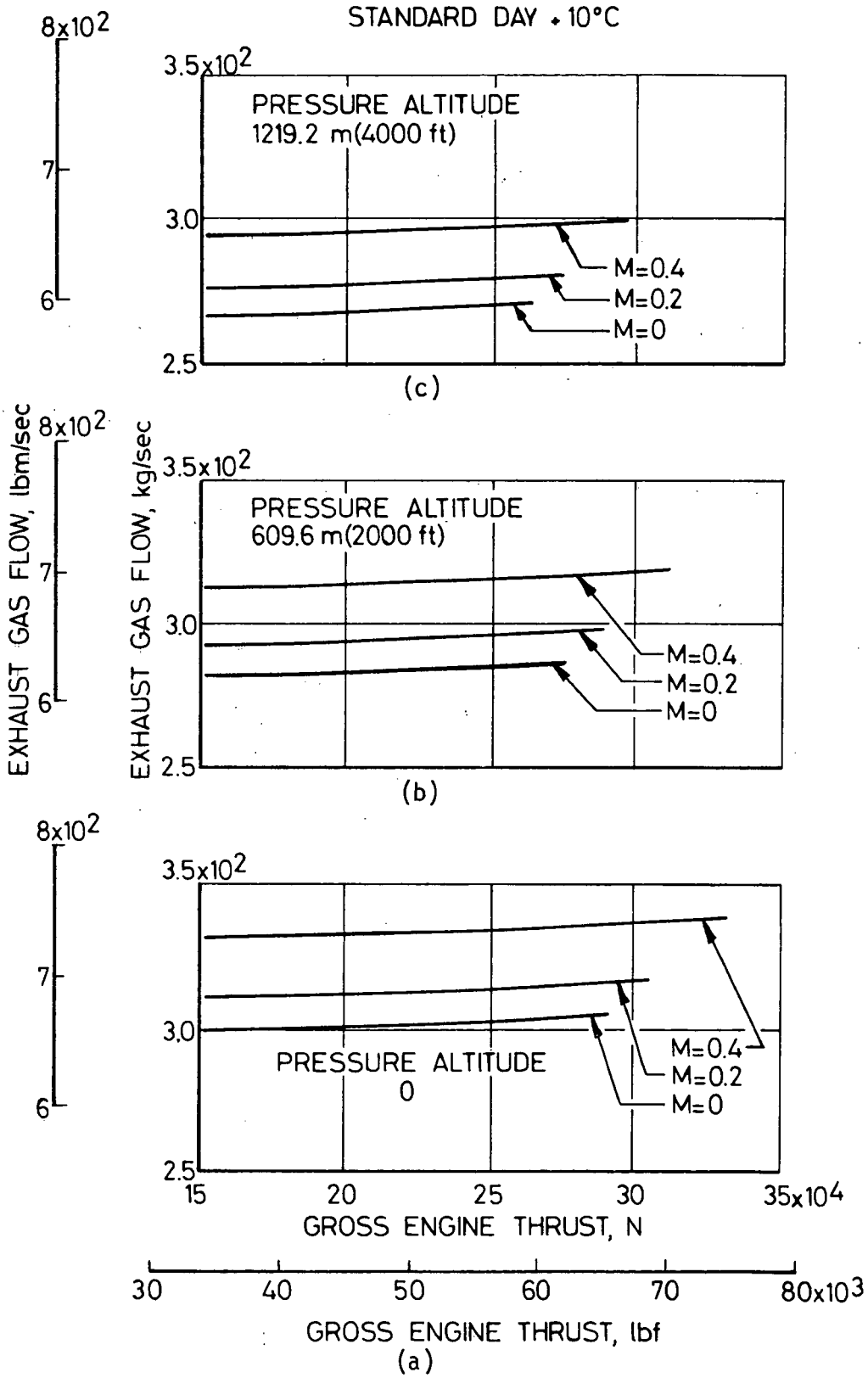

Figure 52 Installed Exhaust Gas Mass Flow for Takeoff and Part Power Cruise

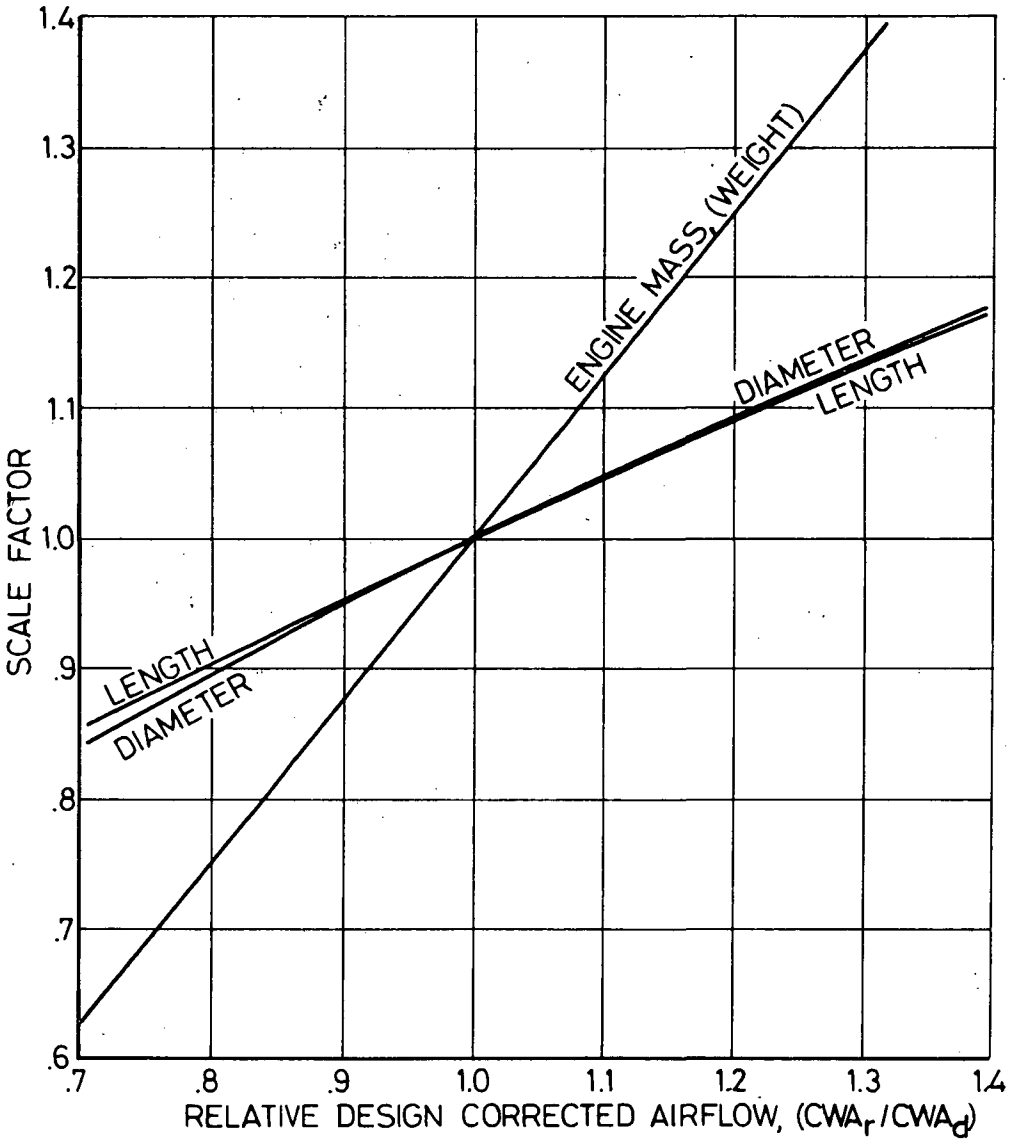

Figure 53 Engine and Nacelle Scaling Factors

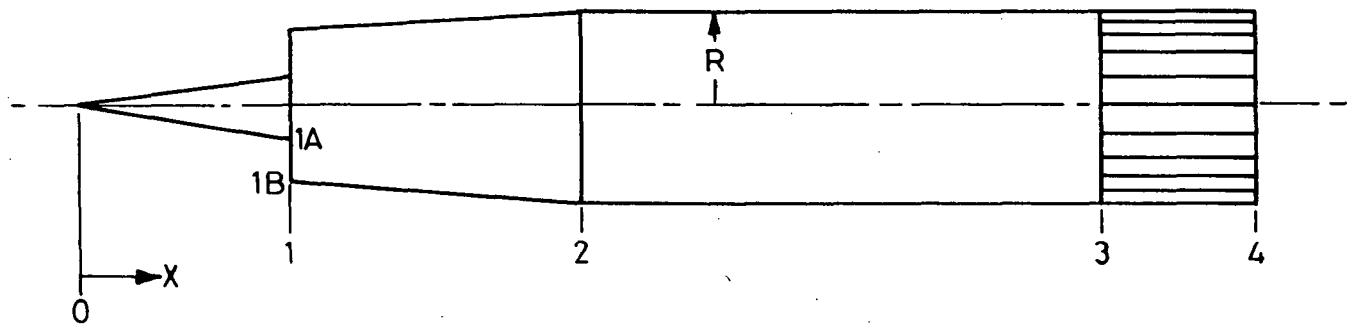

STATION NUMBER	X		R		AREA	
	m	in	m	in	m^2	ft^2
0	0	0	0	0	0	0
1A	2.050	80.7	.320	12.6	.32	3.45
1B	2.050	80.7	.855	33.7	2.30	24.73
2	5.870	231.1	1.052	41.4	3.48	37.43
3	12.499	492.1	1.052	41.4	3.48	37.43
4	13.932	548.5	1.052	41.4	3.48	37.43

Figure 54 AST-JP-2 Engine Nacelle

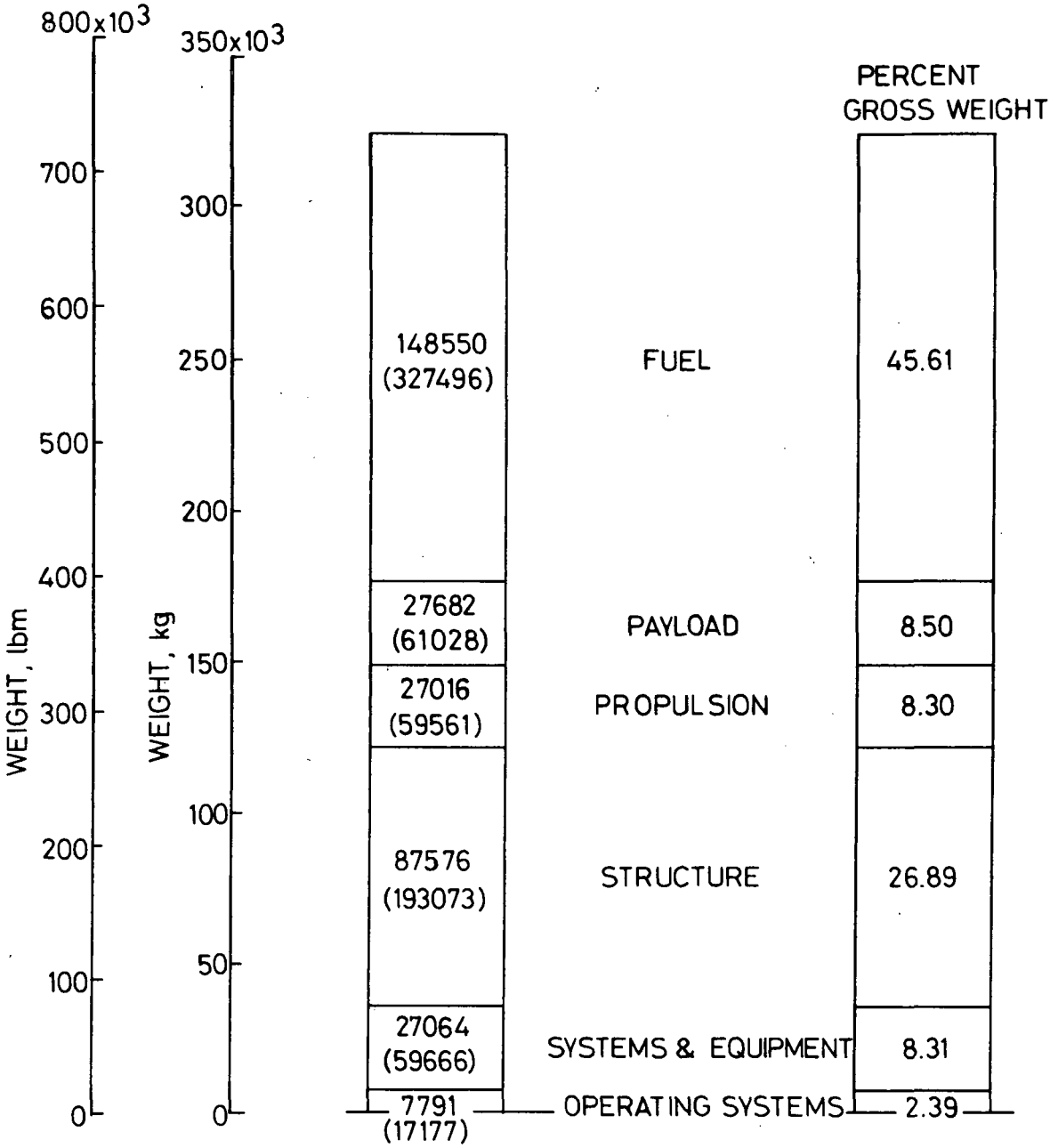

Figure 55 Gross Weight Breakdown

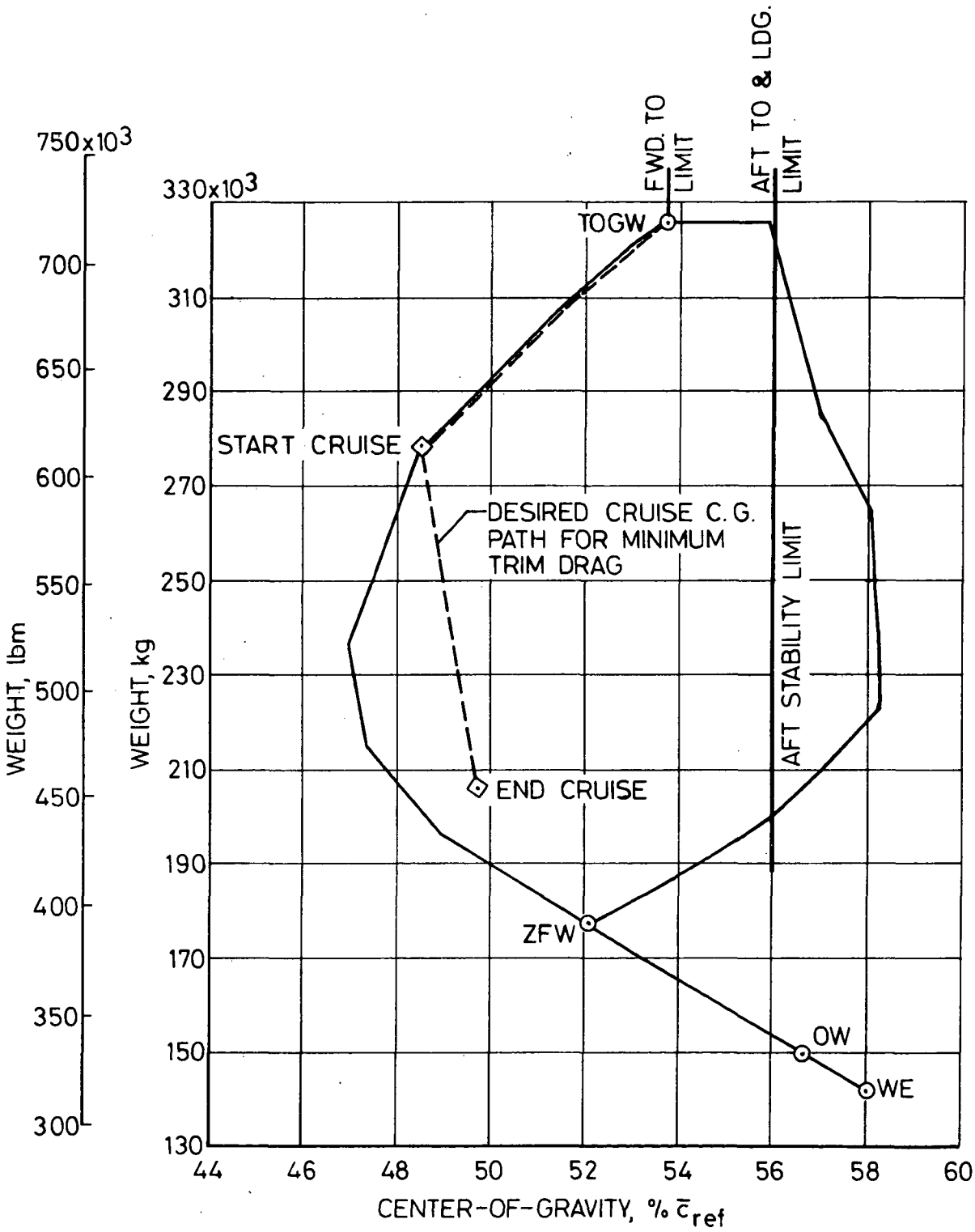

Figure 56 Center-of-gravity Travel Diagram

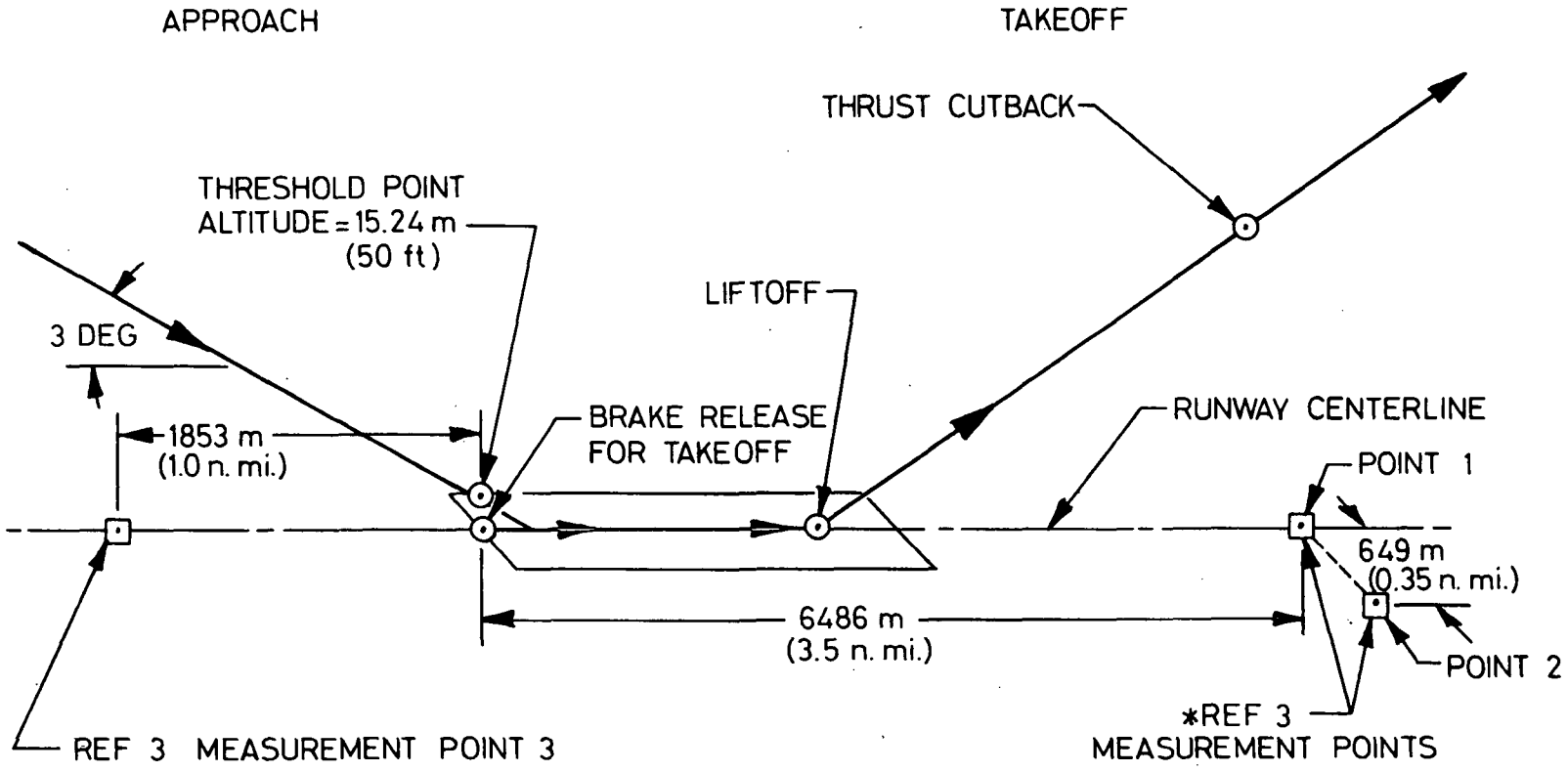

*NOTE: SIDELINE NOISE IS MEASURED WHERE NOISE LEVEL AFTER LIFTOFF IS GREATEST

Figure 57 Noise Measurement Locations for Approach and Takeoff

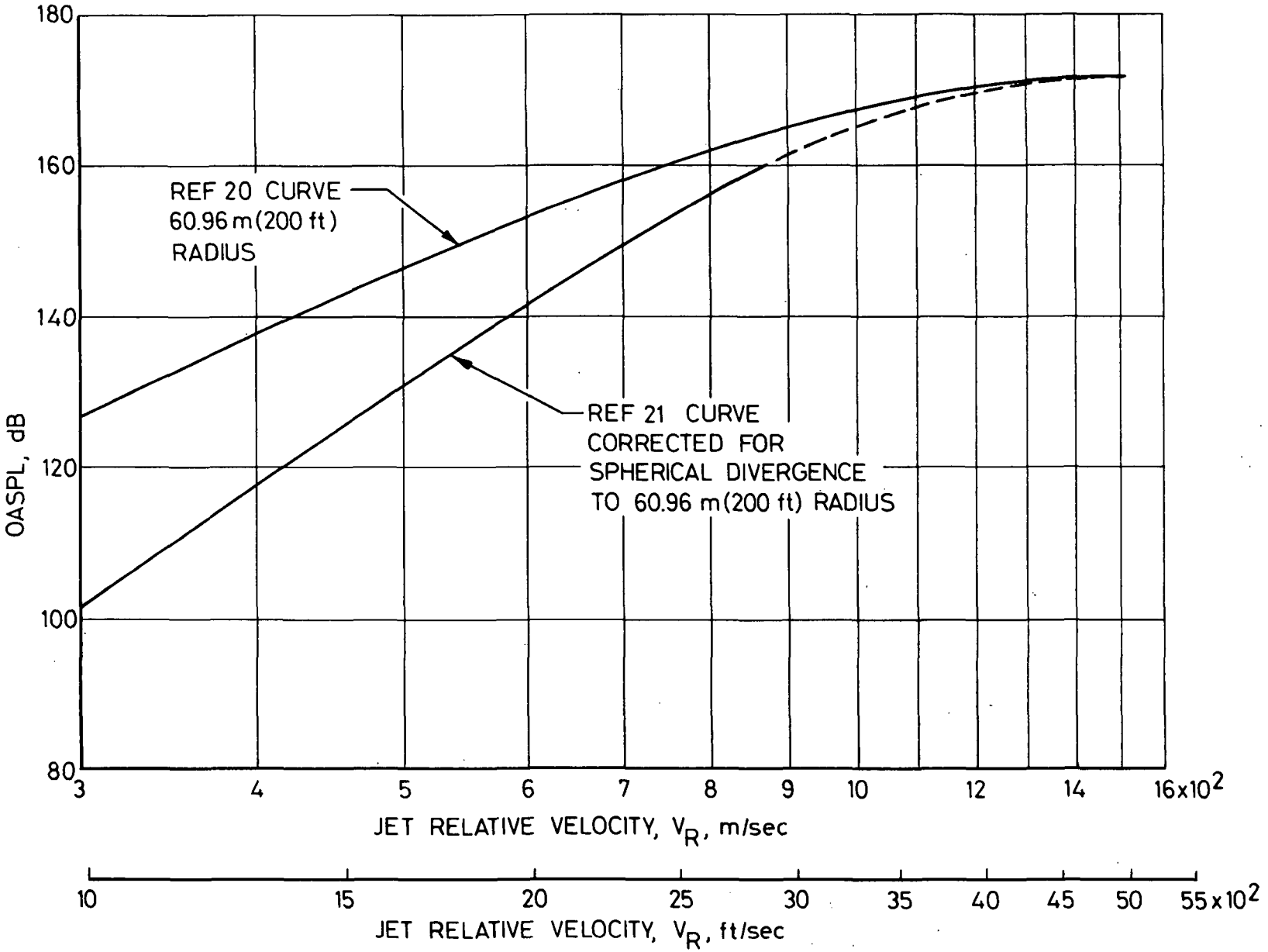

Figure 58 Overall Sound Pressure Level Variation With Jet Relative Velocity

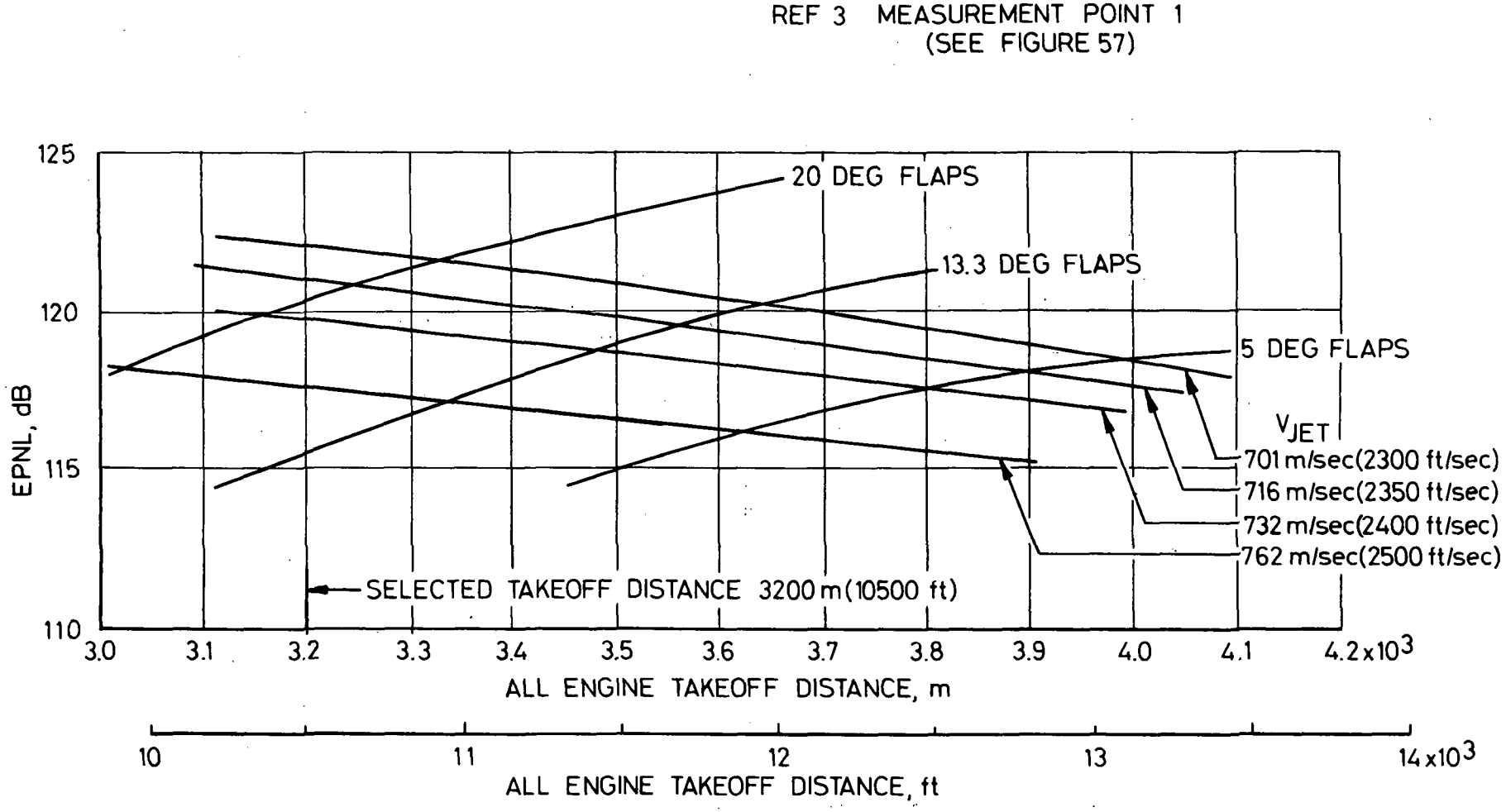

Figure 59 Runway Centerline Noise Level at 6486 m (3.5 n.mi.) Point From Brake Release

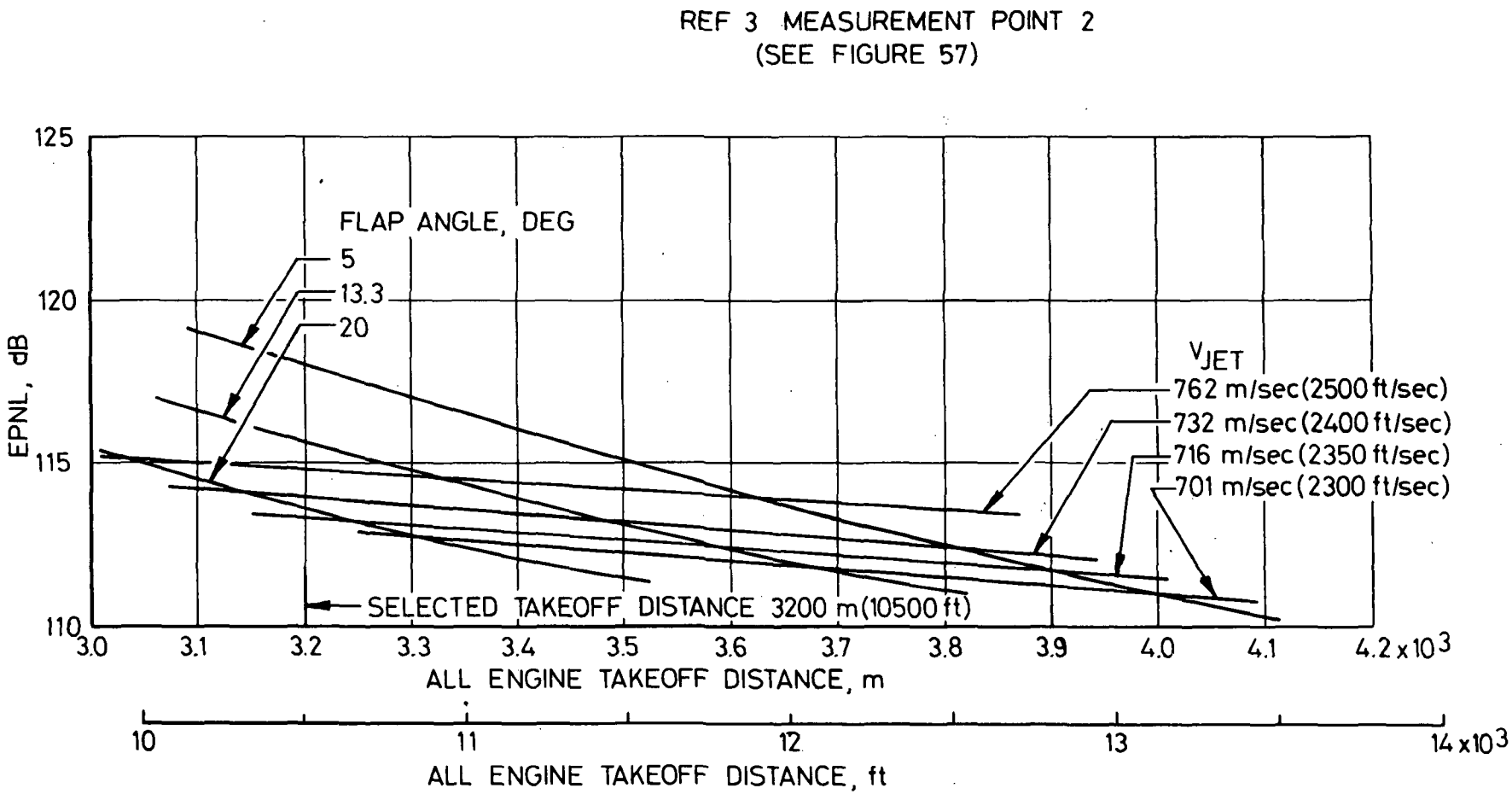

Figure 60 Maximum Sideline Noise Level at 649 m (0.35 n.mi.) From Runway Centerline

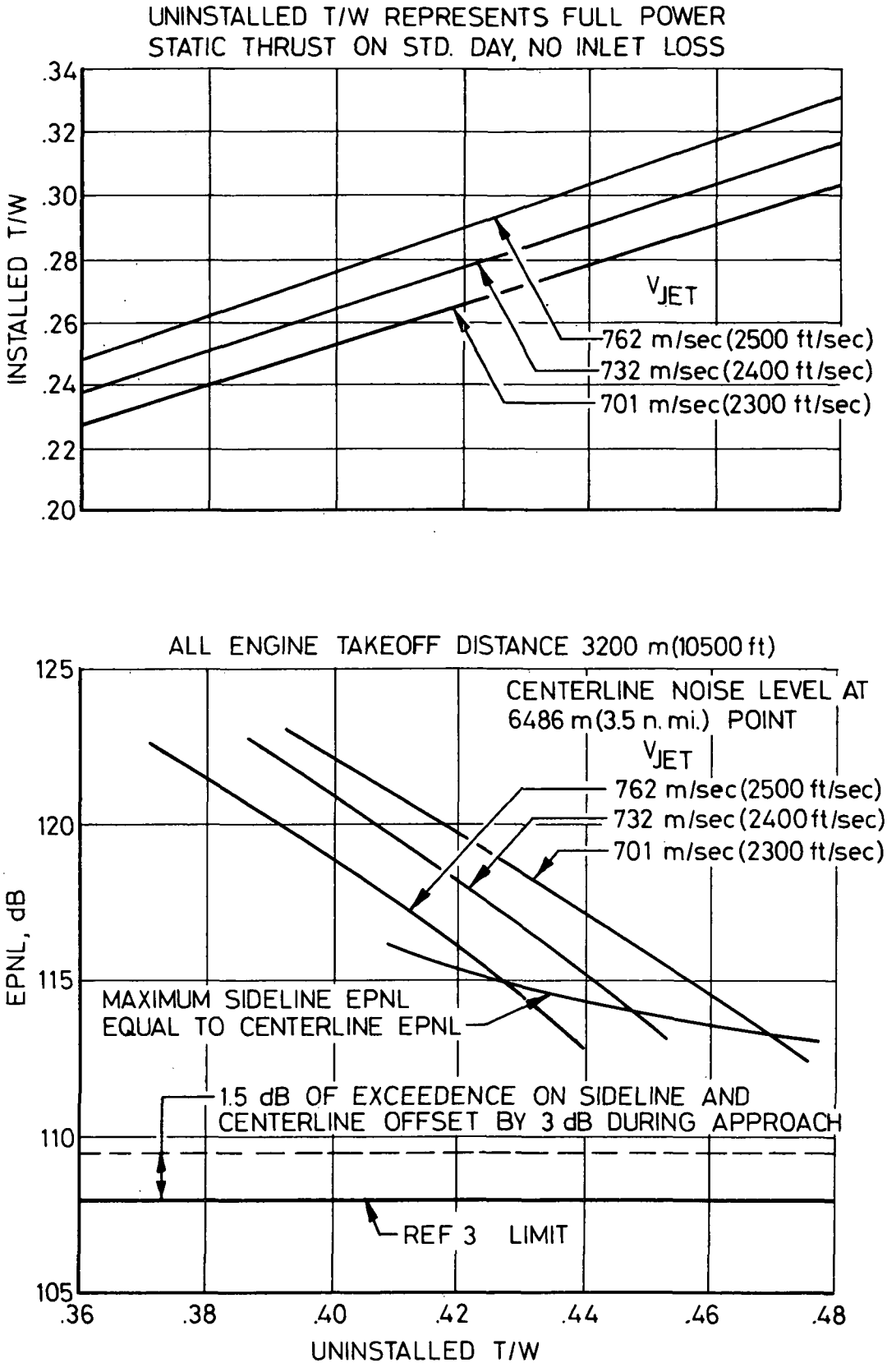

Figure 61 Takeoff Noise Level and Installed T/W Ratios for Uninstalled T/W Ratios

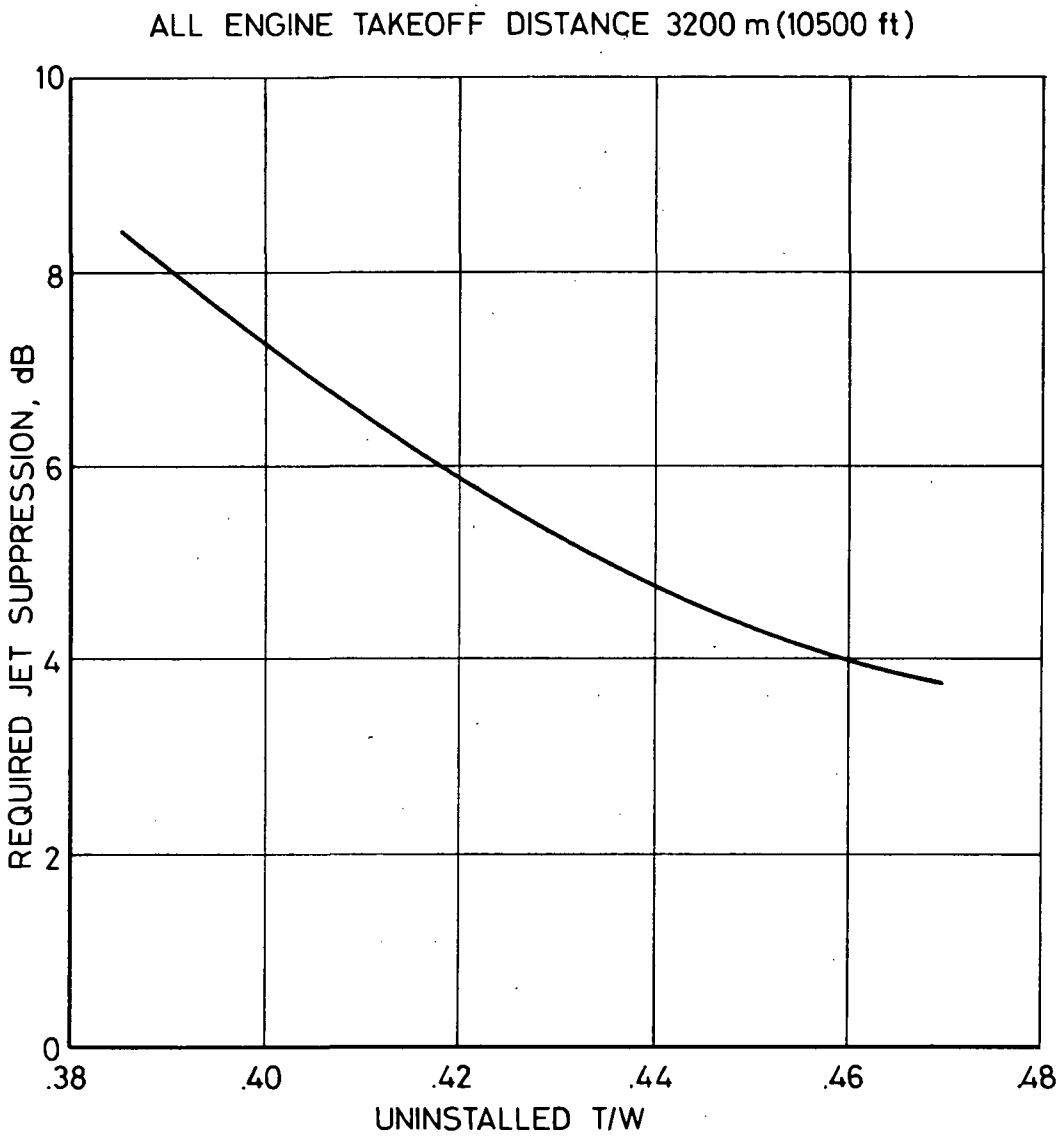

Figure 62 Required Suppression For Uninstalled T/W Ratios

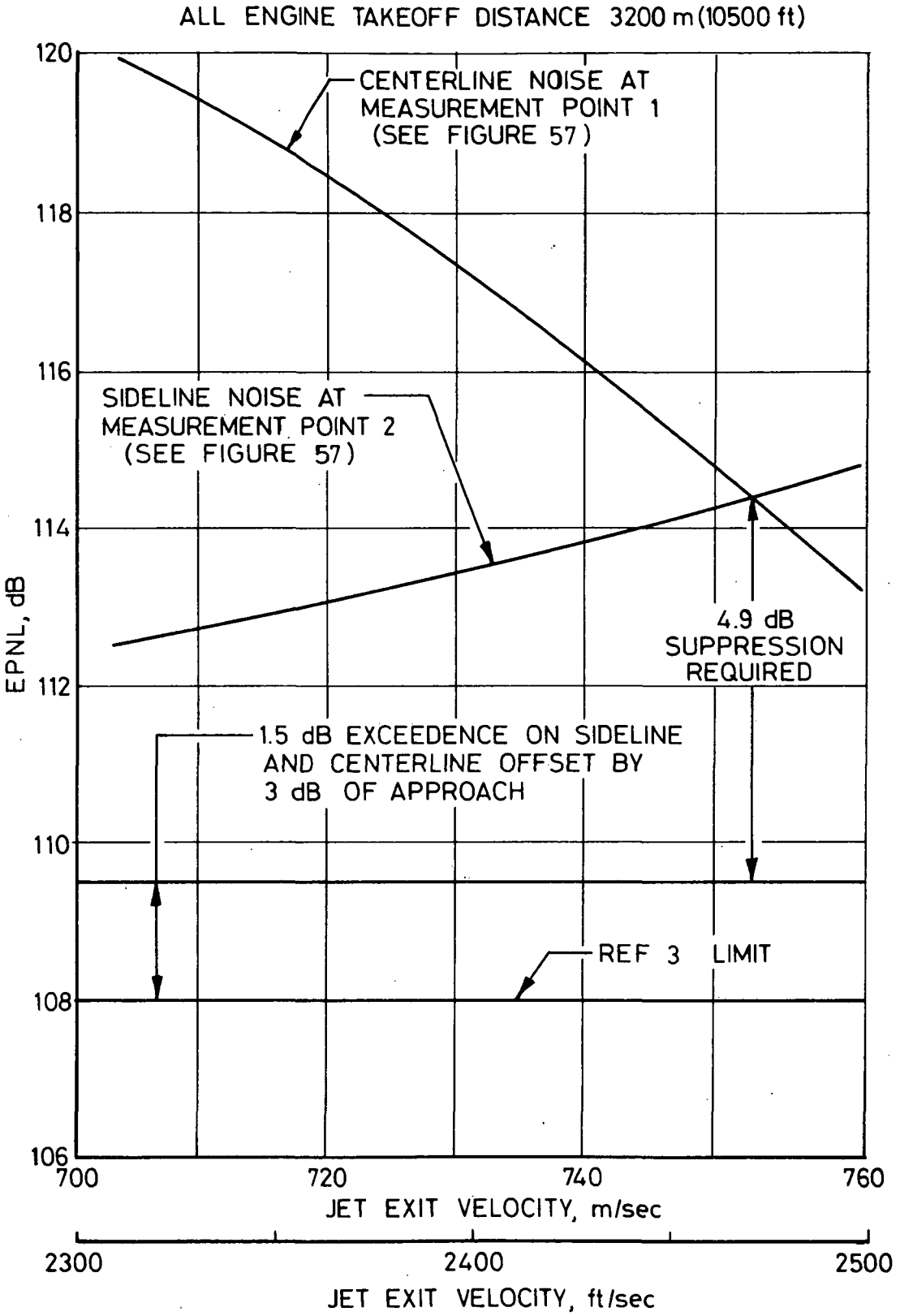

Figure 63 Variation of Effective Perceived Noise Level with Jet Velocity

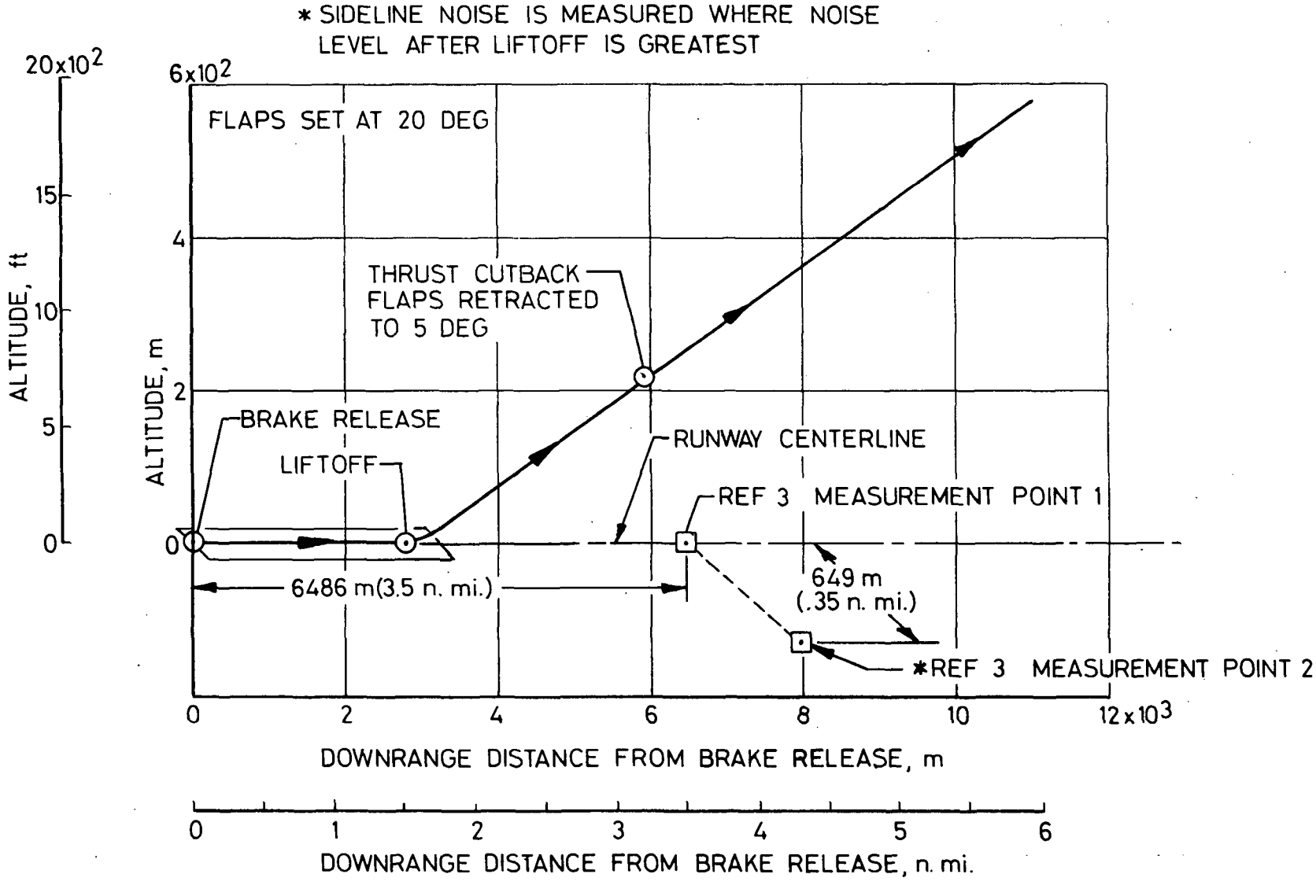

Figure 64 Takeoff Profile

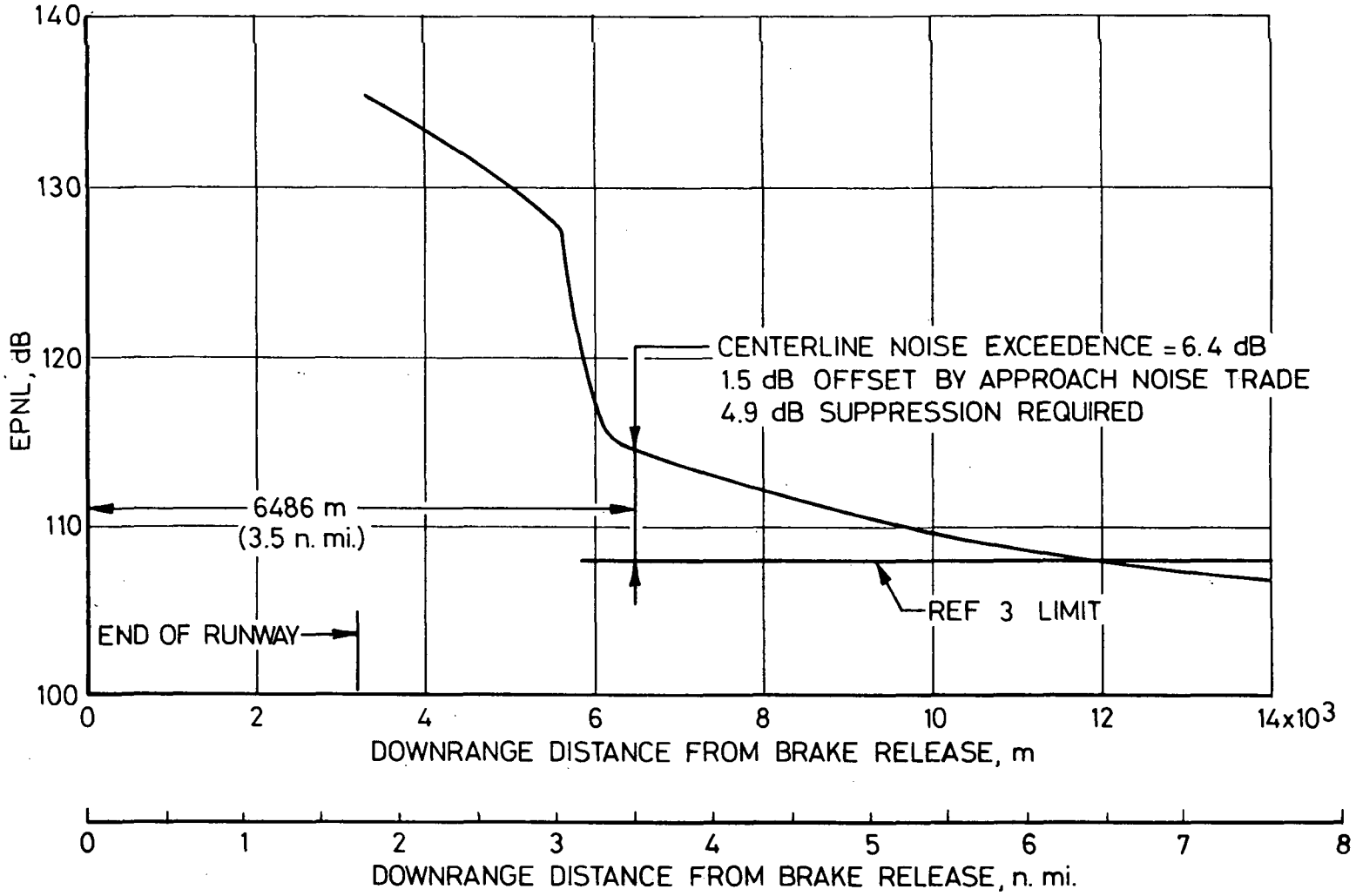

Figure 65 Effective Perceived Noise Level Along Runway Centerline During Takeoff

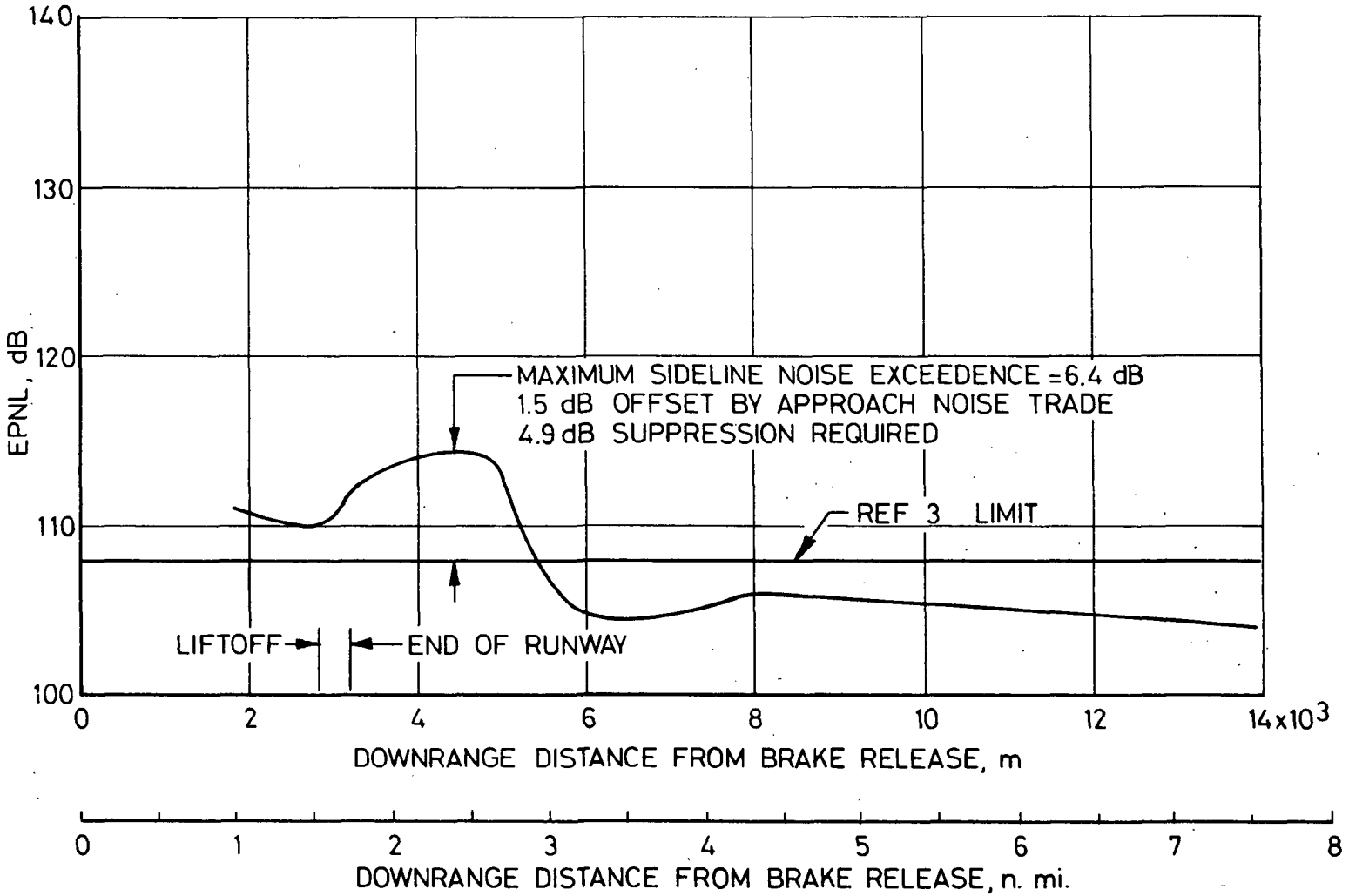

Figure 66 Effective Perceived Noise Level Along Sideline During Takeoff

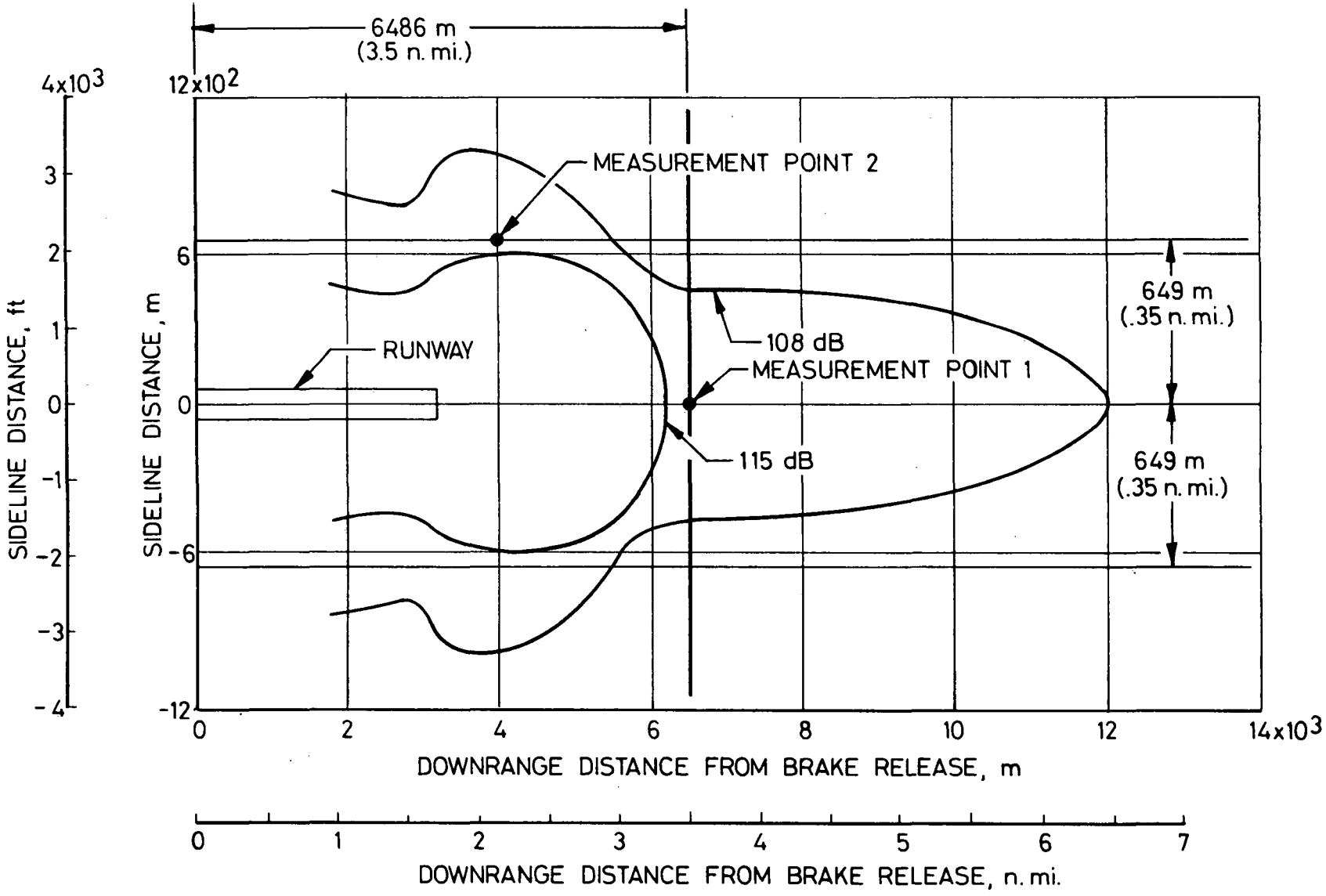

Figure 67 Constant Effective Perceived Noise Levels During Takeoff

JET EPNL AT MEASUREMENT POINT 3 = 103.1 dB
AIRFRAME OASPL AT MEASUREMENT POINT 3=107 dB

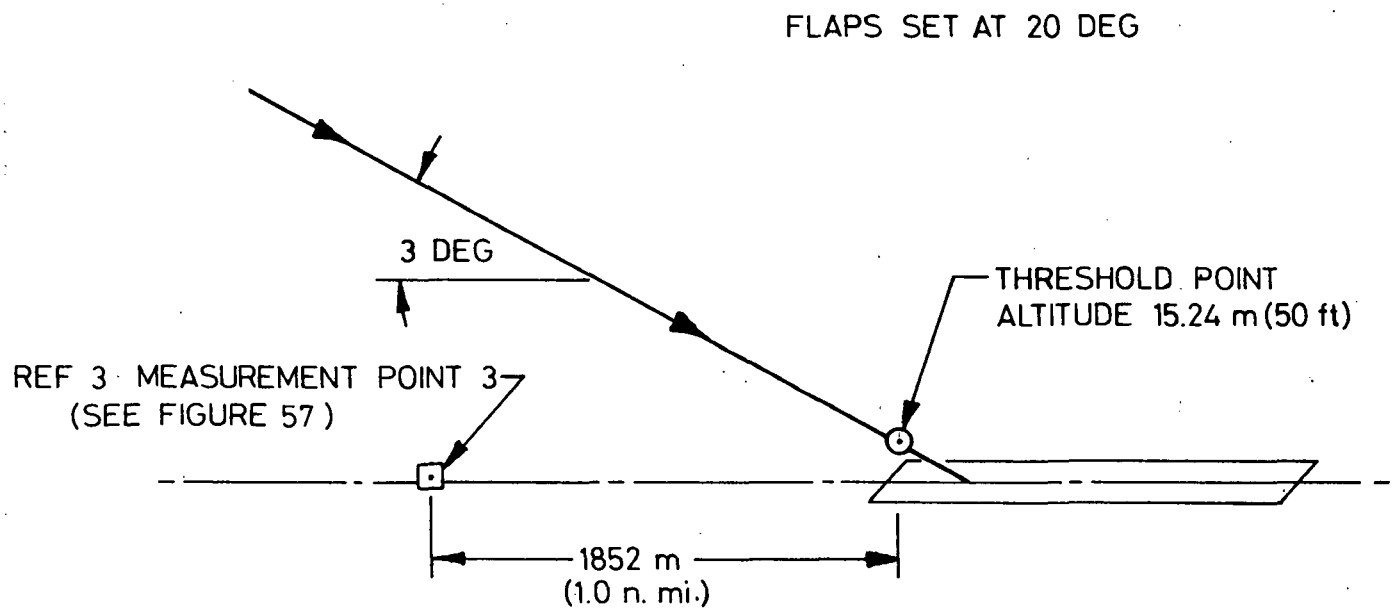

Figure 68 Landing Profile and Approach Noise

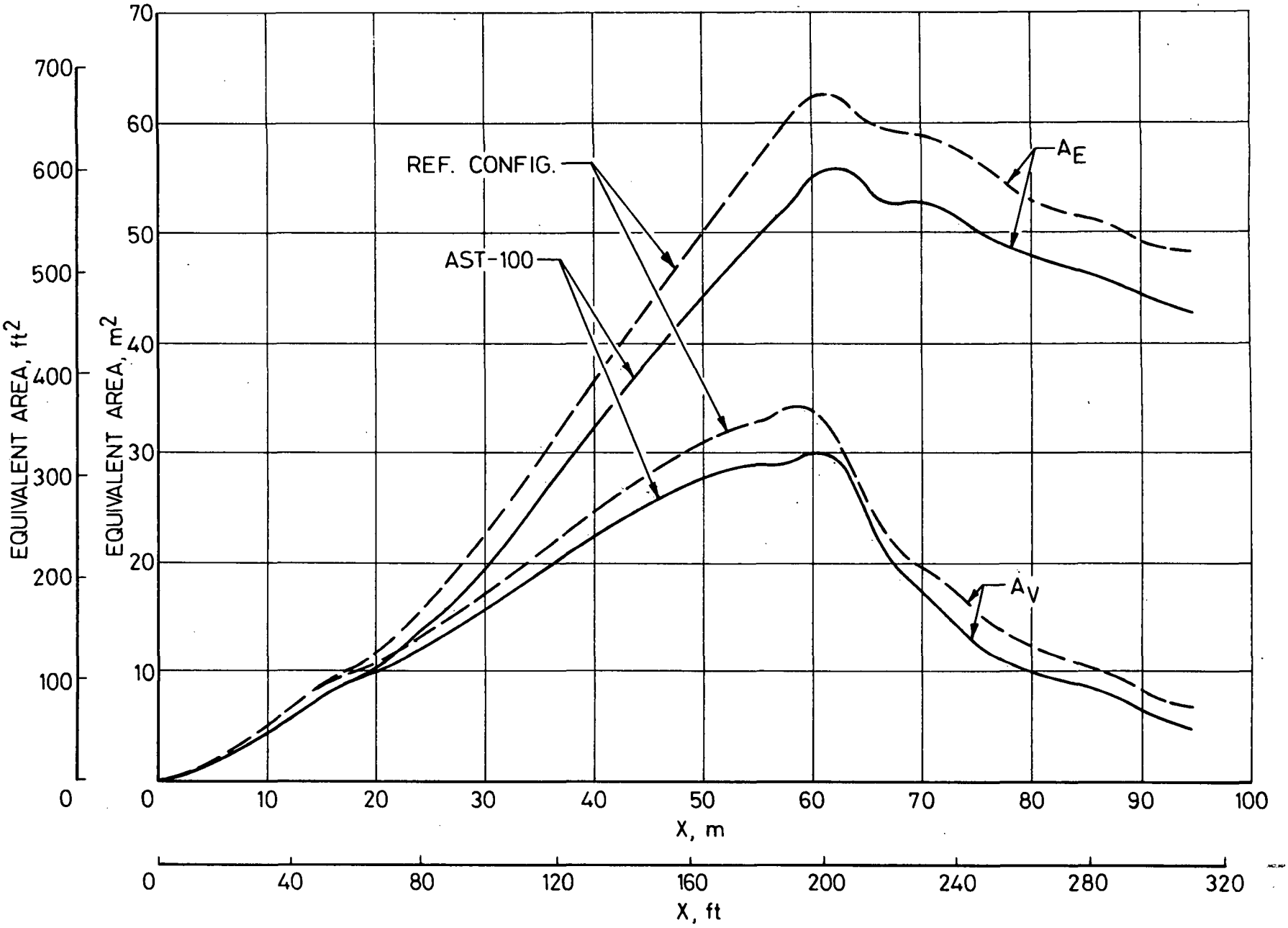

Figure 69 Equivalent Area Distribution at M = 1.175

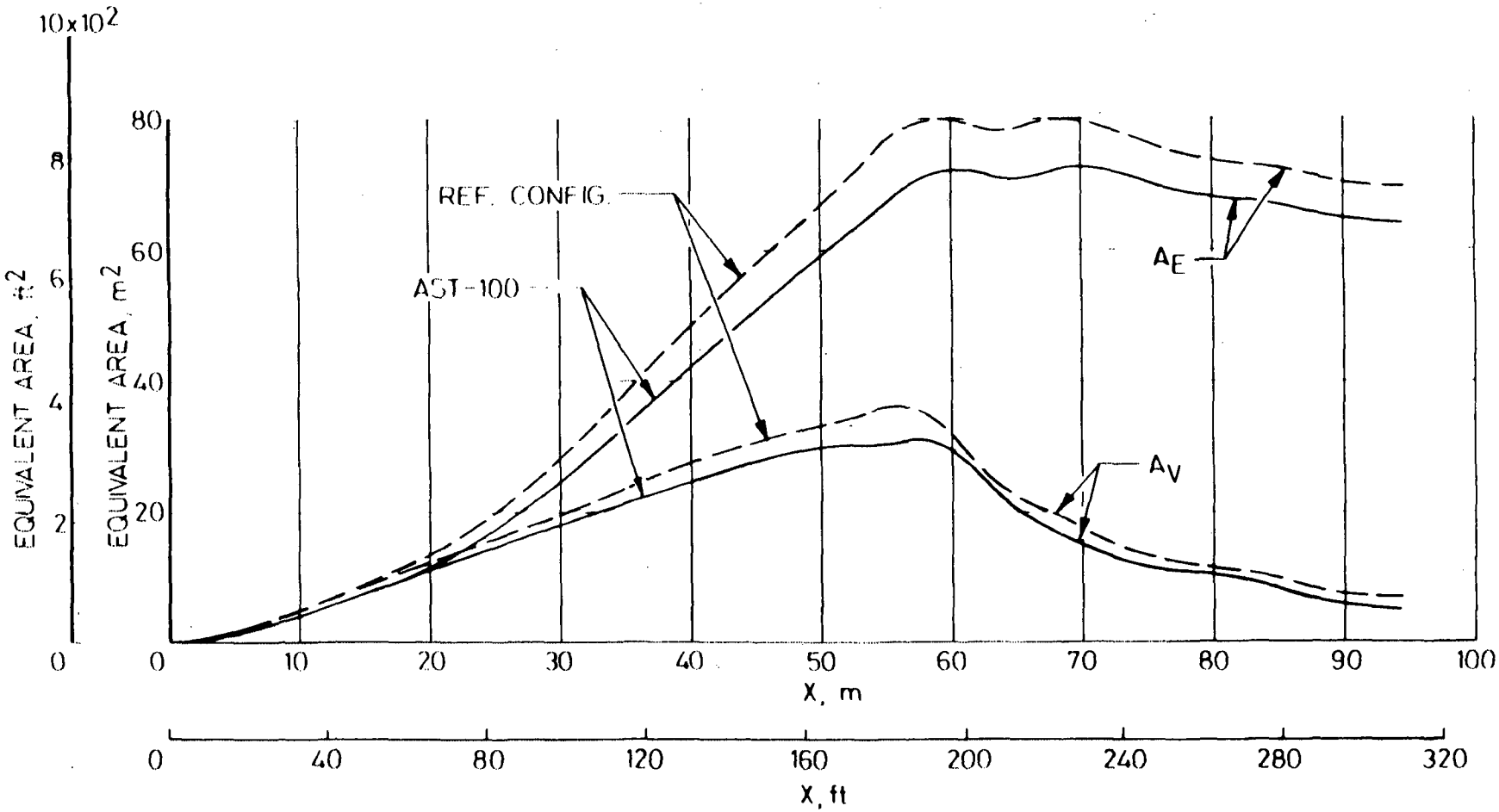

Figure 70 Equivalent Area Distribution at M = 1.6

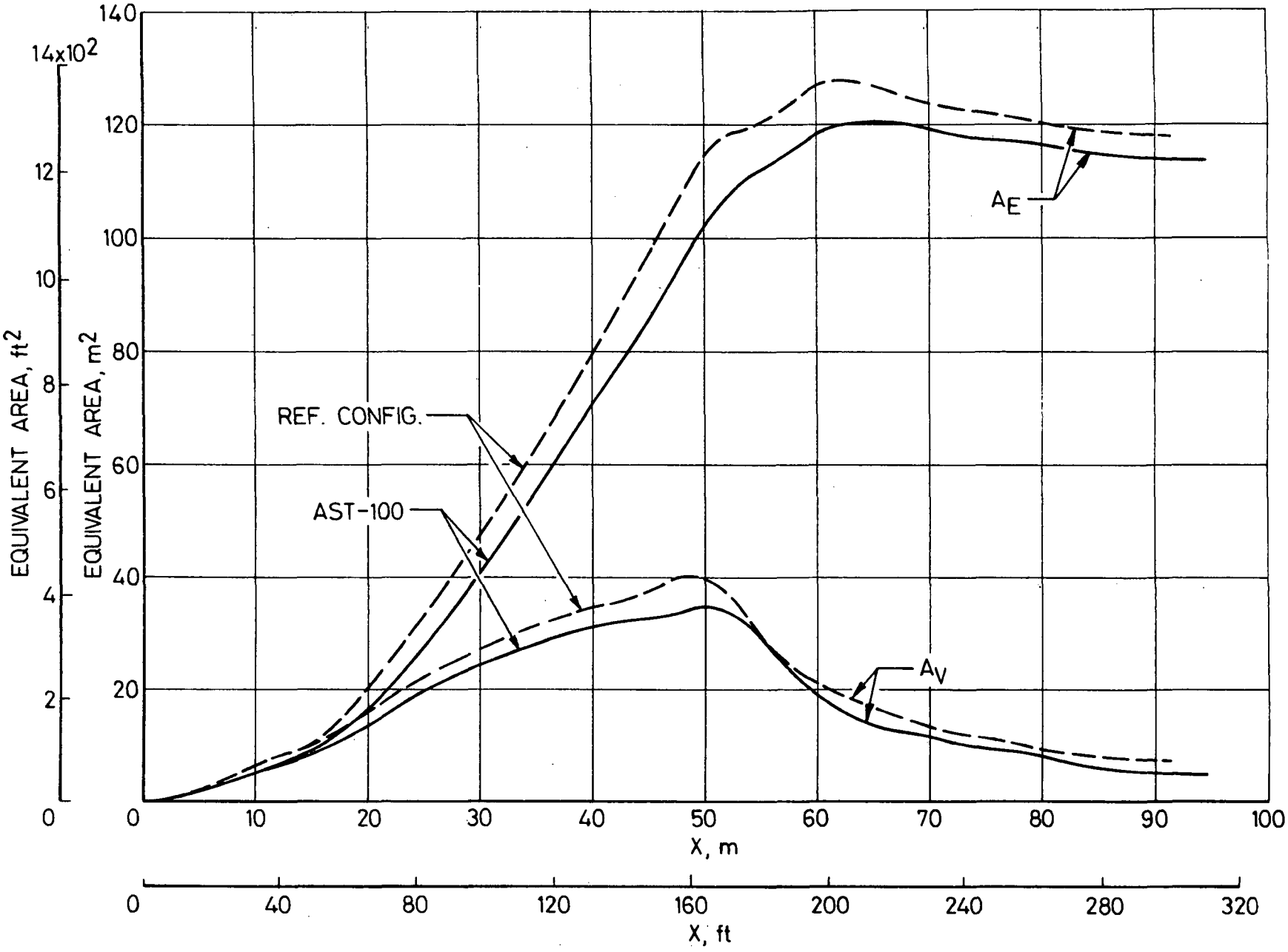

Figure 71 Equivalent Area Distribution at Start of Cruise

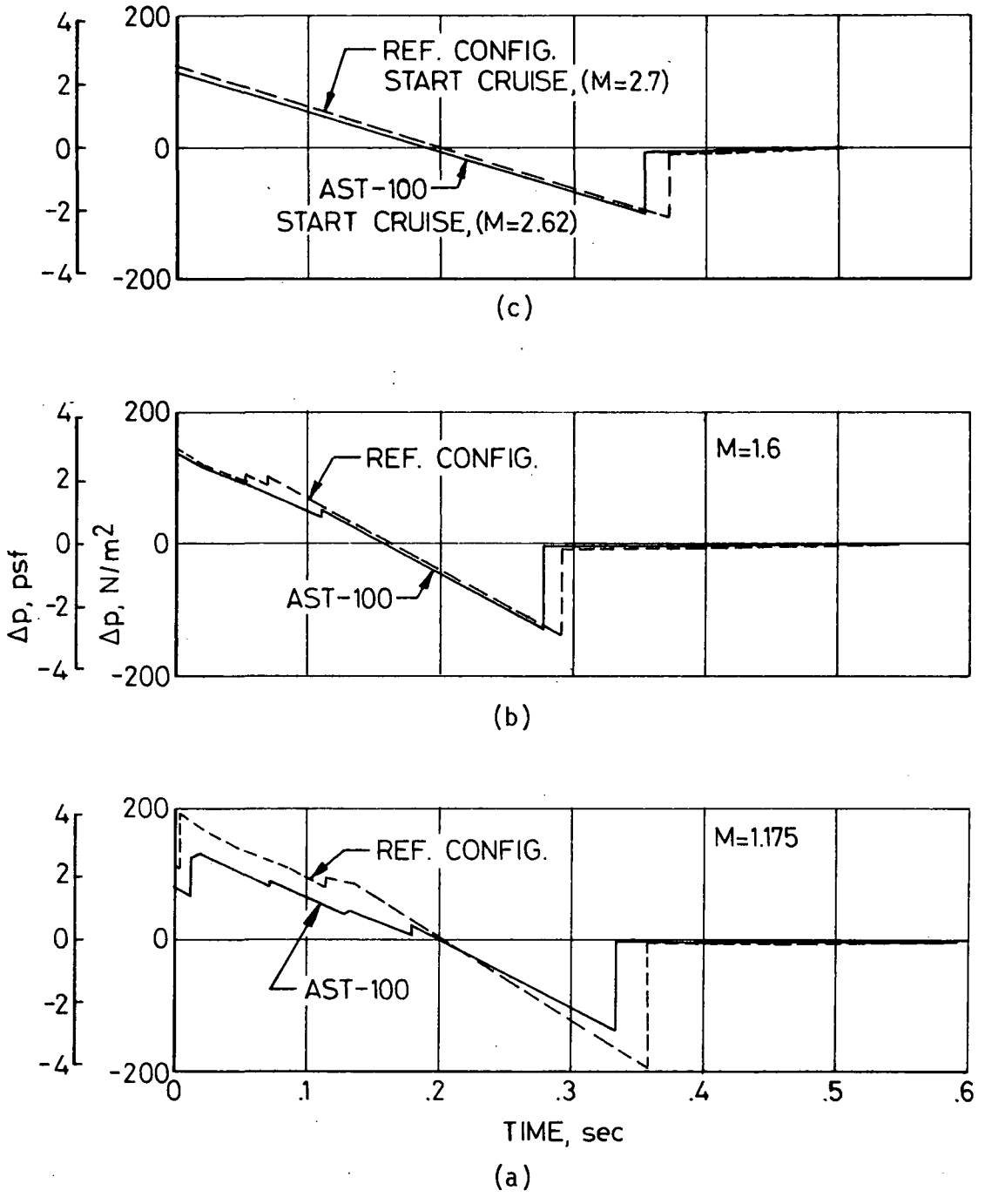

Figure 72 Sonic Boom Signatures

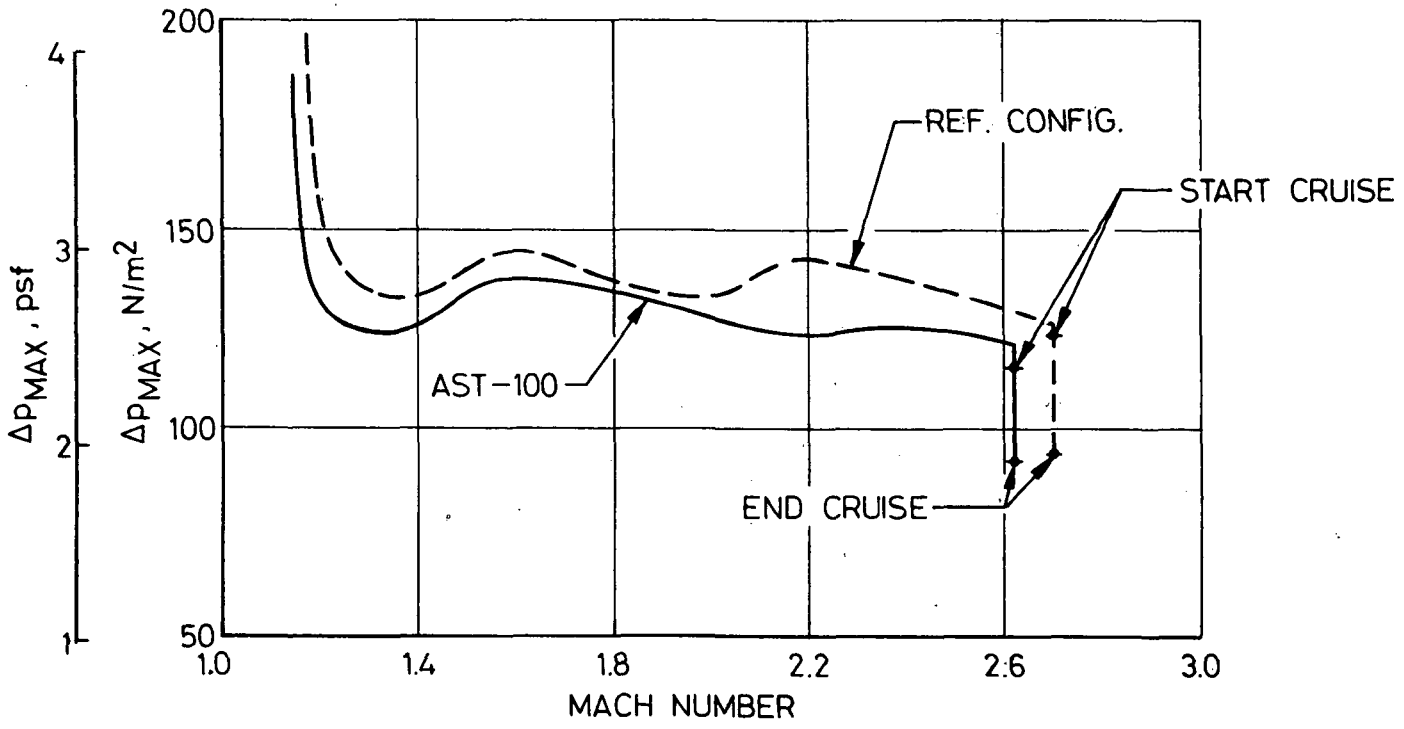

Figure 73 Maximum Overpressures During Climb and Cruise

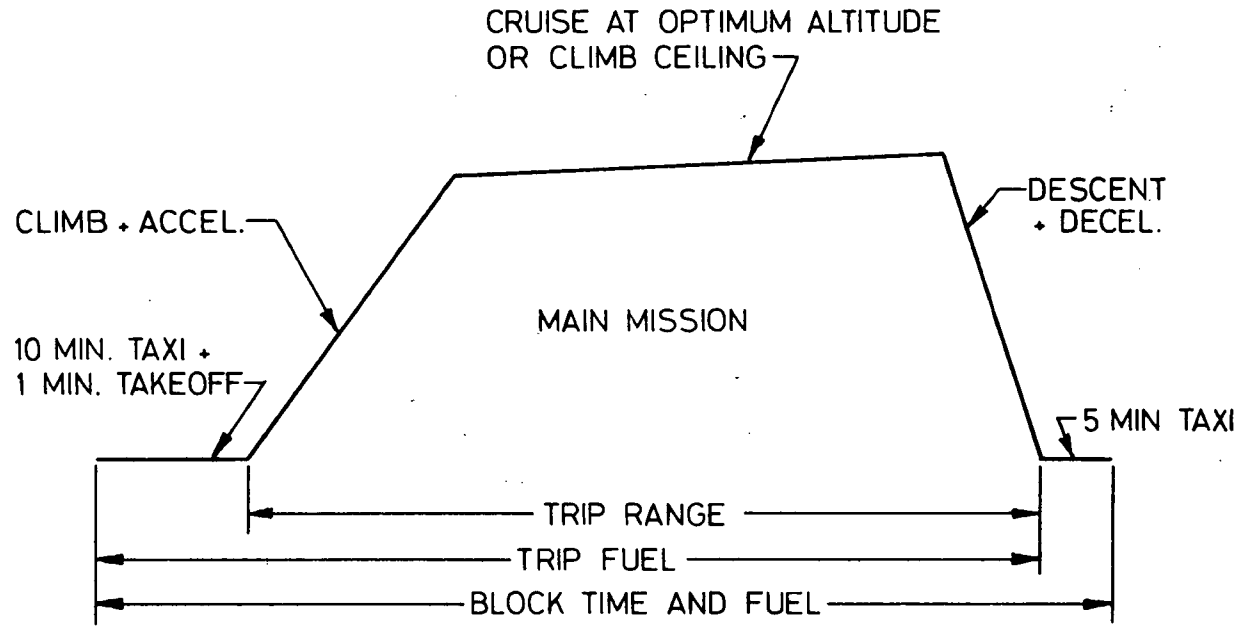

NOTE : C.A.B. RANGE = TRIP RANGE MINUS TRAFFIC ALLOWANCE
AS SPECIFIED FOR SUPERSONIC AIRCRAFT

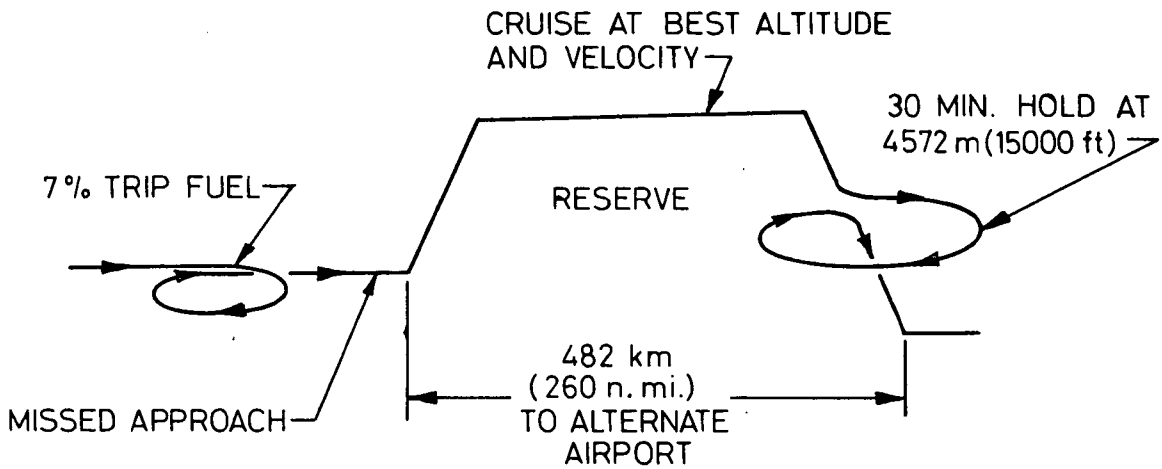

Figure 74 Mission Profile and Reserves

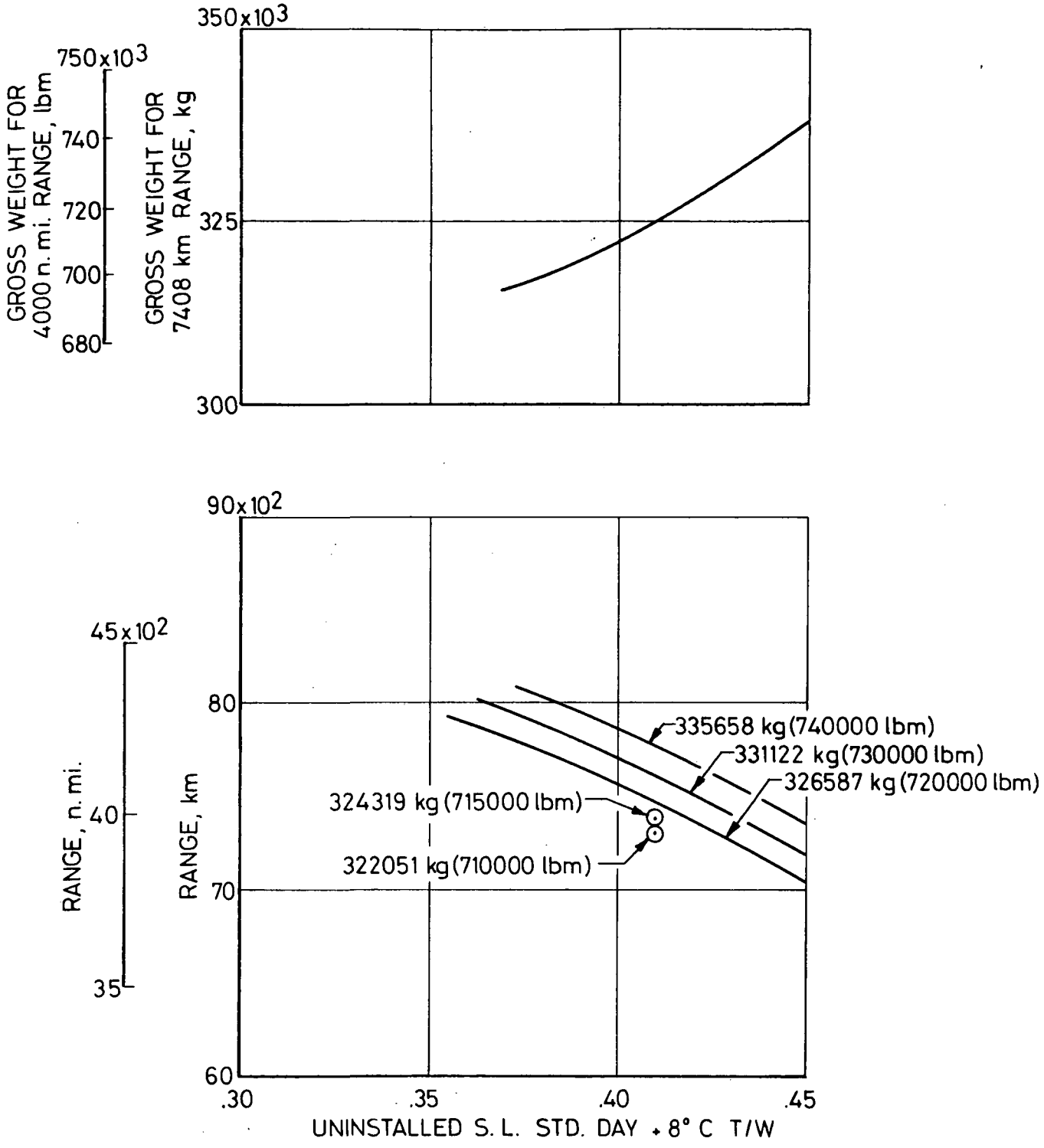

Figure 75 Effect of T/W (Uninstalled) on Range For Various Takeoff Gross Weights

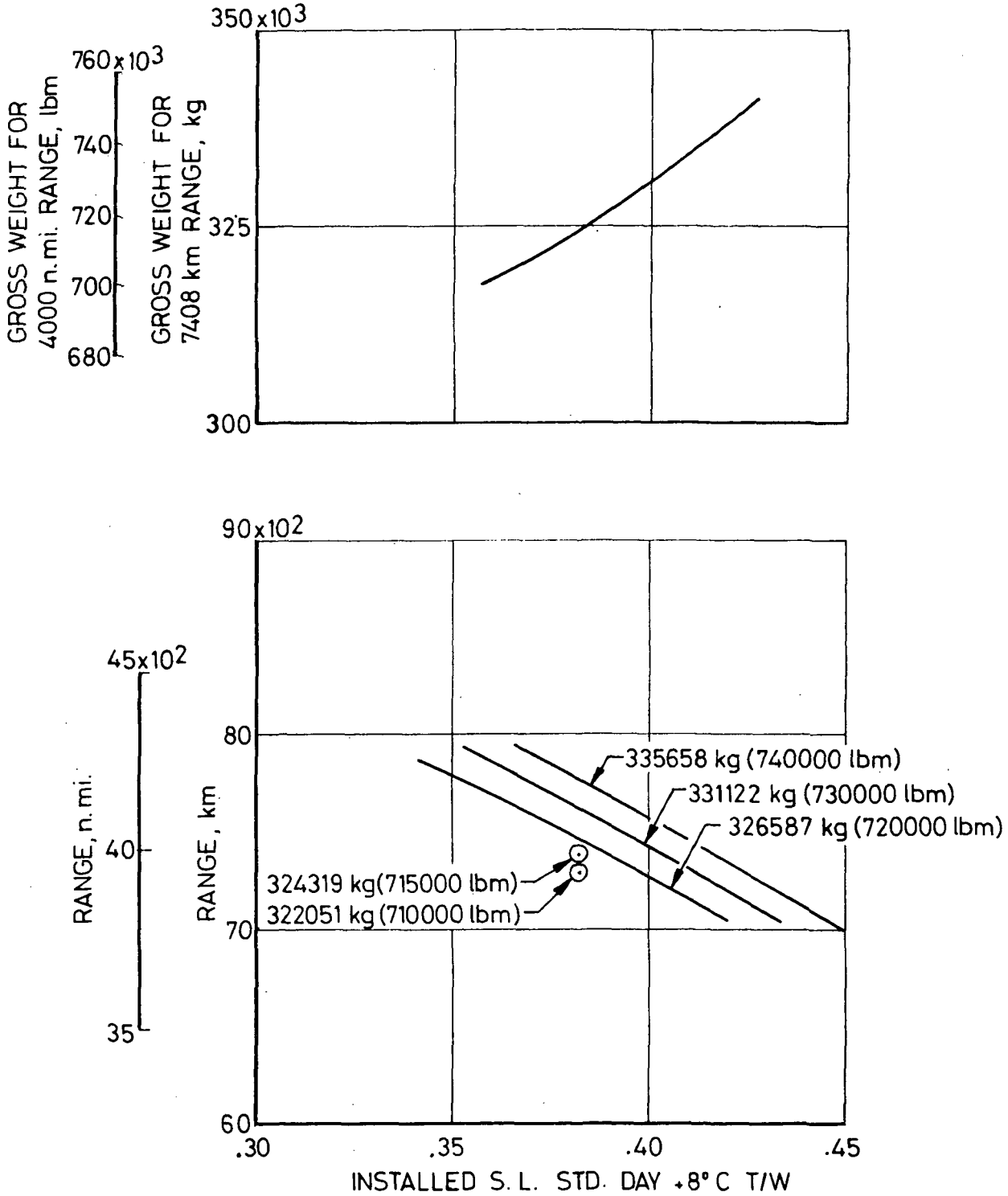

Figure 76 Effect of T/W (Installed) on Range for Various Takeoff Gross Weights

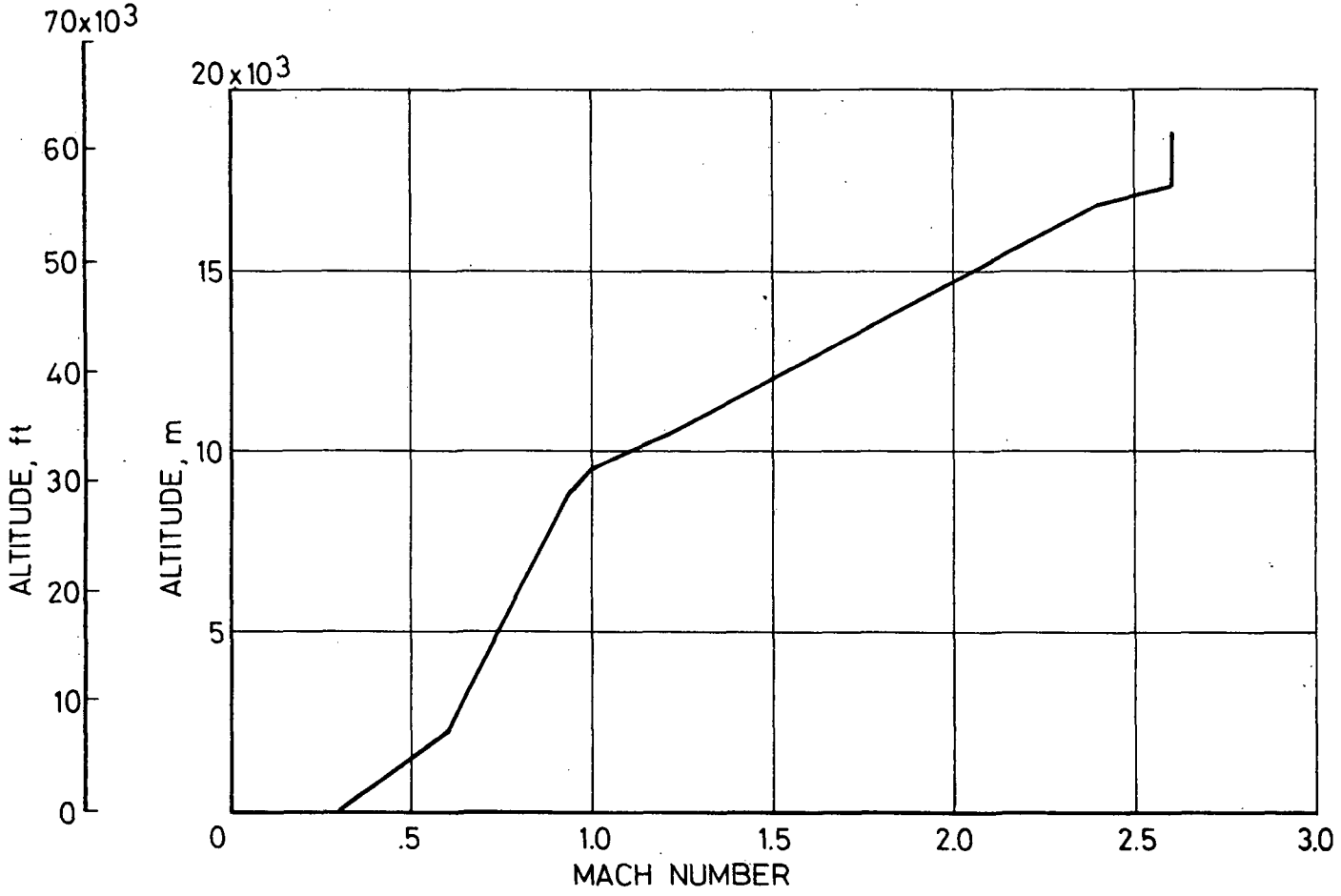

Figure 77 Climb Speed Schedule

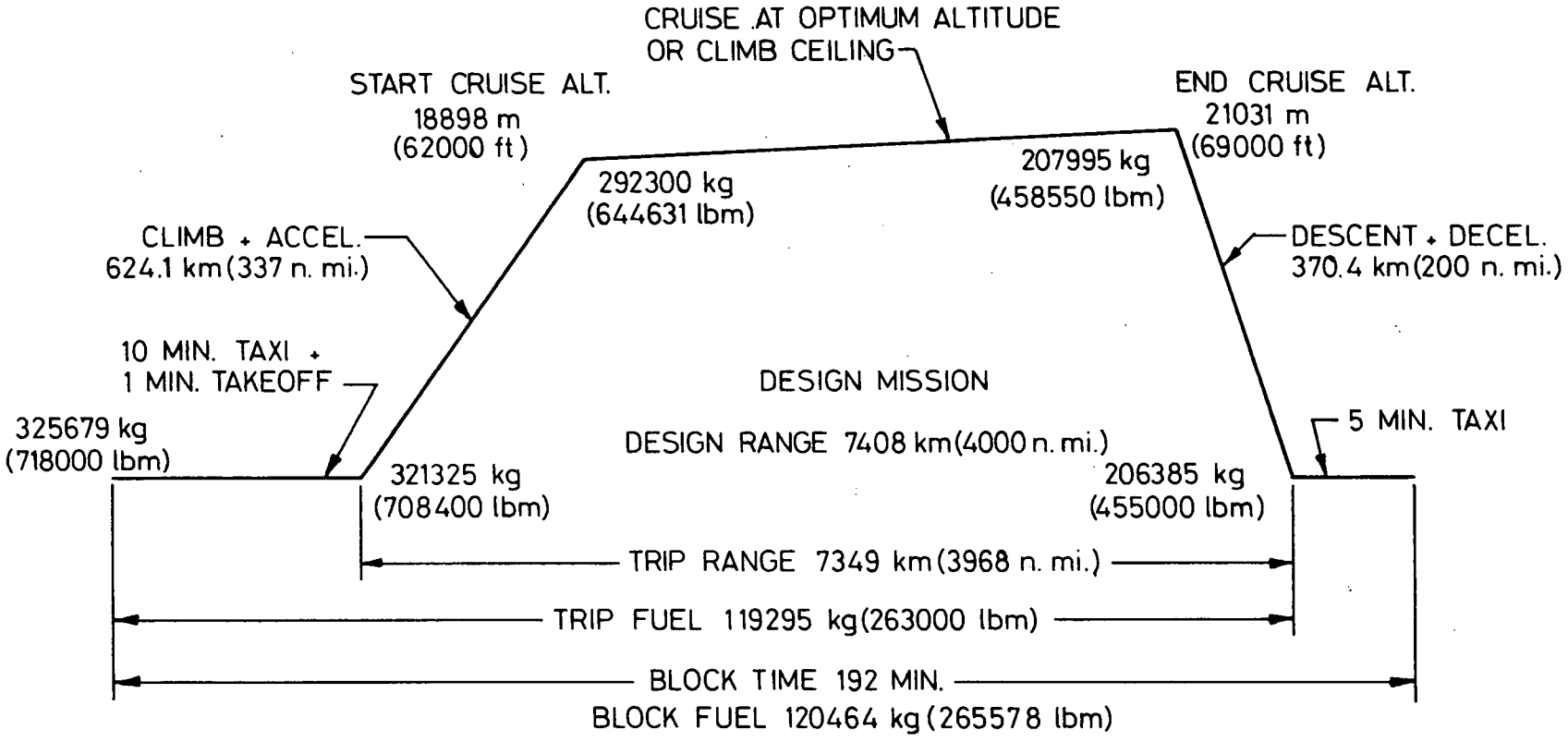

NOTE: C.A.B. RANGE = TRIP RANGE MINUS TRAFFIC ALLOWANCE
AS SPECIFIED FOR SUPERSONIC AIRCRAFT

Figure 78 Design Mission Performance Profile

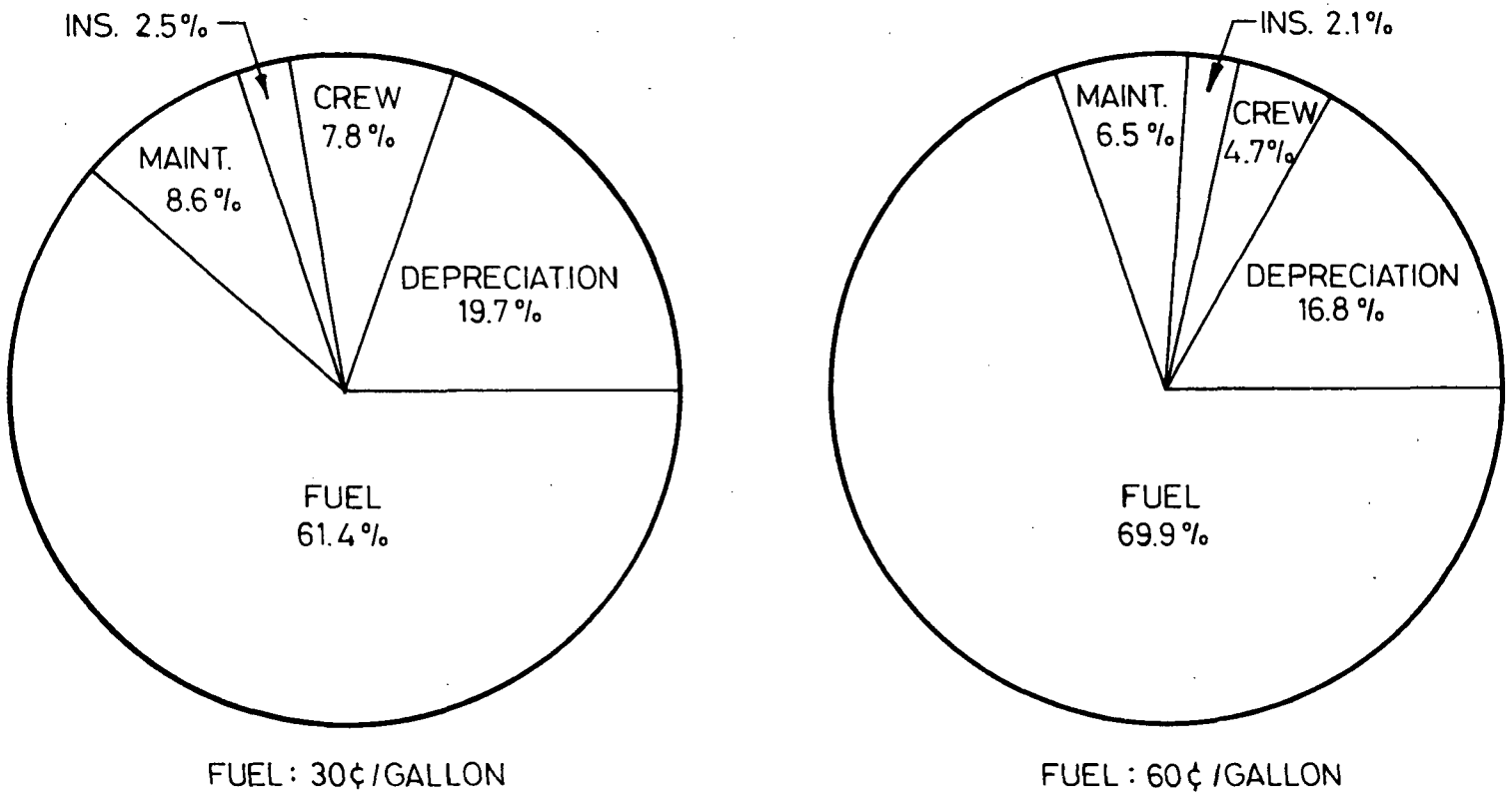

Figure 79 Direct Operating Cost Breakdown

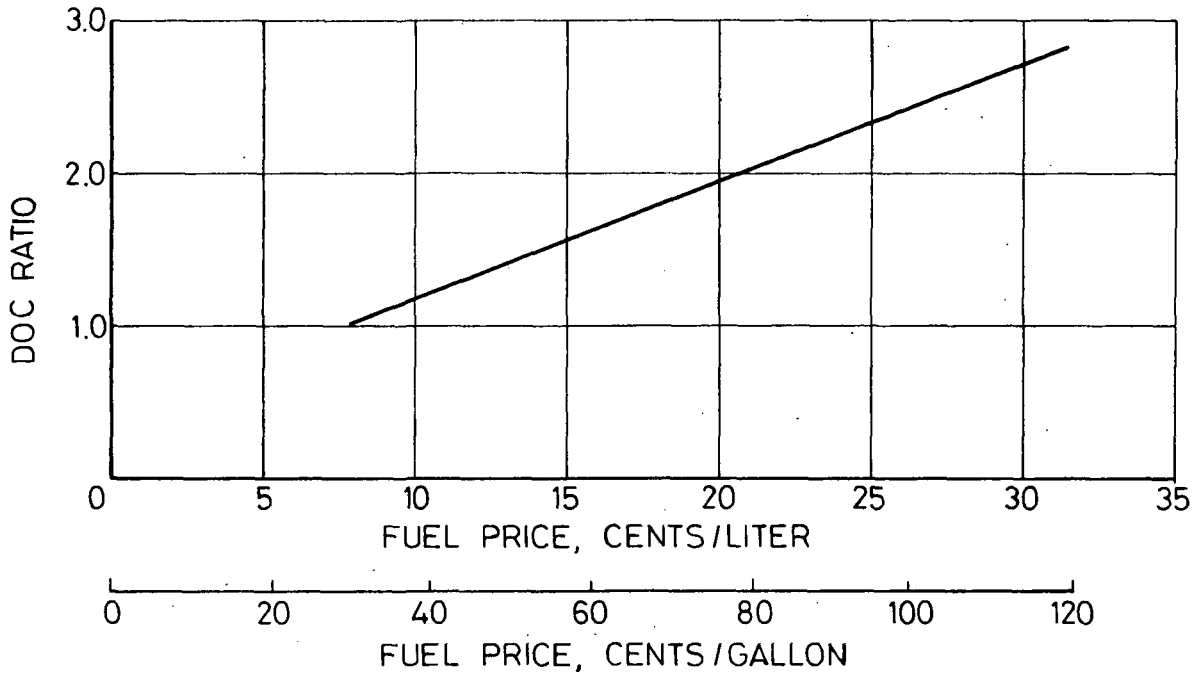

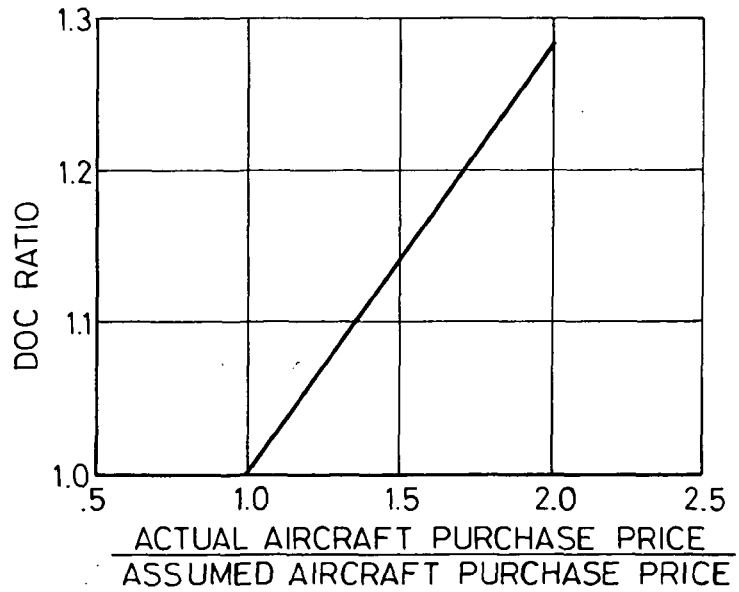

Figure 80 Direct Operating Cost Sensitivity

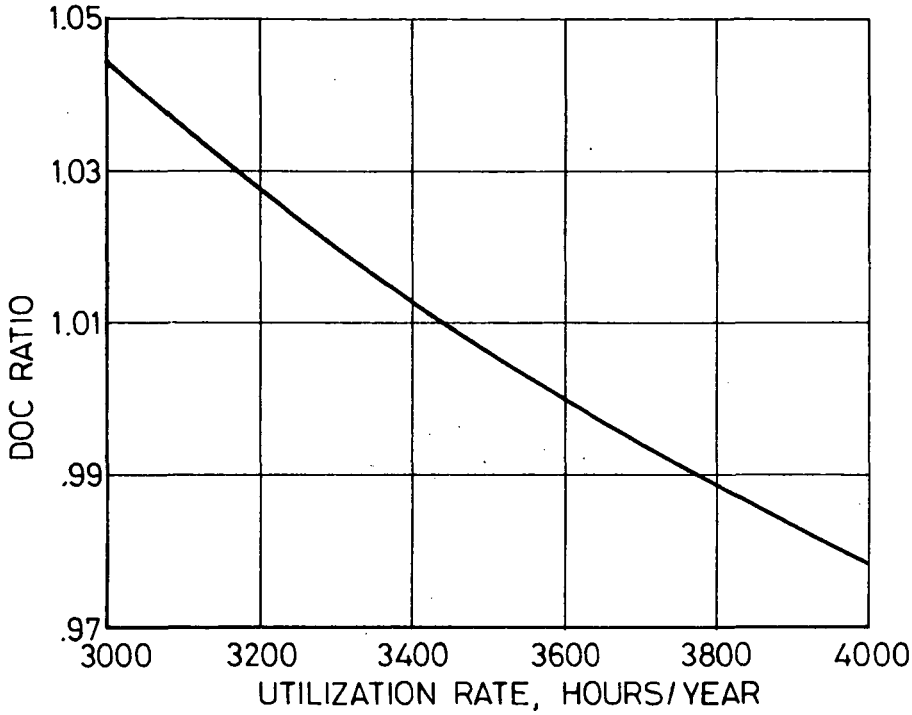

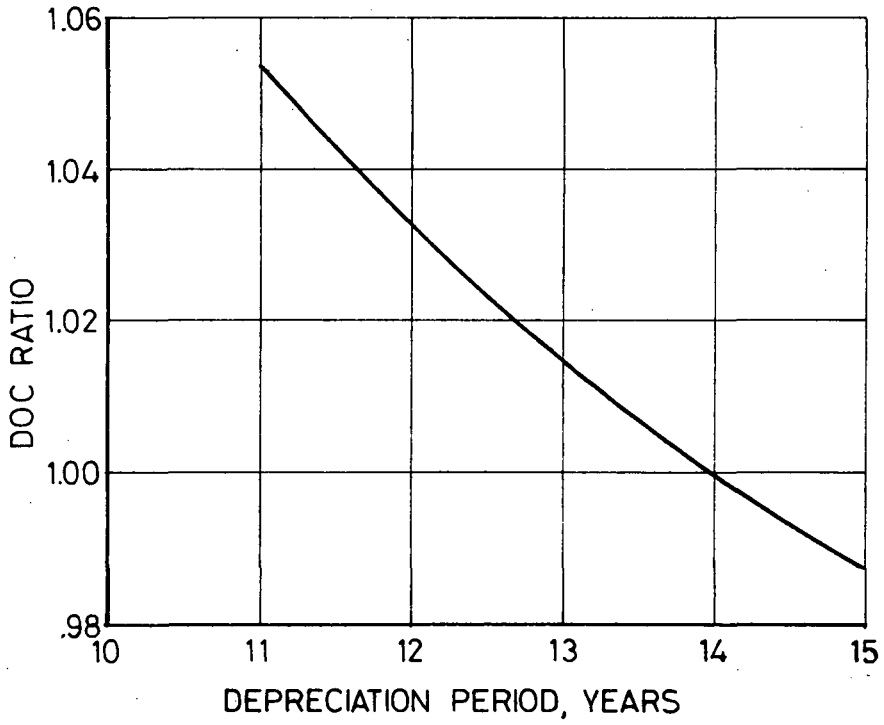

Figure 80 (Concluded)

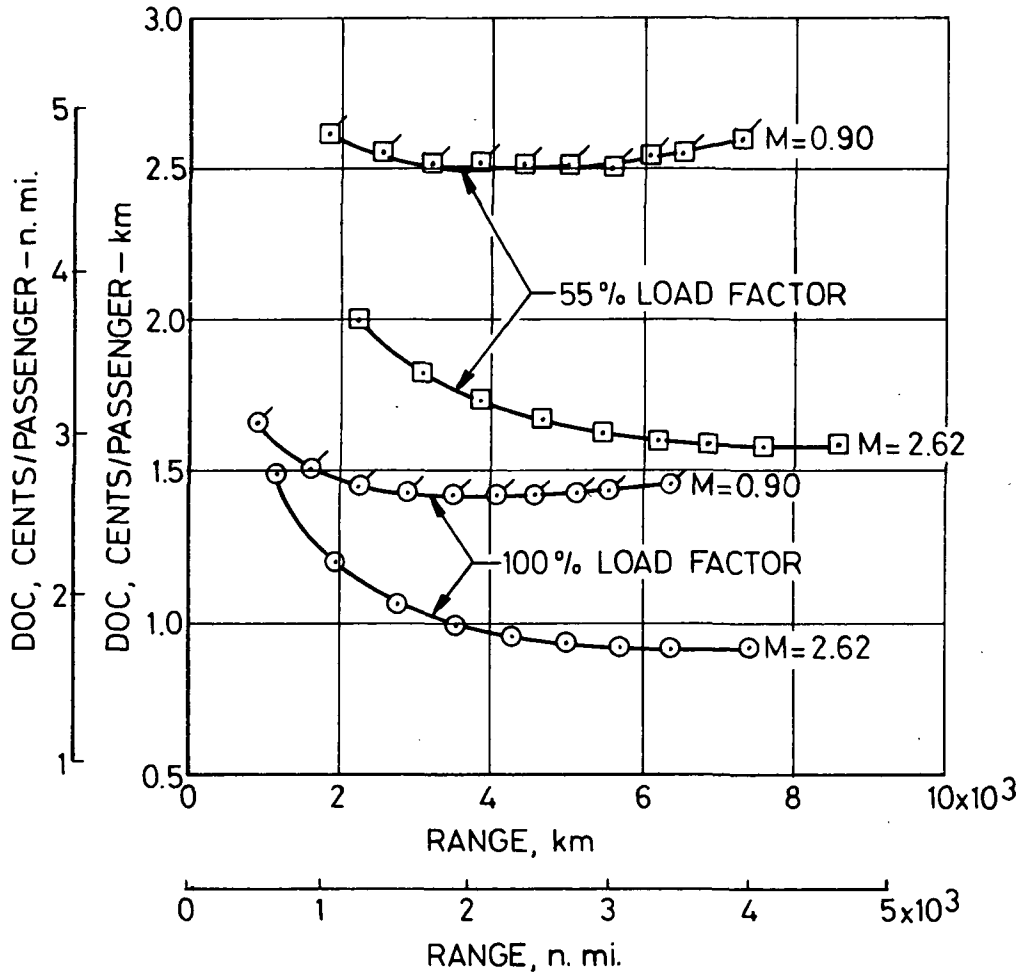

Figure 81 Effect of Load Factor and Cruise Speed on Direct Operating Cost